Università degli Studi di Genova

DIPARTIMENTO DI NEUROSCIENZE, RIABILITAZIONE, OFTALMOLOGIA, GENETICA E SCIENZE MATERNO-INFANTILI
Scuola di Scienze e Tecnologie Biomediche

Tesi di Dottorato di Ricerca

Sit-to-Stand Phases Detection by Inertial Sensors

Coordinatore:
Ch.mo Prof. Angelo Schenone

Supervisore della ricerca:
Dott. Marco Testa

Candidato:
Anna Di Marco
Matricola 4081308

Anno Accademico 2018-2019 — Ciclo XXX

A chi purtroppo non c'è più.

I have no use for people who have learned the limits of the possible

[Terry Pratchett]

Acknowledgements

Quasi (anzi totalmente) incredula, sto scrivendo i ringraziamenti della tesi di Dottorato. E' stata una lunga avventura, fatta di alti, bassi, idee geniali e "*schianti contro i muri*"(Tanti schianti NdA). Non ce l'avrei mai fatta senza l'aiuto di chi in questi anni mi è stato vicino. O, forse ce l'avrei fatta, ma con qualche neurone in meno.

Innanzitutto, vorrei ringraiare il Prof. Marco Testa che in una mattina di Febbraio (O Marzo) ha dato inizio a questa avventura. Grazie per avermi dato fiducia, per avermi consigliato, per avermi supportato e sopportato. Insieme al Prof. Testa, vorrei includere nei ringraziamenti anche il Gruppo di Ricerca di Savona: Tommaso, Luca, Giacomo, Antonello e la new entry Mirko. E' stato un piacere saldare stagno, monitorare judoka e qualsiasi altra. Grazie per l'ampia libertà operativa concessami e per la vostra amicizia, nonchè fiducia (soprattutto nel darmi in mano un saldatore).

"Educational" refers to the process, not the object (*Terry Pratchett*). Quando ho letto questa frase non ho potuto fare a meno di pensare al Dr. Leonardo Gizzi, meglio noto come Dr. Evil, una sorta di mentore a distanza. Grazie per i tuoi *cattivi* consigli, regolarmente non seguiti -no, dai a volte sì.

Un grande e sincero "Grazie" lo vorrei dedicare al "*Popolo*" del Campus di Savona, da Caterina e Pino a tutto il personale delle sgreterie/ professori e quanto altro che ho regolarmente disturbato in questi anni. Un grazie particolare ai ragazzi

delle "Residenze", sia nuove che vecchie. Voi siete stati i miei "*Nipoti*" (e sempre sarete), i miei compagni di viaggio, la mia ispirazione alla leggerezza. E' stato un onore essere la "Nonna" del Campus. Grazie per le risate, le partite a Risiko e a "Battaglia Giamaicana", i giochi finlandesi-di-cui-non-ricordo-il-nome e le domeniche della nonna. E' stato un onore essere vostra Nonna. Raga, non vi cito tutti sennò mi ci vogliono altre dieci pagine di tesi e quaranta fazzoletti per asciugare le lacrime... Insieme ai ragazzi delle Palazzine, vorrei menzionare nei ringraziamenti anche i ragzzi della "*Sala Studio della Carote*" , fra cui Alice, Polly, Konci, Jacopo, Holly, Rouge, Como...

Le ragazze e la società del Cogoleto Rugby mi hanno insegnato che : "*Il rugby è un'ora e mezza di battaglia che può cementare amicizie per tutta una vita.*"(*Henri Garcia*). Grazie. Senza di voi non avrei mai potuto conoscere la bellezza di questo sport; apprezzarne il sacrificio comunitario di fondo. Sopratutto, non vi avrei mai conosciuto. Le ragazze, i dirigenti e gli allenatori del CUS PISA Rugby, invece, non hanno fatto altro che confermare che: "La mischia è la mia famiglia" (*Mauro Bergamaschi*). E in Mischia includo anche i Trequarti. Cos'è un Trequarti se non un pilone che non ce l'ha fatta? Grazie per avermi accolto a Pisa, per avermi permesso di allenarmi con voi; grazie per avermi reso una vostra compagna e una vostra amica.

Grazie alle amicize Pisane che in questo ultimo anno sono stato di gran supporto sia fisico che morale. Questo ultimo anno ho avuto bisogno di un supporto considerevole. In particolare Mimma, Luciano, Laura e Matteo, Vettovaglie alle 5 di mattina senza di voi non sarebbero state le stesse....

Grazie anche ai miei colleghi di ION Trading per la loro comprensione e pazienza, ma soprattutto per il corso intensivo di toscano/livornese.

Grazie Mamma. Grazie Papà. Grazie Michele. Grazie per il vostro costante supporto, i buoni consigli e della buona dose di testardaggine che mi avete dato.

Grazie a tutti gli altri che non ho citato. In questi anni, ho apprezato il contributo

di tutti e tutto in questi anni nel perseguire questo Boss Finale di tutte le tesi. Anche di MATLAB.

Summary

The Sit-to-Stand(STS) is defined as the transition from the sitting to standing position. It is commonly adopted in clinical practice because musculoskeletal or neurological degenerative disorders, as well as the natural process of ageing, determine an increased difficulty in rising up from a seated position.

This study aimed to detect the Sit To Stand phases using data from inertial sensors. Due to the high variability of this movement, and, consequently the difficulty to define events by thresholds, we used the machine learning. We collected data from 27 participants (13 females,24.37±3.32 years old). They wore 10 Inertial Sensors placed on: trunk,back(L4-L5),left and right thigh, tibia, and ankles. The participants were asked to stand from an height adjustable chair for 10 times. The STS exercises were recorded separately. The starting and ending points of each phase were identified by key events. The pre-processing included phases splitting in epochs. The features extracted were: mean, standard deviation, RMS, Max and min, COV and first derivative. The features were on the epochs for each sensor.

To identify the most fitting classifier, two classifier algorithms,K-nearest Neighbours(KNN) and Support Vector Machine (SVM) were trained. From the data recorded, four dataset were created varying the epochs duration, the number of sensors. The validation model used to train the classifier. As validation model, we compared the results of classifiers trained using Kfold and Leave One Subject out (LOSO) models. The classifier performances were evaluated by confusion matrices and the F1 scores.

The classifiers trained using LOSO technique as validation model showed higher values of predictive accuracy than the ones trained using Kfold. The predictive accuracy of KNN and SVM were reported below:

- KFold
  - mean of overall predictive accuracy KNN: 0.75; F1 score: REST 0.86, TRUNK LEANING 0.35,STANDING 0.60,BALANCE 0.54, SITTING 0.55
  - mean of overall predictive accuracy SVM: 0.75; F1 score: REST 0.89, TRUNK LEANING 0.48,STANDING 0.48,BALANCE 0.59, SITTING 0.62
- LOSO
  - mean of overall predictive accuracy KNN: 0.93; F1 score: REST 0.96, TRUNK LEANING 0.79,STANDING 0.89,BALANCE 0.95, SITTING 0.88
  - mean of overall predictive accuracy SVM: 0.95; F1 score phases: REST 0.98, TRUNK LEANING 0.86,STANDING 0.91,BALANCE 0.98, SITTING 0.92

Contents

List of Tables

List of Figures

Introduction

The functional evaluation is a relevant component of the physical examination as it objectifies the loss of functioning of the patient. Furthermore, it constitutes a base for evaluating the effect of rehabilitation therapy. Among the functional tests, the Sit to Stand (STS), defined as the transition from the sitting to the standing position[1], is a basic ability performed many times daily[2], and therefore it is considered a fundamental prerequisite for gait performance or postural transition[3]. It is commonly adopted in clinical practice because musculoskeletal or neurologic degenerative disorders, as well as the natural process of aging, determine an increased difficulty in rising from a seated position [4]. Moreover, the STS has been used to predict the fall risk among elderly or frail subjects[5], as a reduced performance during the STS has been associated with loss of lower extremities strength, postural and balance control [6] and the extent of disability.

Although the STS is performed as a test itself, it also constitutes a portion of the Timed-Up and Go Test (TUG), the Five Time Sit To Stand Test(FTSTS) and the 30-second chair stand test (30s CST). The TUG test measures the time that a person takes to rise from a chair, walk three m, turn around, walk back to the chair, and sit down[7]. It is widely used to evaluate balance, mobility and fall risk [8, 9, 10]. Usually, the single outcome of the test is its duration. The FTSTS measures the time taken for completing as quick as possible 5 STS cycles[11], while the 30s CST counts the number of STS cycles performed in 30 second[12]. Although the tests appear similar and the movements required for completing the task are

almost the same, it has been theorized that FTSTS could be an indicator of lower limb speed and power, while the 30s CST could be an indicator of lower limb endurance [13].
So, the parameters utilized for the evaluation of the performance are the time taken to complete the task or the number of repetition in a known period. Also, qualitative aspects such as the visual observation of the trunk leaning and/or the alignment of the body segments during the performance are useful for the caregiver. Although observation of these parameters has an important role in clinical practice, they are biased by subjectivity and human error. The adoption of objective methods during the functional evaluation is mandatory for every clinician and has been frequently highlighted [14]. In previous works, the camera-based system and force plates made possible the objective quantification: the analysis of the biomechanics of the movement, degrees etc.[15, 16] The use of optoelectronics system or force plates confines the studies on kinematic in a laboratory setting, and their results are not directly applicable to real-life conditions of patients [17]. Furthermore, this instrumentation is expensive.

Small wearable sensors as the inertial sensors, instead, are light-weighted and portable; less expensive. They provide information during the daily living task and performed outside the laboratory environment[18].The Inertial Sensors usually include accelerometers and gyroscopes.

- Accelerometers are electromechanical devices that measure the static force of acceleration(gravity) or dynamic forces of acceleration (vibration and movement). Estimation of muscle power[19] and joint angle [20] and activity classification[21] can be executed using acceleration signals.

- Gyroscopes measure the angular velocity: they are particularly useful for postural displacement detection [22, 23].

The spreading of inertial sensor based clinical applications increased simultaneously with the introduction of MEMS technology and the wide occurrence of ubiquitous smart devices, especially smartphones and tablets. Inertial sensors have been used i in numerous clinical applications , that include assessing and quantifying kinematic variables related to functional tasks or functional status [24, 25], classification of physical activities[21], falls detection[26, 27] and gait analysis[28, 29, 30, 31], sport monitoring[32, 33]. The sensorization of STS (and its variants) by inertial sensors is nothing new[34, 23].The STS monitoring by inertial sensors could improve the fall risk assessment [22, 35, 36, 37, 38]. For example, it has been showed that parameters such as jerk (the third derivative of position), or the postural sway could be more discriminant than time for separating elderly fallers and not fallers [35, 37, 38].

The purpose of this study is to characterize the dynamic events occurring as rising from a chair. The study of distinct events-or phases- of the STS movement would result in a most effective description about:

- the contribution of each single body element involved in the movement;
- kinematic and kinetic variables involved during the movement and their changes related to specific diseases;
- the pain points that could cause the failure of the movement.

[15, 16]
Previously, the identification of STS events or phases has been performed applying specific thresholds to joint angles, velocity changes, torques, and momentum. The high variability of the movement both between and within individuals makes it difficult to find common thresholds[15].
The Machine Learning (ML) could be a solution for solving the above-cited problem. Machine Learning is the process to generate a set of rules from real data [39]. There are many application in medical field such as diagnosis of a disease[40, 41, 42],

prediction of disease[43, 44, 45]. It is an instrument very versatile, and have been used in many clinical fields such as human activity recognition[46], gait analysis or fall detection. Following we reported some examples.
ML has been used in the gait analysis for automatic recognition of gait pattern changes due to aging [47]; gait event detection for the functional electrical stimulation [48]. ML allowed researchers to identify the falls, but also to the classify the type of falls[49].

This study aimed to detect the Sit To Stand phases using data from inertial sensors. Due to the high variability of this movement, and, consequently the difficulty to define events by thresholds, we used the machine learning. In particular, we compared the performances of two classifiers model in order to find the most efficient model. The phases detection should help the recognition of the causes that lead to the falls. The knowledge about the factors that cause falls could help the caregivers to assess specific rehabilitation programs.
This study would be the first step of the implementation of a system able to detect the STS phases in real time. The measurement method should not restrain the subject with too many sensors in order to reduce the time to wear them and to encourage the use of the system in clinical rehabilitation. For these reasons, the phases detection have to be correct also using features computed on small sample size and from fewer sensors. We addressed this problem arranging the data collected from the sensors in 4 datasets:

- Two datasets included the data from all the sensors; the features were computed on epochs of 0.1s and 0.2 s
- Two datasets included the data from only the sensors placed n trunk and thighs; the features were computed on epochs of 0.1s and 0.2 s

Chapter 1

Sit To Stand

1.1 General Overview

The functional evaluation is a relevant component of the physical examination as it objectifies the loss of functioning of the patient. Furthermore, it constitutes a base for evaluating the effect of rehabilitation therapy. The adoption of objective methods during the functional evaluation is mandatory for every clinician and has been frequently highlighted [14].

Among the functional tests, the Sit to Stand (STS), defined as the transition from the sitting to the standing position[1], is an essential ability performed many times daily[2], and therefore it is considered a fundamental prerequisite for gait performance or postural transition [3]. It is commonly adopted in clinical practice because musculoskeletal or neurologic degenerative disorders, as well as the natural process of aging, determine an increased difficulty in rising from a seated position [4].

Moreover, the STS has been used to predict the fall risk among elderly or frail subjects[5], as a reduced performance during the STS has been associated with loss of lower extremities strength, postural and balance control [6] and the extent of disability. The parameters utilized for the evaluation of the performance are the time taken to complete the task or the number of repetition in a known period.

In addition, qualitative aspects such as the visual observation of the trunk leaning and/or the alignment of the body segments during the performance are useful for the rehabilitator. Commonly, STS includes four phases:[15, 16, 50]

1. Flexion momentum phase: The initiation of the movement coincides with the trunk flexion and pelvis rotation. The lifting of the buttocks from the chair is the end of the first phase. The main muscles involved are the hip and ankle flexors.

2. Transfer phase: It starts when the buttocks leave the seat, and it ends with the maximum ankle dorsiflexion and maximum forward flexed position. During the second phase, the maximum hip and knee torques are reached, also if the main muscles involved are the knee extensors.

3. Extensor Phase: This phase precedes the upright stance. The knee and hip extension velocities increase until the maximum. Then the knee extension and hip extension velocities reduce until 0 °/sec. The hip extension velocity reached 0 °/ sec is the final event of phase III.

4. Stabilization phase: The upright stance is achieved. The ankle plantar flexors stabilize the body to achieve the maintenance of the balance and postural stability. Usually, subjects experienced more postural sway.

It's a complex movement: it requires muscular strength and coordination[51, 52]. Studies confirmed that the STS requires more muscular strength than activities such as stair climbing [53].
Three main standing strategies performed by elderly and neurodegenerative patients have been individuated : [54]:

- Arm strategies: Pushing or swinging the arms against the chair is the most common strategy for facilitating the rising. It is used by neurodegenerative patients, disabled persons, elderly with difficulties getting up. Those at lower

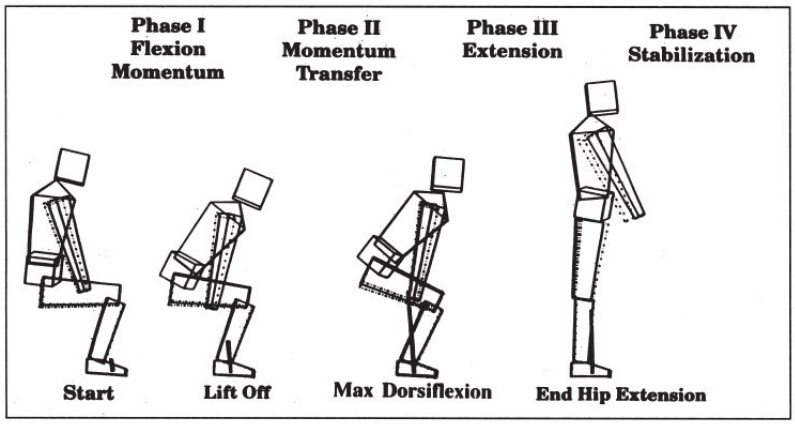

Figure 1.1: *The STS is defined as the transition from the sitting position to the standing position. It could be divided into 4 phases. Phase: From the starting of the movement (the beginning of the trunk flexion) to the maximum trunk flexion; Phase II: from the maximum trunk flexion to the LIft-off; Phase III: from the lift-off to the hip extension; Phase IV: The maintenance of the standing position [16]*

functionality spectrum push the arms against the chair, while the subjects more functional may swing the arms without looking for any support.

- Momentum Transfer Strategy: In phase I, the trunk flexion generates a momentum that will be transferred to the total body contributing to the rising. Generally, it is used by young and healthy adults because it requires much strength.

- Stabilization Strategy: The compensation relies more on little frequent movement than on the momentum generated by the trunk.

[15, 55, 56]

1.2 Sit To Stand Test

The STS requires strength, coordination and balance[51, 52]. Generally, clinicians and physiotherapists use it as subject's performance test. It has been used as indicator of postural control, fall risk, lower extremity strength, and proprioception

and as measure of disability. It is a powerful test, but the main difficulty is to determine the quality of the subjects' "chair rising." Various methods have been used for measuring the quality of STS. The next paragraph is a general summary of the most famous and used tests in clinical use/practice.

1.2.1 Five Times Sit To Stand

The five Time Sit To Stand Test (FTSTS) was introduced for the first time in 1985[11]. Subjects stand up five times as quick as possible. The time required for completing the test is the main outcome. Originally, this test was introduced for measuring lower limb extremities strength, recently is used to assess functions, too. The study reported in [57] showed that FTSTS improve the discriminating ability of ABC[1] and DGI[2] to identify people with balance dysfunction. In addition to balance, motor control and strength, FTSTS requires the ability to integrate visuospatial information[58] found an association between the FTSTS and cognitive function assessed by Pfeiffer's short Portable mental state questionnaire[3]. In particular, if subjects completed the FTSTS within 15 s, then they were less likely to suffer from cognitive dysfunction. Interpretation of tasks longer than 15 s was misleading because so long time could be due to both cognitive and musculoskeletal impairments.

[1]The Activities-specific Balance Confidence Scale (ABC) is a self administered questionnaire tool used to assess the confidence is performing various ambulatory activities without falling or experiencing sense of unsteadiness. BC scale consists of less and more challenging daily activities: walk around the house, walk up or down stairs,...

[2]The Dynamic Gate Test is an 8-test to assess to quantify the dynamic balance abilities. It has been demonstrated to be very sensitive test, since it evaluates walking during challenging tasks.

[3]The Pfeiffer's Short Portable Mental State Questionnaire (SPMSQ) is used for the assessment of organic brain deficit in elderly patients.

Many studies focused on the FTSTS ability to asses elderly fall risk. It has been shown that slower FTSTS performances had been associate do to high fall risk[59, 60, 61]. Unfortunately, in this case, the main limitation is the identification of the right time threshold. The time needed to complete the task is not enough as the main performance measure. The quantification of postural sway and the smoothness of the transition could be added as quality performance indicators.

1.2.2 30s chair test

The 30-second chair stand test (30s CST) consists of counting the number of completed stands in 30 s with the hands crossed against the chest. The total number of stands completed is used to score subjects performance. The timed-sit-to-stand tests involve recording the amount of time to perform a prearranged number of STS repetitions. The 30s CST was introduced for avoiding the floor effect associated with the timed-sit-to-stand test,i.e. the difficulty of many patients to complete the chair stand test including even five STS repetitions[12]. The 30s CST protocol allows all subjects to receive a score, even zero, increasing the evaluation range and the discrimination ability of the test[62]. As other chair stand protocol, it was used as indicator of lower limb strength[13, 62]. The admission procedure in an emergency department short-stay unit provides for patients' physical performance. Among the tests, the most used is the DEMMI test. This test measures mobility across the spectrum from bedbound to independent mobility[63]. It includes 51 items, and it is time-consuming. The 30s CST is faster and easier to deliver. Bruun et al.[64] demonstrated the association between the 30s CST and the DEMMI. A threshold of 8 repetitions could distinguish between patients with low physical performance and high physical performance implying the possibility of implementing the 30s-CST in acute settings with limited time and space for testing.
The fitness test is used to assess the motor abilities and establishes the quality of life. The most used scales are based on the observation of common daily activities.

The Fullerton Test is mainly intended to identify highly-active older adults who are at an increased risk to experience fall-related injuries due to sensory impairments. The test uses both dynamic and static balance under different situations to identify balance deficits in older adults. The test includes the 30s CST used for assessing the endurance and lower body strength[65].

1.2.3 Timed Up and Go Test

The Timed Up and Go (TUG) test was introduced in 1991 by Podsiadlo and Richardson as modification of the former Get-Up and Go test[4][7]. The TUG measures the time in seconds for a person to rise from sitting from a standard armchair, walk 3 meters, turn, walk back to the chair, and sit down. The person wears regular footwear and uses his/her customary walking aid. The original purpose of the TUG was to test basic mobility skills of frail older adults.
The test has been used in other populations, including people with arthritis [66, 67, 68] and stroke [69, 70]. The TUG may be particularly well suited for the quantification of disorders resulting in poor sequencing of well-learned motor skills, which is a problem in people with PD [71, 72].

1.3 Sensorization of the Sit To Stand

The parameters utilized for the evaluation of the performance are the time taken to complete the task or the number of repetition in a known period. In addition,the qualitative aspects useful for the rehabilitator the visual observation of the trunk

[4]The Get Up and Go, as the timed up and go test, consists of the observation of the subjects rising from the sitting position,walk 3 m, turn around, walk back and sitting again. The performance was assessed qualitatively observing the task. The introduction of the time taken to complete the task made the test more objective.

leaning and/or the alignment of the body segments during the performance. Although observation of these parameters has an important role in clinical practice, they are biased by subjectivity and human error. The adoption of objective methods during the functional evaluation is mandatory for every clinician and has been frequently highlighted [14]. The STS movement can be described through kinematic and kinetic variables, obtained using devices such as force plates, video analysis, optoelectronic systems, and inertial sensors[37].

1.3.1 Force Plate

A Force Plate is a rectangular metal plate instrumented as load cells. The force plate produces an electrical output proportional to the force applied to it. Force platforms may be classified accordingly to the sensors used. The piezoelectric and the strain gauge sensors are the most commonly used. The force plates are used to measure three orthogonal ground reaction forces (GRF), moment components and center of pressure[5]. In the Biomechanics research, the force plates are used across several movement tasks:

1. Gait Analysis: The gait analysis is the systematic study of how a person walks. It may be conducted for a clinical purpose (diagnosis, assessment, monitoring the results of treatments) or for research purposes. The analysis of the ground reaction forces during walking can give valuable information about basic locomotor and provide data which can be used to evaluate normal or pathological gait. Indeed, the normal gait is a repetitive cycle that exhibits a precise pattern, as shown by the figure 1.2. The Pathological gait is an altered gait pattern due to deformities, weakness, or other impairments.

2. Jumping and landing technique: Jumping and landing activities are major

[5]The point of the application of the ground reaction forces under the feet[73]

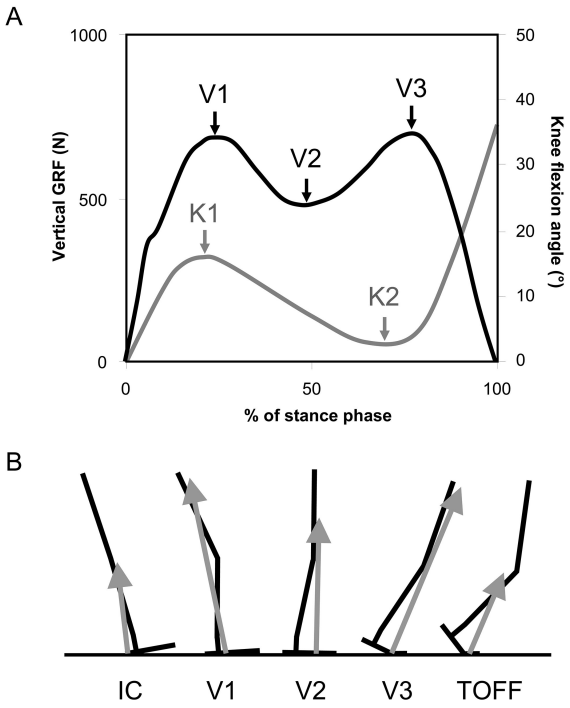

Figure 1.2: *A. Kinetic events (V1, V2, V3) indicated on the trace of vertical ground reaction force (black line), and kinematic events (K1, K2) indicated on the trace of angular displacement of the knee (grey line). B. Scheme of the ground reaction force (GRF) vector and limb segments orientation at the kinetic events. IC,initial contact; V1, first peak of vertical ground reaction force; V2, mid-stance minimum of vertical ground reaction force; V3, second peak of vertical ground reaction force; TOFF, toe off; K1, maximum knee flexion angle at the first half of stance; K2, minimum knee flexion angle at the second half of stance[74]*

components of some sports such as volleyball or basketball: testing GRF during landing can identify injury risks or predict reoccurring injuries.

3. Balance tasks: Standing balance is essential in daily living. The postural stability decreases , or it decreases due to neurodegenerative pathologies as stroke [75]. The measure of the balance of a patient could be used as quantification of the improvements due to the rehabilitation treatment, identify the risk of falls [76].

Analysis of the STS by Force Plate

The force plate has been used to describe the STS. Numerous studies (using different devices) described the STS producing different results. More than any other human movement, the STS is characterized by high inter and intrasubject variability [15]. Two STS performances are never equal, but unequivocal movements can be identified and standardized, as researchers standardized the gait analysis events (heel-ground contact, swing and toe off). [15] Etnyre et al.[15] proposed a reference

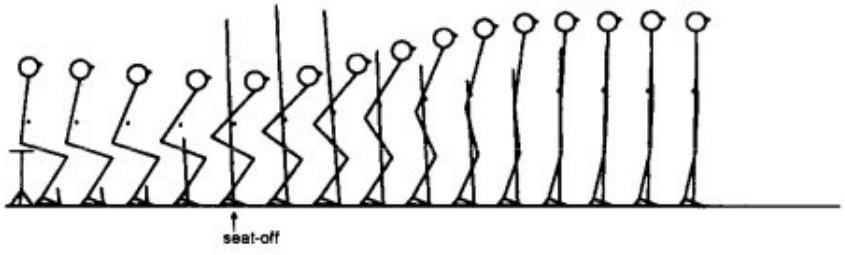

Figure 1.3: *Stick Figure of STS movement, the ground reaction force, the solid line, and the center of mass, the black dot, are plotted. At the instant of seat-off the ground reaction force(solid line) was directed slightly backward and passed anterior of the hip and ankle joint and far posterior of the knee joint[77].*

standard for STS analysis using a force plate based on the identification of eleven events in the 3-dimensional space, as shown by the figure 1.4. The study compared four different STS conditions: arms free, arms crossed, hands on knees and hands-on armrest. The figure 1.5 shows the comparison of VGRF during STS in healthy

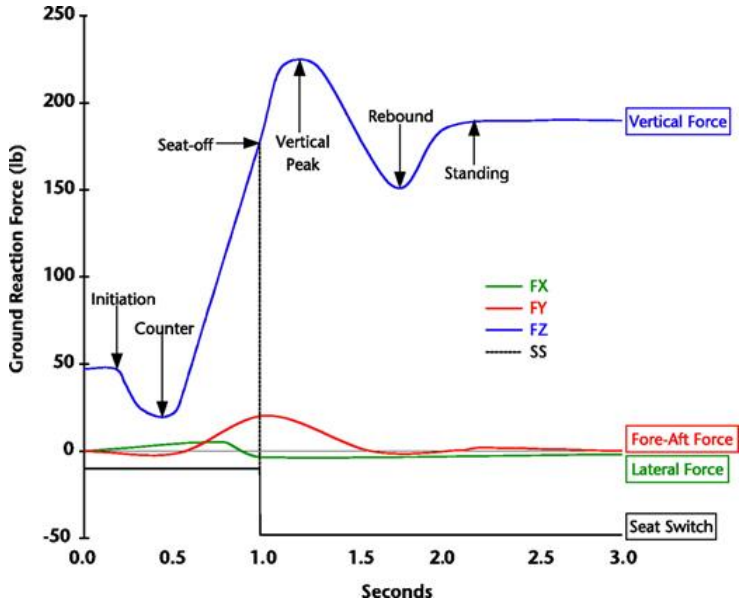

Figure 1.4: *Three Orthogonal Ground reaction Force during standing for a single participant (arm-crossed condition). The graph highlights the six events individuated by Etnyre in vertical axis: Initiation(the first deflection from the baseline); Counterforce(the minimum peak following the start of the movement); Seat Off (The buttocks rise from the chair); Peak Force(The greatest vertical force recorded); Rebound (the lowest force value following the peak); Standing (the participant recovered the postural stability)[15] .*

subjects, stroke, and stroke fallers. The fall risk increased in stroke patients due to their pathological condition. The analysis of GRF helped to distinguish stroke patient and fallers stroke patients in order to provide the most suitable rehabilitative program to reduce the fall risk[78].

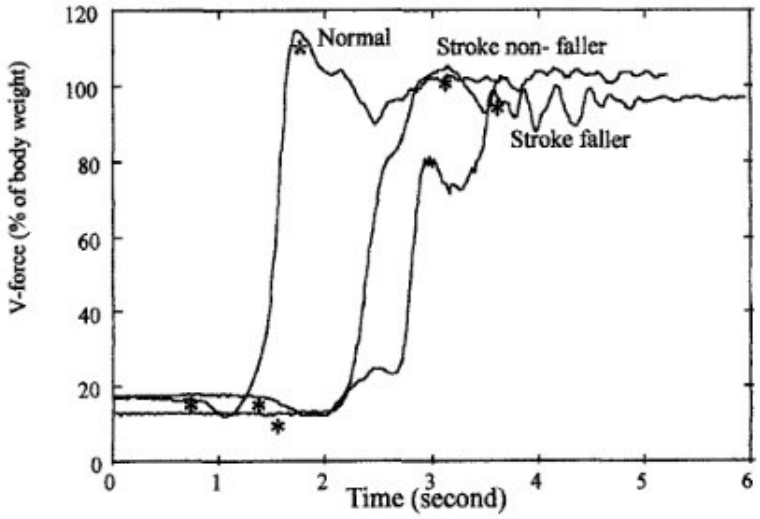

Figure 1.5: *Comparison of vertical force in healthy subjects, stroke patients and stroke fallers patients during rising. The graph shows the force change during the movement. In the first phase of STS, the force was steady due to the weight of feet. When the rising begun, the force decreased and then increased until the maximal vertical force is reached. This force peak is due to the body acceleration. The force decreased until the BW. The asterisks on the graphs indicated the limit points of the rate of rising in force slope: the stroke fallers patients have a lower rate rise[78]*

- Difference in time: Stroke patients need more time to stabilize the cop during rising;
- Stroke Fallers patients showed high Medio Lateral (ML) COP sway. The higher COP oscillation in the ML plane indicates poor stability and high fall risk;
- The stroke fallers patients exhibited less peak power;
- Stroke patients distributed the body weight (BW) asymmetrically, in particular, they put more weight on the healthy leg when rising.

- The rate of rising (dF/dT) was lower in stroke fallers patients than in stroke patients or healthy people.

1.3.2 Electromyography

The Electromyogram(EMG) is the representation of muscles electrical activity during the contraction, i.e., the potential electric field generated by the depolarization of the sarcolemma. The first EMG signals investigator was H. Piper in 1912 [79]. The EMG signal can be detected by two techniques:

- Surface EMG: The signal is recorded by a pair or an array of electrodes placed on the skin. The application is easier than the needle technique, but only surface muscles activity can be detected; noise due to the cross-correlation effect with other muscles. Better suited for studies related to EMG pattern and muscular fatigue.

- Needle EMG: The signal is recorded by needle electrodes inserted into a muscle. This technique can record action potential of spontaneously contracting single muscle fibers (it is not possible by Surface EMG). The aim is to study the physiology and pathology of the Motor Unit[6]

[79] The common applications of EMG are:

- Investigate the motor control strategy [80, 81] and in particular pathological alterations [82], in order to understand the muscles' functionality, diagnosis and improve the rehabilitative treatment.

- Investigate muscular fatigue. The muscular fatigue defined as the "failure to maintain the required or expected force" [83] can be detected only when

[6]Motor unit consists of a motor neuron and the skeleton muscles innervated by the motor neuron.

it occurs. It is based on force measurement during muscle contraction [84]. The EMG analysis of muscular fatigue reports the modification of the fatigue associated with biochemical and physiological changes [84, 85]. The Median frequency and the mean frequency are the spectral parameters commonly used for analyzing the EMG spectrum. Studies have shown that MF and MDF shift towards low frequencies, while the value of RMS increased, probably due to the recruitment of more MU.

EMG Signal During STS The Tibialis Anterior(TA), the Bilateral Quadriceps(QUA), the medial Hamstring(HAM), the soleus(SOL) are essential during the STS. They are in charge of the anteroposterior stabilization of the and ankle joint. In the initial phase of STS, the TA muscle is the first muscle to be activated [87, 86]. Its activation increased proportionally to the weight shift. Almost simultaneously, the QUA was activated. It contributed to the early stabilization of the knee before the knee extension. The TA and QUA activities increased until the reaching of the standing phase when they became inactive. The HAM, main stabilizer of the knee during the standing phase, is the third to be activated. The SOL was the last muscle activated. It contributed to postural stability. The HAM and the SOL are active during the standing phase (figure 1.6).
The analysis of the EMG pattern activation during STS or the individuation of the muscular deficit is useful for designing a more effective rehabilitative treatment program.
Different pattern activation of the lower limbs between stroke hemiplegic patients and healthy patients was found. The figure 1.7 shows the different patterns of leg muscles activation during the STS in three different groups: Healthy subjects, Stroke Fallers, and Stroke non-Fallers.

- The stroke fallers patients activated the Soleus muscles prematurely or excessively. The premature or excessive activation of the SOL might cause stiffness

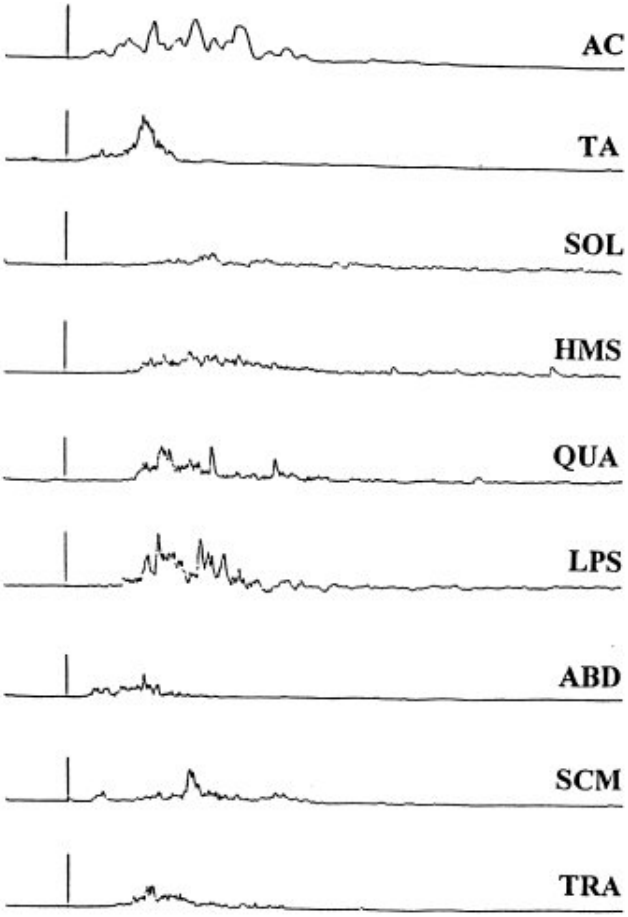

Figure 1.6: *EMG signals recorded during STS. The healthy subject sat in the natural position: feet flat on the floor, ankle joint laid in a plan slightly posterior to the knee joint, trunk relaxed and head facing forward. The vertical line indicated the time of the "go" signal. Accelerometer (AC), tibialis anterior (TA), soleus (SOL), quadriceps (QUA), hamstrings (HMS), abdominals (ABD), lumbar paraspinal (LPS), sternocleidomastoid (SCM) and trapezius (TRA). The TA was the first muscle to be activated, followed by the LPS, QUA and HMS. These muscles were activated near the take-off. The SOL is the last muscle recruited [86]*

of the ankle, resulting in instability.

- The stroke non-fallers patients exhibited prolonged activities of the TA and QUA muscles of the unaffected side, probably due to a compensatory strategy. The muscles of the unaffected side were recruited as early as possible and with greater amplitude to compensate the weakest muscles of the hemiplegic side. This compensatory strategy could protect them from falling.

- The Stroke fallers patients exhibited no TA muscle activation or low amplitude. The TA was an ankle stabilizer, the absence of the TA activation could indicate that stroke fallers utilized less the ankle musculature than healthy subjects or stroke non-fallers patients [87].

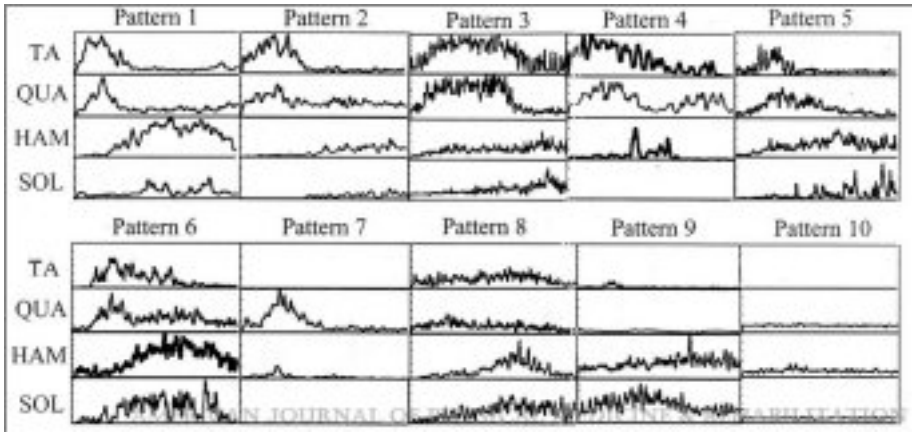

Figure 1.7: *Different pattern of leg muscle activation in three different groups during STS. TA, Tibialis Anterior; QUA Bilateral Quadriceps; HAM, medial Hamstring; SOL, soleus. These four muscles are essential in controlling anteroposterior stabilization of the knee and ankle joint in a healthy subject. The activation sequence for healthy subjects is TA, QUA, HAM, and SOL(Pattern 1). The muscle activation of the unaffected side (Pattern 2, 3, 4, 5) of the stroke patients (both fallers and non-fallers) is quite similar to the healthy subjects activation. Prolonged activation of TA and QUA has been detected in stroke non-fallers, while in stroke non-fallers the amplitude activity of the TA muscle decreased (or interrupted). The muscle activation of the affected side of the stroke fallers is quite varying (pattern 6,7,8,9,10). Stroke fallers exhibited an absence or reduction of motor output or interrupted motor unit activation [87].*

The knee Osteoarthritis (KOA) is related to knee pain [88]. The knee pain and

disability is associated with the Quadriceps Femoris[7] muscles weakness resulting in a diminished force output from one muscle group on one side of the knee and creating joint instability [89, 90]. Patients affected by KOA used a compensatory strategy for rising from a chair. In particular, they tend to load the hips more than healthy subject and generated less knee joint torques. This could increase the risk to develop Osteoarthritis at hips too and lead to knee muscle atrophy and weakness [91]. The affirmation is confirmed by the evidence that knee extensor muscles of women with KOA are less efficient than healthy subjects. Moreover, the Biceps Femoris (BF) activity of women with OA is higher than controls [92]. The BF is a biarticular muscle involved in both the knee flexion and hip extension. During STS, the force generated at the hip by the BF muscles is transferred to the knee joint through the recto femoris [77]. Likely explanations are:

- Patients affected by KOA use more the hip muscles than the knee muscle transferring the load from the knee to the hip;
- The higher BF activation is used for stabilizing the knee and reducing the pain [92].

Patients with KOA performed the Total Knee Arthroplasty (TKA) as a remedy for alleviating the knee pain. Despite the functional improvements, they continued to obtain a lower score than healthy controls on the functional test. The investigation on the STS performed by subjects three months and one year following the TKA highlighted that 3 months after the TKA the Quadriceps Femoris is still weak. Subjects 1 year following TKA recovered the Quadriceps Femoris strength, but they continued to use a compensatory strategy during STS. This finding highlighted the need for retraining after the intervention because resolving the impairment did not automatically lead to regaining the correct use of muscles [93].

[7]The Quadriceps Femoris is a muscle group (Rectus Femoris, Vastus Lateralis, Vastus Intermedius) involved in the extension of the knee joint.

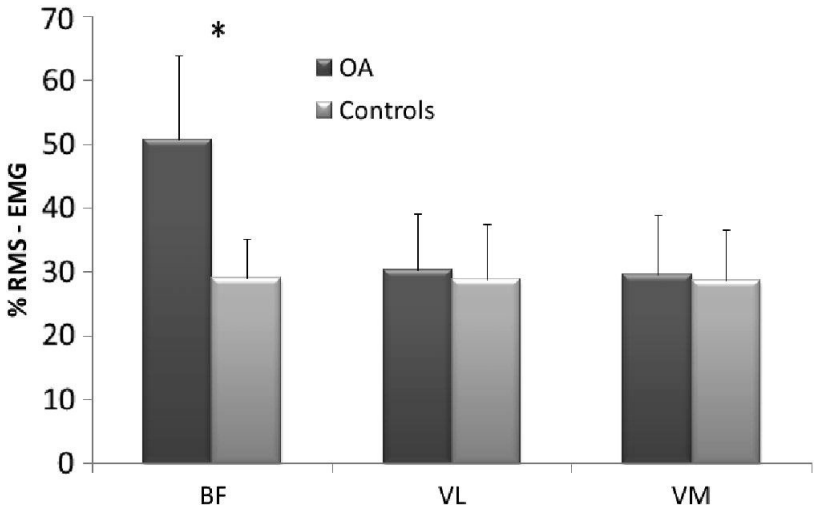

Figure 1.8: *The RMS-EMG activity of Biceps Femoris (BF), Vastus Lateralis(VL), and Vastus Medialis (VM) during STS in women with knee osteoarthritis (OA) and controls. VM and VL did not show any statistically significant difference between the two groups. The main difference between the two groups is the BF activity, significantly higher in OA group [92]*

1.3.3 Optolectronic system

In literature, the Optoelectronics system is considered a gold standard in human movement analysis [17]. The system detects light and uses this detection to estimate the 3D position of marker via time-of-flight triangulation. The markers can be:

- Active Markers: They use LEDs that shine a light toward the camera. Each active markers can flash at a different frequency that makes marker tracking easier.
- Passive Markers: Passive Markers are reflective and bounce light back at the cameras where they can be detected.

The Optoelectronics system in biomechanics is particularly useful for:

- calculation of the center of Mass: The center of Mass (CoM) is the unique position at which the weighted position vectors of all parts of a system sum up to zero. It is the point where any uniform force on an object acts. In

other words, it is the balance point of an object's mass. This simplifies the motion description of oddly-shaped objects and the complicated system as the human body. In general, the CoM can be found by vector addition of weighted position vectors which point to the center of mass of each object in a system. The human body is a system of segments linked to each other at the joints: mass distribution changes as the body posture changes making the CoM changes continuously. The human body consists of several segments: the overall mass distribution within the body is a function of the mass distribution within the individual segments and the body posture. The body posture, in particular the join position and angles, can be estimated from the optical motion system, while the segment body mass distribution can be estimated by anthropometric tables [94].

- Evaluation of body segment position: the kinematic data, acceleration, velocity, angles are indirectly measured.

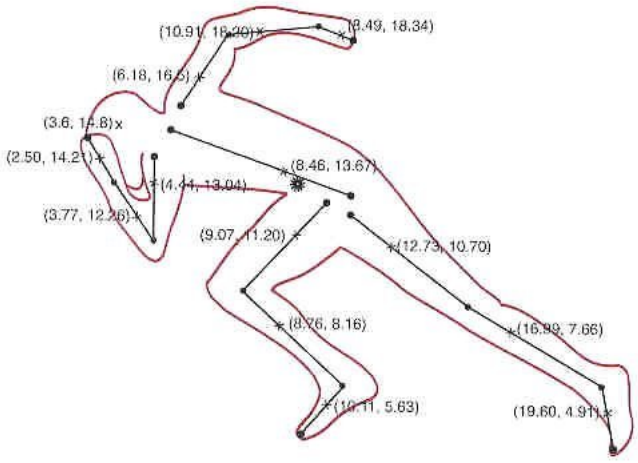

Figure 1.9: *The Center of Mass (CoM) is the balance point of an object mass. Its calculation simplifies the description of the mechanics of an object. The position of CoM in the human body changes and body posture changes. The human body consists of several segments; the CoM can be estimated combining the information about each segment mass distribution and the body posture. [95]*

Analysis of STS by Optoelectronic System The figure 1.10 shows the displacement of the CoM during STS: in the first part of the movement, it moved forward by the rotations of the upper body; then it moved upward by the legs extension. The velocity pattern of the CoM is used by Roebrock et al. [77] to distinguish three different phases:

- The acceleration phase: The CoM accelerated horizontally. The phase started at the beginning of the movement and ended when the CoM reached the maximal horizontal velocity.
- The transition phase: The CoM horizontal acceleration decreased, while the CoM vertical acceleration increased. The phase started when the maximal horizontal accelerations are reached, while the conclusion coincides to the reaching of the maximal vertical velocity.
- The Deceleration phase: The vertical velocity decreased until the end of the movement. The horizontal velocity fluctuated around zero.

Schenckman et al.[16] used a simple motion capture system to describe the STS. The study individuated four key events, as shown in figure 1.1. The motion analysis is based on the flexion and extension angles of ankle knee, hip, trunk, and head. The key events are the maximum values achieved and the timing of maximum join angles, velocities, and torques.
Obesity is a chronic disease whose incidence is increasing among children and adolescents. The altered weight distribution and muscular weakness caused the use of a motor strategy that can negatively affect the joints. Obese patients could suffer from lower back pain due to postural changes. The STS performance detected by an Optoelectronics system evaluated the different rising strategy used by obese patients and the control group. The control group lean forward the trunk and keep the initial foot position. Instead, the obese group limited the trunk flexion and moved the feet backward respect to the initial position. The limitation of the

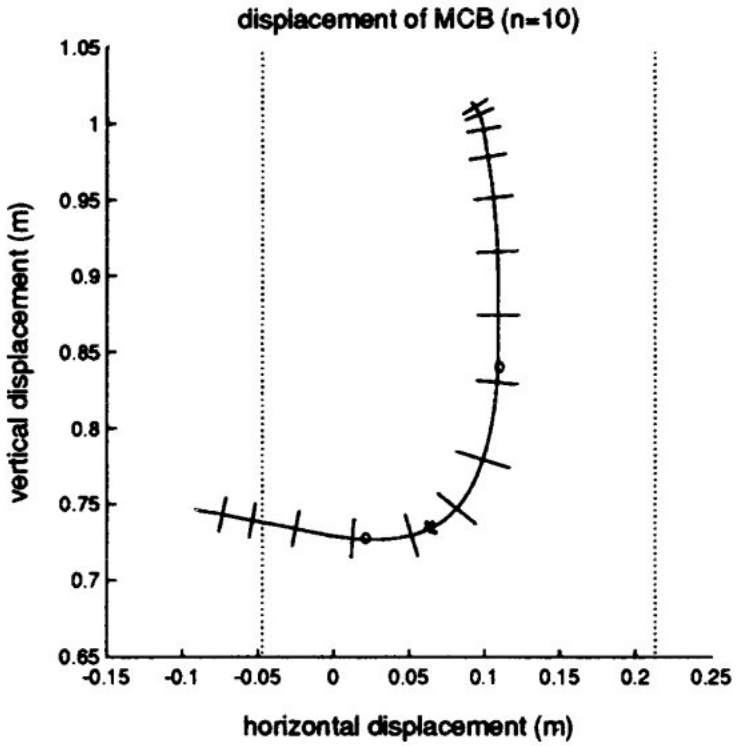

Figure 1.10: *Horizontal and vertical velocity of the CoM during STS. The solid line represented the horizontal velocity, while the dotted one the vertical velocity. Based on the CoM patterns three phases were distinguished. The vertical lines indicated the limits between the three phases. Phase 1: the movement began and horizontal velocity increased until its maximal point. Phase 2 started when the CoM reached the maximal velocity; in this phase, the vertical velocity began to increase. The phases concluded when the horizontal velocity is near to zero, and the CoM vertical velocity reached the peak. Phase 3 started when the CoM reached the maximal vertical velocity; the vertical velocity decreased until the end of the movement. The horizontal velocity fluctuated around zero.[77]*

trunk flexion is probably due to the lower back pain. Furthermore, this strategy exposed the knee to high load and increased the muscular fatigue [96, 97].

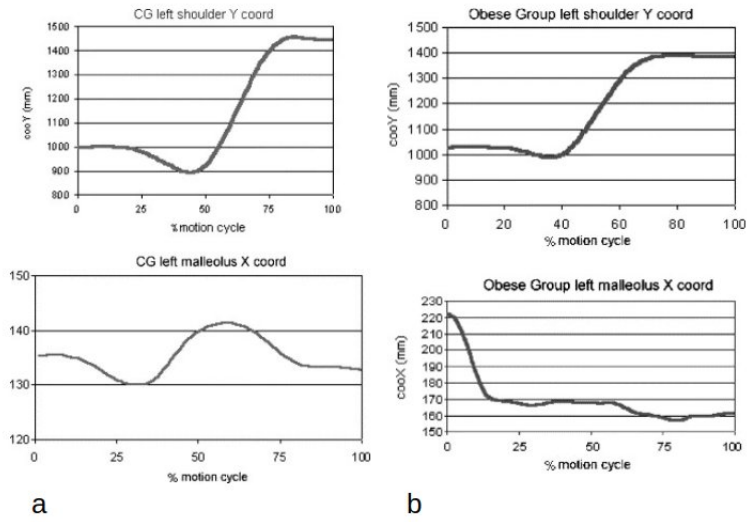

Figure 1.11: *STS performance of Control Group (a) and Obese Group (b). The position of the left shoulder and left malleolus are reported. a) The control group used a rising strategy characterized by a high degree of the trunk flexion. The feet movement are near to zero. b) The obese group limited the trunk flexion and moved backward the feet. This strategy is very inefficient because the momentum on the knee joint increased accelerating the muscular fatigue.[97]*

1.3.4 Inertial Sensor

The use of optoelectronics system or force plates confines the studies on kinematic in a laboratory setting, and their results are not directly applicable to real-life conditions of patients[17].

The sensorization of STS by MEMS may enhance its objectivity through the measurement of different kinematic variables such as trajectories and accelerations of the involved body segments.

The clinicians evaluate the performance of the STS using parameters such as the time taken to complete the task, the visual examination of the movement and the number of repetitions in a known period. Usually, clinicians use a stopwatch to

measure the task duration, but it may be imprecise and may lack specificity.
In clinical practice, the movement fluency helps evaluate the functional status of the patient but its evaluation with visual observation may limit its validity and reliability and may rely upon the experience of the observer [98]. The use of inertial sensors allows the calculation of several indices of the smoothness of the movement. The most known index is the Jerk, i.e. the third derivative of the position. It lacks a univocal definition: it can be obtained from the first derivative of the acceleration [35] or as the slope of the Antero-Posterior acceleration-time curve [38]. The use of inertial sensors for monitoring the STS will be discussed in Chapter 2

Chapter 2

Inertial Sensors

2.1 General Overview

Inertial Sensors are sensors based on inertia. They usually include at least an accelerometer and a gyroscope.

Micro-Electro-Mechanical Systems is a technique of combining Electrical and Mechanical components to produce a system of small dimensions. The main advantage of MEMS technology is the low cost and the little dimensions [99]. The spreading of inertial sensor based clinical applications increased simultaneously with the wide occurrence of ubiquitous smart devices, especially smartphones and tablets.

Nowadays, the integration of inertial sensors in smart devices has become a standard procedure [100]. Inertial sensors embedded in smart devices have been used in numerous applications, that include assessing and quantifying kinematic variables related to functional tasks or functional status [24, 25], classification of physical activities [21], falls detection [26, 27], and gait analysis, sport monitoring [32, 33]. The smart devices as the smartphones have the main advantage to be not perceived as invasive by users, making them more collaborative [27]. The Inertial Sensors have few advantages in the clinical practice compared to a monitoring system such as optoelectronics system or force plate [17]. The Inertial Sensors could be placed on

several body regions accurately and reliably [101].

2.1.1 Accelerometers and Gyroscopes

Accelerometers are electro-mechanical devices that measure the static force of acceleration(gravity) or dynamic forces of acceleration (vibration and movement). Figure 2.1 shows a simplified model of an accelerometer. It consists of a proof mass (M), a spring-damper (k,c) system suspended in an outer casing behaving like a second order mass-damper-system. External accelerations cause the displacement of the mass; the spring stretches with a force that corresponds to the acceleration. The acceleration is measured using the distance of the spring stretch (proportional to the stretching force) [102].

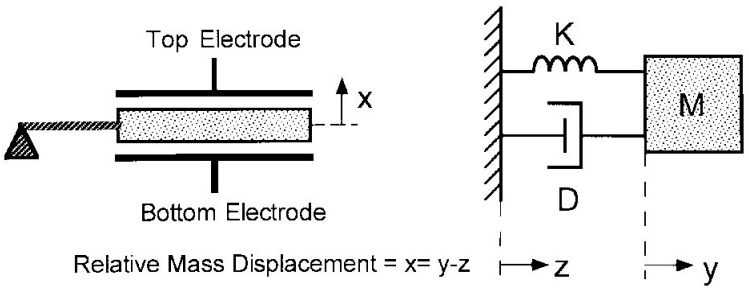

Figure 2.1: *General accelerometer structure and its mechanical model. The accelerometer consists of a spring-mass (M), and a damper-spring system. It behaves as a second-order spring-mass-damper system. External acceleration causes the displacement of the outer case. The mass stretches the spring in the direction opposite to the movement of the outer case. The acceleration is derived from the force exerted on spring by the mass is measured by the relative displacement x [103].*

Here are reported a few examples of the most used transducers for building the accelerometers.

- **Piezoelectric Sensors**: Some materials, such as the quartz, generate an electrical charge when deformed. The mass is attached to the piezoelectric crystal. When the outer case moves, the mass compresses the crystal, which in turn generates an electrical charge. They are not suited for steady or quasi-steady

measurements, because, during the action of a static force, the charge will decay with time. They are particularly recommended for measuring vibration.

- **Capacitative Accelerometers**: The acceleration is measured by detecting the change in capacitance due to a moving plate or sensing element [102, 104]. The capacitance can be measured using electronic circuitry. They have high sensitivity, good dc response and noise performance, low drift, low-temperature sensitivity, low power dissipation, and a simple structure.

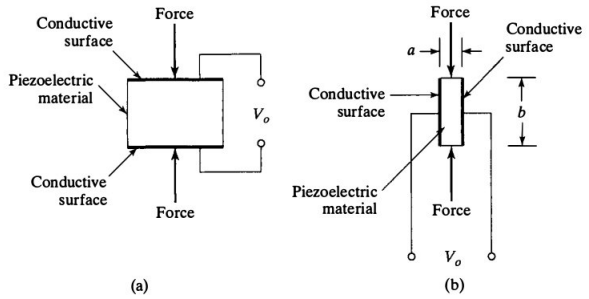

Figure 2.2: *Piezoelectric Sensors: they employ the piezoelectric effect of some crystals, i.e., the ability to generate an electric charge when the crystal is deformed. The piezoelectric material is placed between two conductive plates (for example, silver). When a force is applied, an electric charge is generated by the movement of the electrons from one side on fo the conductive surface to another. The charge generated is stored in the inherent capacitance of the piezoelectric material itself. a) Longitudinal effect: The Charge is given by $Q = F * d$, where F is the applied force and d is the piezoelectric coefficient of the material. d b) Transverse effect: The Charge is given by $Q = F * d * b/a$ if the ratio of the dimensions, b/a, is greater than 1 (the usual case), the transverse effect will produce a greater charge than the longitudinal effect.[103]*

The Gyroscopes are used for measuring the angular velocity. Conceptually, they consist of a spinning wheel in which the axis of rotation is free to assume any possible orientation. During the rotation, the orientation of this axis remains unaffected by tilting or rotation of the mounting, according to the conservation of angular momentum. Due to this principle, a gyroscope can lead to the measurement of orientation and its rate of change. The basic structure is similar to the acceleration sensors: a mass supported by springs. The angular velocity is obtained by

measuring the Coriolis Force[1] on the vibrating mass. Data from accelerometer and gyroscope can be used to estimate the orientation of the inertial frame[2] [105].
The dead reckoning is the process of estimating the sensor orientation and position. The procedure involves the use of the data from Accelerometers and Gyroscopes. The integration of the gyroscopes measurements returns information about the sensor orientation. The sensor position is obtained from the double integration of the acceleration. Before to integrate, the subtraction of earth gravity is required, hence the need to know the sensor orientation[106].
Despite the theory, it is quite hard to obtain the " perfect pose" estimation because of measurement noises and time slowly time-varying bias. Due to the bias, the Inertial Sensors output is non-zero also in the absence of any input. The bias is a time-depending error added to the measured signal. Furthermore, the integration of measurements leads to error accumulation [106, 107].
The solutions proposed to overcome the drift problem included the wavelet analysis[3]. This technique is used for removing the drift before the integration [109].
It has been proven that the incorporation of additional sensors such as magnetometers and the application of proper fusion filter (as the Kalman filter) reduced the drift and improved the accuracy [110, 111]. The magnetometers are highly sensitive to magnetic field disturbances generated by ferrous materials that usually there are in any laboratory [112]. To reduce the errors due to magnetic disturbances in the

[1]The Coriolis Force: an inertial force described by Coriolis. The effect of the Coriolis force is an apparent deflection of the path of an object that moves within a rotating coordinate system. The object does not deviate from its path, but it appears to do so because of the motion of the coordinate system.

[2]The inertial frame is the stationary frame. The Inertial sensors measure linear acceleration and angular velocity with respect to this frame.

[3]Wavelet analysis. The wavelets transform was introduced by Morlet and Grossman, and it allows analyzing the signal in both the time and frequency domain. A signal can be decomposed in terms of wavelets, which are generated from a fixed function called mother wavelet [108]

laboratory, Musić et al. replaced the magnetometers with a dynamic human body model. The human body model simulated the STS motion. Three segments constituted the model: shank, thigh and Head-Arms-Trunk (see the figure 2.3). The accelerometers (placed on shank, thigh, and shoulder) data were integrated into the data obtained by the human body model by the Kalman Filter [113].

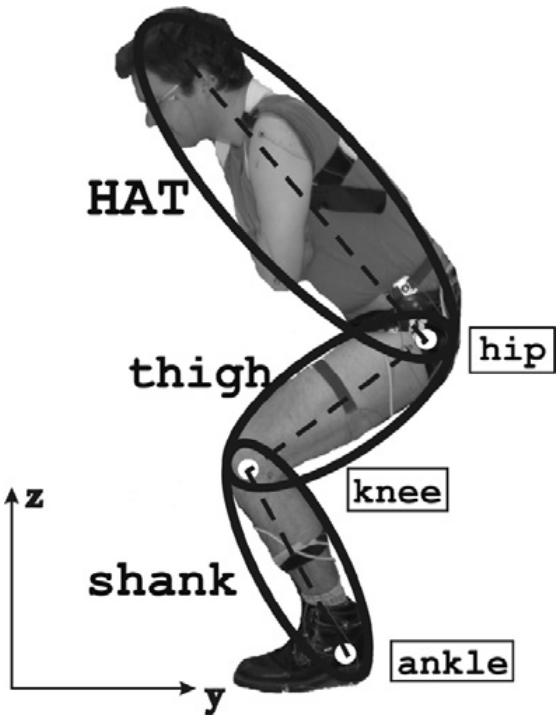

Figure 2.3: *Standing up motion human body model proposed by Musić. The body model replaced the use of magnetometers to improve the accuracy of the accelerometers and gyroscope to detect the STS. The model constituted by shank, thigh, and Head-Arms-Trunk. The joints in the ankle, knee, and hip connected the three segments. The Kalman filter has been used to integrate the data from the accelerometers (placed on shank, thigh, and shoulder)to the data obtained by the body model. [113]*

An attitude and heading reference system (AHRS) consists of various sensors along the three axes: accelerometers, gyroscopes, and magnetometers. Onboard processing in an ARHS, which provides information about the own orientation device, differentiates it from the inertial sensors. Indeed the inertial sensors collect data and deliver them to a computational device [114]. This system was born in the avionics field to measure the attitude and heading of aircraft; it has been adopted in

the biomechanics field to measure segments and joints kinematics in a wide variety of contexts [115].

2.2 Clinical Application

2.2.1 Gait Analysis

Gait is an important skill for ensuring independent living. The study of gait parameters can indicate deteriorating functionality and increasing falls risk: for example walking speed, stride time, stance, and swing time can be used as falls predictors [116, 117]. Temporal parameters, such as the gait time, can be detected by accelerometers placed on heel, thigh and waist [118], while sensors placed on both legs have provided information about the stride symmetry [118, 119]. The walking speed can be estimated by a single accelerometer placed on the trunk or by a triaxial accelerometer attached to tieback and a uniaxial accelerometer attached to the top of the right heel [119, 120].

The accelerometer required additional signal processing for compensating the influence of gravity. The data integration can be affected by drift. Another accelerometer pain point is the attachment point of the sensor on the body and skin artifact during the movement [121]. Parameters as the duration of swing, single and double stances during a gait cycle can be detected by knowing the heel strike and toe-off for each legs. These can be measured also by stand-alone Gyroscopes. Greene et al. [31] used an adaptive threshold algorithms for detecting the Initial Contact and the Terminal Contact during the gait cycle. The algorithm showed good results at normal walking speeds, but it had difficulties when shuffling gait is recorded. The wavelet analysis fit for the gait analysis identification [122]. The shank angular velocity measured during the gait, showed peaks when the heel strike and toe-off occurred. These peaks varied their amplitude accordingly to subject weight or velocity, painful articulation and so on. They can easily detected by decomposing the

shank angular velocity into wavelet packages [122].

The gyroscopes are insensitive to the influence of the gravity and are easier to place on the body [121, 123], but the measurements from gyroscopes are less reliable change direction[123].

The fusion of data from gyroscopes and accelerometers resulting in more robust

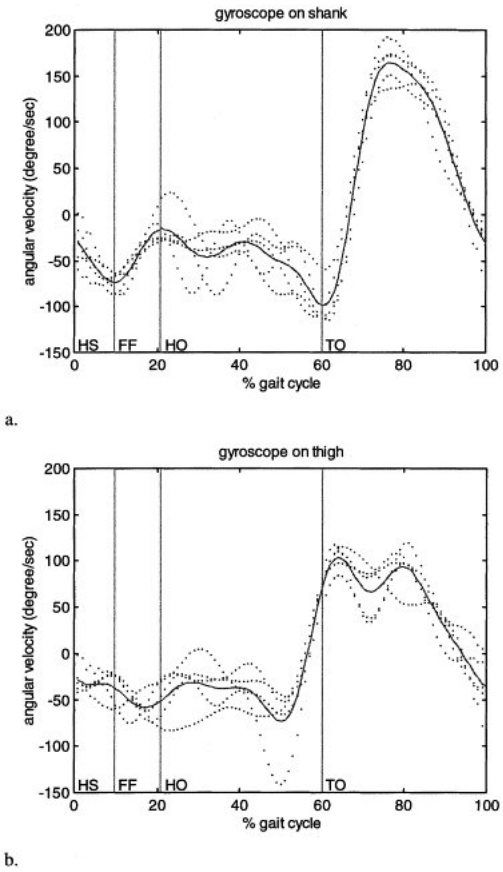

Figure 2.4: *Shank and thigh gyroscope signals in a normalised gait cycle. The vertical lines mark the heel strike (HS), foot flat (FF), heel off (HO), and toe off (TO). The dotted line is the angular velocity in each gait cycle and the solid line is the average value for angular velocity. The signals from the gyroscope placed on the shank had an higher correlation with the Vicon motion analysis system than the signals from the gyroscope placed on the thigh.*

estimations [124]. As highlighted by [124], the joint estimation calculated by integrating the difference of two angular rates around the corresponding coordinate axis is accurate on short time, but it is affected by the slowly-time drift. The effect

of the drift on the gyroscope can be reduced using the acceleration based joint angle found without integrating. However, the accelerometer-based angles affected by the accelerometer noise and seems to be less reliable in moments of large acceleration changes. The combination of both angles by a standard fusion tool (as the Kalman Filter) resulted in angle accurate on small and large time scales as shown in the picture 2.5.

The detection of the gait events by foot switches is strongly dependent on thresh-

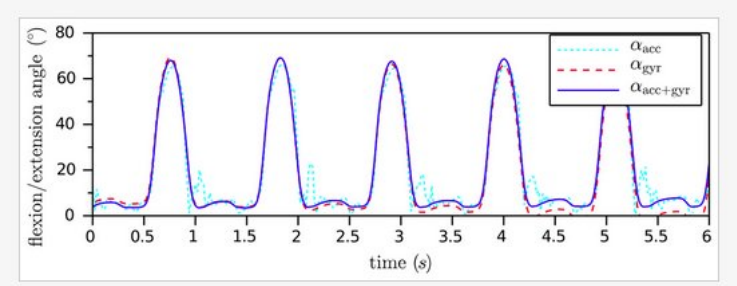

Figure 2.5: *Sensor Fusion of the Gyroscope-based and the accelerometer-based knee angle of a leg prosthesis. The a_{gyr} is accurate on short time but affected by drift. The a_{acc} angle is not affected by drift but is less reliable in moments of large acceleration angles. [124]*

old choice. Inertial sensors places on foot are possible to detect gait events, such as the foot-switches [30, 29]. Additionally, the information from the Inertial sensors can be used for reconstructing the trajectory of the foot where the sensor was placed [30] 2.6.

The smartphones are more advantageous than inertial sensors. They are ubiquitous; they can save and process data; the data can send by mail, wi-fi application and Bluetooth. The gate parameters obtained by the smartphones are reliable, as shown in [28]. The study compared the data obtained by the triaxial accelerometer and the data from the sensors embedded in smartphones. They found that the waveforms of the embedded sensors and triaxial accelerometer are similar, and the parameters obtained by the smartphone are highly correlated with the data from the triaxial accelerometer [28].

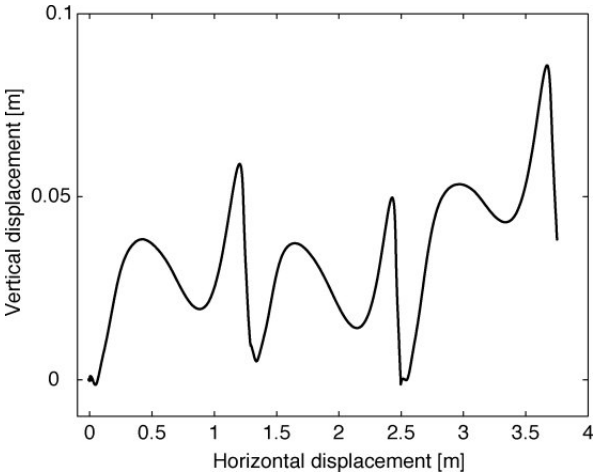

Figure 2.6: *The inertial sensor was placed on the foot in order to replace the foot switches. Indeed, the gait events detected using the foot switched are dependent on the choice of the thresholds. By combining the data from gyroscope and accelerometers of the inertial sensor is possible to reconstruct the trajectory in the sagittal plane of the foot where the sensor was placed.[30]*

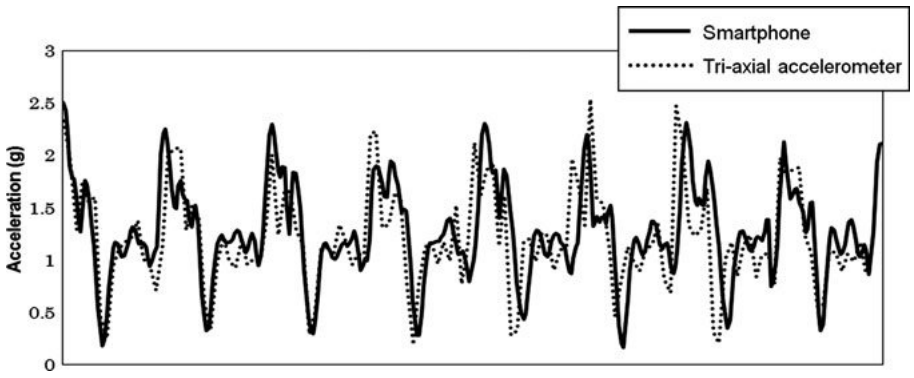

Figure 2.7: *Acceleration signals from smartphone and triaxial accelerometer (dotted line). The waveforms are quite similar and the parameters obtained from the smartphones are highly correlated with data from the triaxial accelerometer used as reference in the study [28]*

2.2.2 Fallers

Falls are one of the major hospitalization cause, above all among the elderly. Falls are often associated with fractures, fear of falling that lead to a sedentary life resulting in a reduction of quality life. Despite there is not a unique and " gold standard" definition of what Fall means [77], the risk factors for falls are several

and commonly approved: previous falls, balance impairment, muscle weakness, visual impairment,... just to cite a few [125]. The motor performance during the STS may be used as a predictor of frailty status, even if it may be influenced by somatosensory afferents, balance, and psychological status [126][8, 9]

The clinician evaluates the performance of the STS using parameters such as the time taken to complete the task, the visual examination of the movement and the number of repetitions in a known period. The task duration is an important parameter during the clinical evaluation of the fall risk or frailty assessment as fallers needed more time for completing the task [60]. Despite its relevance in the clinical practice, some studies disagreed on time as a discriminant feature for separating fallers and not fallers. For example, in Weiss et al. [38] the time difference between fallers and the control group was not significant. Doheny, Walsh[35] reported that a classifier with time duration and kinematic features had greater accuracy, sensitivity, and specificity than a classifier including the only time duration. The task duration measured with a stopwatch may be imprecise and may lack specificity, it may be used in combination with other clinical criteria, such as the Fried's criteria [127] and the UPRDS, to perform an initial screening and select those patients in which the sensorization of the STS may be appropriate.

In clinical practice,the movement fluency is helpful for evaluating the functional status of the patient but its evaluation with visual observation may limit its validity and reliability and may rely upon the experience of the observer [98]. The use of inertial sensors allows the calculation of several indices of the smoothness of the movement. One of the most common is the jerk, i.e. the third derivative of position, an index that characterizes the average rate of change of acceleration during a movement [128]. Although the jerk may be an analytical way to objectify the smoothness of the movement, it lacks a univocal definition as it depends mainly on the movement amplitude, the duration and the intervals of arrest [129]. For example, Weiss et al.[38] defined the jerk as the slope of the Antero-Posterior (AP)

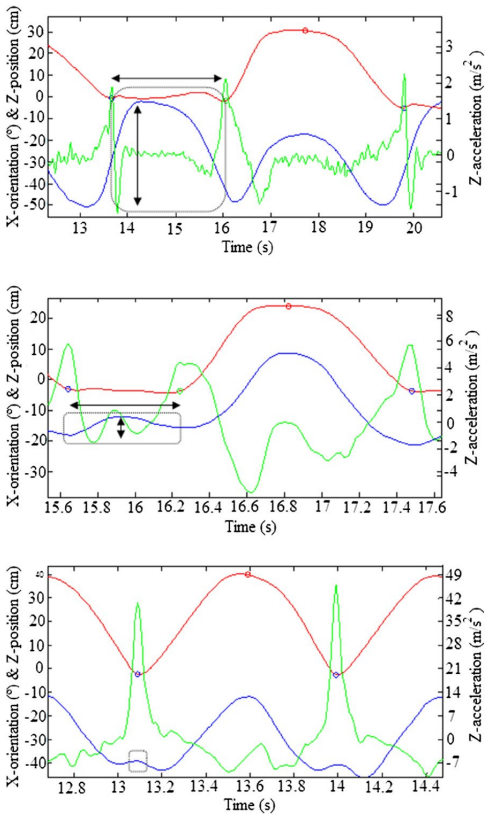

Figure 2.8: *Movement patterns of raw Inertial Signals for frail (a), pre-frail (b) and healthy subjects (c). The blue line is the X-Orientation signal, the green line is the Z acceleration, and the red line is the Z-Position signal.The circle outlines the extra forward and backward lean for more frail subjects, and the arrows feature the time duration and X-orientation range. X-Orientation is the quantification of the trunk tilt evaluated according to the trunk movement. During the Impulse phase (definition on Millor article), the frail subjects had greater X-Orientation Value, indicating that the frail subjects require extra forward and backward leaning to connect one cycle with another. During the standing and sitting, the X-Orientation value of frail subjects differed from Pre-Frail and Healthy Subjects, whereas the difference between these last two groups was not statistically different. Indeed, the frail subjects were not strong enough to produce power output for raising, so they need a more compensatory movement that the healthy subjects. The healthy subjects reached greater "minimum Z acceleration" values during standing and sitting up compared to frail and pre-frail. The minimum Z acceleration values were greater in the pre-frail subjects than in the frail. The maximum Z acceleration was statistically significant for differing the healthy Subjects from the Frail and pre-frail, but no difference was noticed between frail and pre-frail. The explanation could be that the frail subjects have less lower limb power and strength.[37]*

acceleration-time curve during the STS and reported that the fallers exhibited lower jerk compared to controls. Moreover, this parameter was more discriminant than the time duration in detecting the fallers group. In Doheny et al. [35], the jerk, defined as the first derivative of the acceleration, was similar between the groups while the addition of other kinematic features increased the discriminant validity of the classifier. In contrast, Ganea et al. [36] evaluated the smoothness plotting the norm of acceleration versus the trunk angular velocity measured around the ML axis. The quantification of the smoothness was related to the fractal dimension of the movement patterns and showed to be the most discriminant. Therefore, the jerk may constitute an interesting index to measure the smoothness of the STS, despite its additional value in increasing the specificity of an STS movement needs a shared definition and further inquiries. The postural sway is related to balance functions that are important for the fall risk assessment. The sensorization of the STS allowed the measurement of the postural sway even though they proved to not discriminate between pre-frail and healthy subjects [37]. However, in clinical practice, the adoption of two postural strategies, called ankle strategy and hip strategy, is usually assessed to evaluate the ability to maintain the body balance after a perturbation. The ankle strategy repositions the center of mass using an inverted pendulum that moves around the ankle joint, and it is usually lost in the elderly. The hip strategy is based on a two-segment inverted pendulum moving at the hip joint, and it is used when the perturbation is stronger. The STS can be seen as a merging of the two strategies: the hip strategy is used during the rising phase of the movement, while the ankle strategy starts when the person has stood up. However, the sensorization of the STS to measure the goodness of the ankle and hip strategies requires some consideration on the number of sensors and their placement over the body. Positioning one sensor is more comfortable and portable, but its location on the body limits the quantity of information. For example, a sensor located on the sternum could give information about trunk leaning in the

space, but it is unable to detect trunk movements with respect to the lower limbs, that could be components of the postural strategies. Similarly, in many studies, the sensor was positioned over the lumbar spine that, given its high mobility, impeded to study precisely the postural strategies [130]. Therefore, the application of two or more sensors could track not only the body oscillations, that have been proven less effective in detecting the fallers [37], but also could measure whether features characterizing the above mentioned postural strategies are suitable predictors of fall risk.

Finally, we could highlight two limitations of using inertial sensors, accelerometers, and gyroscopes:

1. the discrimination between faller and non-fallers depend on the data processing and, consequently, on outcome features;

2. which sensor placement provide the most important features.

Chapter 3

Sit To Stand Phases Detection

3.1 General Overview

Among all daily life activity, the STS is the most crucial one. It is considered the prerequisite of walking and it is strictly connected to functional independence[131]. The STS is a complex movement and one of the most mechanical demanding [53]. Neurodegenerative diseases, pathologies and the process of ageing make it harder. Indeed, it is commonly used as an indicator of overall functioning and balance performing; as a predictor of fall risk and to assess lower extremity strength and balance [13, 62, 132]. In the clinical practice, the main evaluation parameter is the duration of the performance: prolonged STS movement duration could lead most likely to fall [59, 60, 61]. The visual analysis of the movement helps the caregiver to assess the status of subjects. It is a qualitative analysis and often depends on the caregiver experience and sensitivity. In previous works, the camera-based system and force plates allowed the objective quantification: the analysis of the biomechanics of the movement. This instrumentation is expensive, and the analysis can

be carried out outside the laboratory environment. The inertial sensors, instead, are lightweight and portable; less expensive. They have been used in the daily life activity recognition [133], gait analysis [28, 30, 119, 120, 118] and falls detection [22, 35, 36, 37, 38].

The purpose of this preliminary study is to characterize the dynamic events occurring as rising from a chair. The study of the distinct events-or phases- of the STS movement would result in a most effective description about:

- the contribution of each single body element involved in the movement;
- the kinematic and kinetic variables during the movement and their changes related to specific disease;
- the pain point that could lead to movement failure.

[15, 16]

Previously, the identification of STS events or phases has been performed applying specific thresholds to joint angles, velocity changes, torques o and momentum. The high variability of the movement both between and within individuals makes it difficult to find common thresholds[15]. Although the application of thresholds could lead to misleading results, it has been shown that the trunk angles and orientation can be used for the phases detection [134, 135]. Van Lummel et al. [134] analyzed the variation of trunk angle (ϕ) to detect the STS phases. The figure 3.1 shows the sine of the trunk angle resulted from the application of the wavelet transform. The phases have been detected by the dips and slope changes of the signal [134]. This methodology is efficient, but cannot be applied in real time.

We used the Machine Learning (ML) or data mining to overcome both the threshold limitation and the real-time phase detection.

Machine Learning is the process to generate a set of rules from real data [39]. There are many application in medical field such as diagnosis of a disease [40, 41, 42], prediction of disease [43, 44, 45]. The advantages of the use of ML are: the possibility

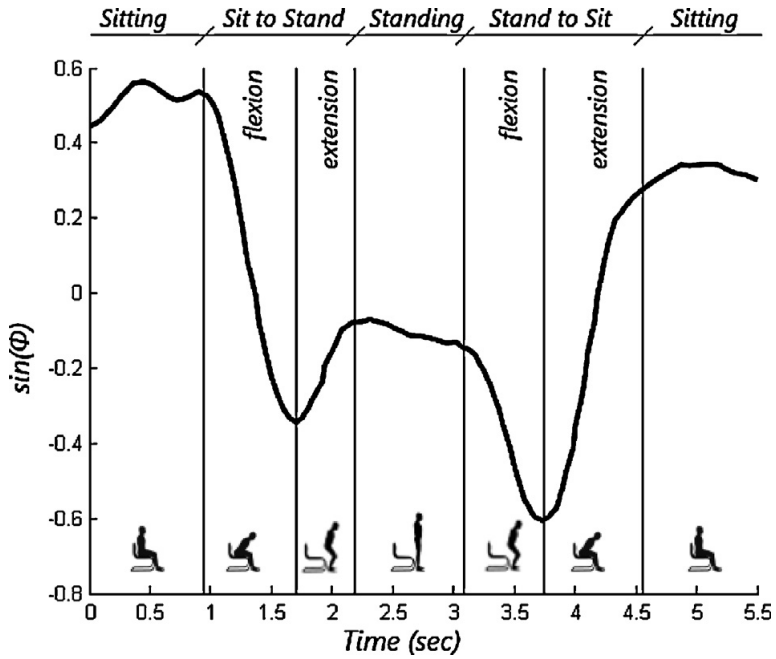

Figure 3.1: *The figure shows the wavelet transform of the sine of the trunk angle,* $dw\_sin(\phi)$. *Wavelet transform has been used to remove the drift and any noise. The vertical lines identify the STS phases. They have been detected by analyzing the dips of the graph [134]*

to the constantly expanding healthcare databases for predicting disease at early stages [44]; or to simplify the diagnosis process [42]. It is very versatile, and have been used in many clinical field such as human activity recognition [46],gait analysis or fall detection. We reported some examples below.
ML has been used in the gait analysis for automated recognition of gait pattern changes due ageing [47]; gait event detection for the functional electrical stimulation [48]. ML allowed researchers to identify the falls, but also to the classify the type of falls [49].

In this study, we trained two classifier models and compared their performances. The inertial sensors data were used to train the classifiers. The preprocessing phase included the STS phases identification based on the definition provided by [16]. The phases' starting and ending points were detected by the identification of some key

events.

3.2 Material and Methods

3.2.1 Data acquisition

Twenty-seven healthy subjects (13 females, 24.37 ± 3.32 years old) participated in the study. Eight wireless inertial sensors (Xsens Technologies BV, Enschede, The Netherlands) were placed on: sternum, back (L4-L5), right and left thigh, tibia and ankle.

The licensed radio data receiver Awinda drove the communication and synchronization between the sensors and enabled the communication with the PC. The MT Manager (Xsens licensed software) acquired the sensors data collected by the radio station. The software automatically set the frequency sampling at 50 Hz.

The participants sit on a height-adjustable chair shown in figure 3.2. An electric switch placed on the chair detected the seat on and the seat off. The chair height was adjusted for each subject so that the knee angle was 90°when the exercise started.

The Data Acquisition device (DAQ) NIUSB 6343 (National Instruments, Austin, TX, USA) recorded the chair's switch electric signal at 1024 Hz. Also, it sent a square wave signal that started and enabled the Xsens data acquisition. The signal frequency was set to 1024 Hz. It was stored with the chair's switch and used for the synchronization between the devices. The data from the DAQ were acquired using a custom script in MATLAB 2016a (MathWorks, Natick, MA, USA).

The MATLAB software has been used for data processing and classifier training. During the exercises, the participants were asked to keep their arms crossed at the chest. They were asked to stand and sit back down for 11 times. The exercises were recorded separately. An operator gave the command for standing up.

Figure 3.2: *The height adjustable chair used in the experiment.*

Two webcams filmed the exercises. An expert clinician watched the video recordings and discarded the tasks performed wrongly.

3.2.2 Signal Processing

Data Processing

The figure 3.3 shows the processing data workflow.

1. *Signal Phases Segmentation.* The signals from each inertial sensor were split into phases. The phases were defined as:

    - Resting: The subjects sit on the chair before or after the movement.
    - Trunk Leaning (TL): The start of the STS movement. This phase began with the flexion of the trunk and ended just before the buttocks lifted from the seat of the chair.
    - Standing (SD): From the seat off to the full extension of hips, knees and, trunk (quiet posture standing)
    - Balance (BL): The subjects reached the quiet posture standing, it ended when they started to sit;

- Sitting (ST): This phase began with the start of the descending movement. It ended when the buttocks sit down on the chair [16].

The phases were delimited by specific *key events*. Refer to 3.2.2 for more details.

2. *Phases split in epochs.* The classifier models should be able to recognize a specific phase using features computed on small samples. Indeed, the next step of this work is to use the trained classifier in real time phases detection. So, each phase was split in not overlapping time-windows(epochs). We decided to use two-time windows corresponding to 0.1 s and 0.2 s [136] of the sensors signal to compare the performances of different datasets. We did not apply the time normalization.

3. *Features Extraction*. The Mt Manager software preprocessed the Xsens raw data. The software applied a fusion filter that estimated acceleration and orientation. For this analysis, we used the accelerometer signal and the Euler Angles[1] resulted from the MT Manager preprocessing. The features were computed on six signals for each sensor: the acceleration signals along the axis and the three Euler angles. The features analyzed were: mean, standard deviation, RMS, Max and Min, COV,and first derivative. The features were computed on the epochs for each sensor.

4. *Database Building.* All epochs of all recordings of all subjects were gathered all together to construct the Classifier Database. We can imagine the database as a matrix: the rows correspond to the epoch, while the columns to the features. The last column contains the labels relative to each epoch (i.e. the

[1]Euler Angles: They are used to describe the orientation of a rigid body with respect to a reference system [137].

label expressed the membership of each epoch to a specific phase). The table 3.2 is an example of the database.

5. *Classifier Training.* We compared the performance of two classifiers for each dataset:

   - K-Nearest Neighbour (KNN)
   - Support Vector Machine

For further details see 3.2.3.

Phases segmentation

A phase is a piece of signal between two key events. We identified five key events: Start of the STS movement, Seat Off, End of Sit-Stand, Start of Stand-Sit, and Seat On. Any piece of signal before the *Start Of the STS Movement* and after the *Seat On* has been included in the *Rest* phase.

Phases	Starting Point	Ending Point
Trunk Leaning	Start Of the STS Movement	Seat Off
Standing	Seat Off	End of Sit-Stand
Balance	End of Sit-Stand	Start of Stand-Sit
Sitting	Start of Stand-Sit	Seat On

Table 3.1: *The phases were identified using six key events. The table shows the starting and ending point of each phase*

Start Of the STS Movement The first event of the STS is the trunk flexion [16]. The start of the movement has been identified using the AP acceleration signal recorded by the sensor placed on the sternum (corresponding to the Z-axis sensor). The signal was divided into epochs of 0.1 s and 0.2 s accordingly to the Dataset. The standard deviation (SD) has been calculated for each signal epoch. The movement began when the SD increased five times the baseline. The baseline

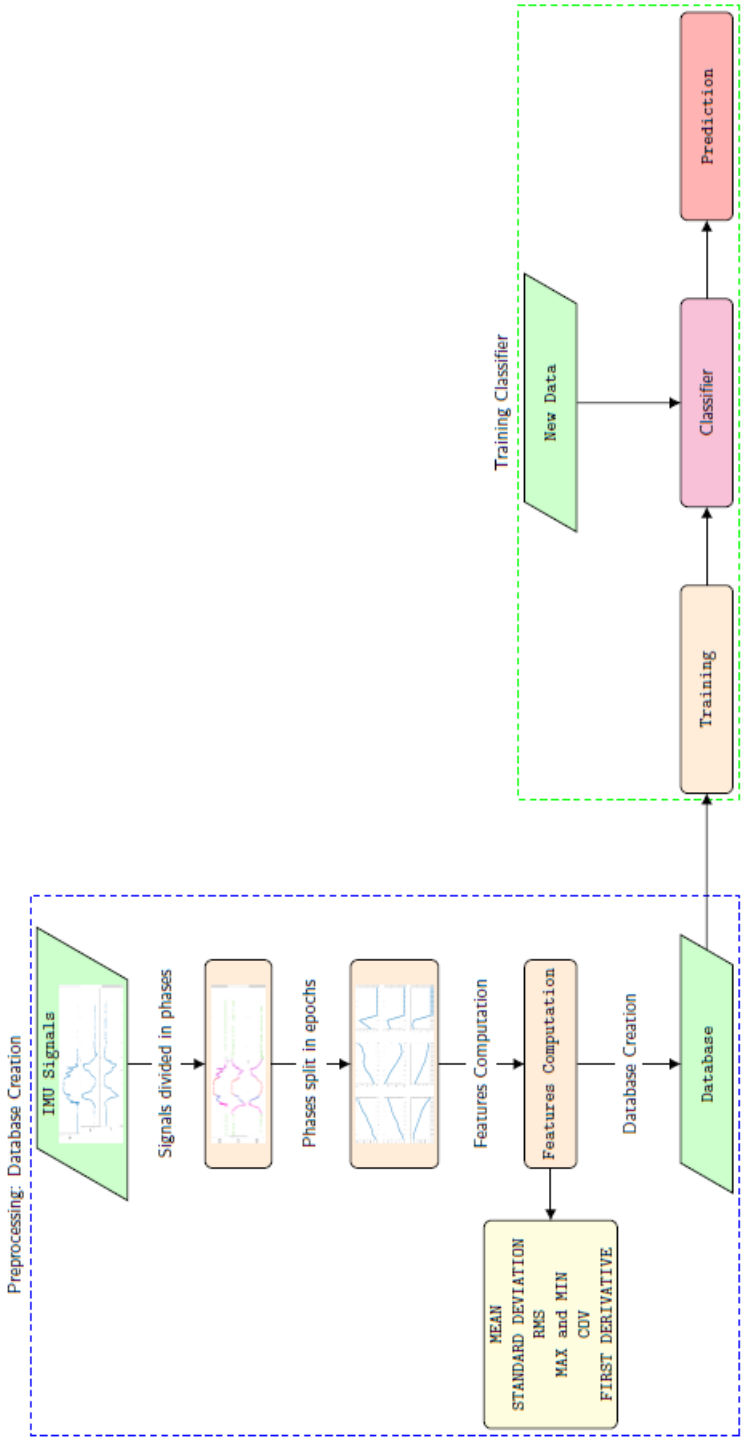

Figure 3.3: *The figure shows the inertial sensors signals processing. We evaluated six signals from the inertial sensors: the accelerations along the three axes and the Euler angles (pitch, yaw and roll). The signals were divided into phases (Resting, Trunk leaning, Standing, Balance, Sitting). Then, they were split into epochs. Temporal features were computed on each epoch- mean, standard deviation, RMS, Max and Min, COV and first derivative. The features were gathered to build up the database that was used to train the classifiers.*

is the absolute value of the mean of the standard deviation computed on the first three signal epochs.

Seat Off and Seat On Detection An electric switch on the chair detected the *Seat Off* (when the buttocks left the chair) and the *Seat On* (when the buttocks reached the chair again). The switch signal was acquired by the DAQ Device(National Instrument, Austin, Texas, US) at 1024 Hz. It has been re-sampled at 50 Hz, the same sampling frequency of the inertial sensors. The *Start of The Movement* and *Seat On* delimited the Trunk Leaning phase.

End of standing and start of sitting The events were identified using the femoral acceleration, as described in [35]. Doheny et al. [35] used the femoral acceleration to isolate the STS phases during the FTSTS. The fig 3.4 shows the triaxial accelerometers signal recorded and processed by the above cited authors. Initially, they identified the minimum acceleration over the total FTSTS, A_{min}. Successively, they used it to locate the minimum acceleration for each STS phase, referring them as mid-stand-points(A_{ms}). Empirical thresholds were used to establish the phases of STS:

- Start of Sit-stand transition: the signal amplitude fell below 0.2 A_{ms}
- End of Sit-stand transition: the signal amplitude fell below 0.8 A_{ms}
- Start of Stand-sit transition: the signal amplitude increased above 0.8 A_{ms}
- End of Stand-Sit transition: the signal amplitude increased above 0.2A_{ms}

The figure 3.5 shows the vertical acceleration (corresponding to X-axis) recorded by the sensors we used. The accelerometers data were low pass filtered at 5 Hz using a 4th order Butterworth filter.
The positive direction of the vertical axis is opposite compared to the positive direction of the sensor used in the reference study [35]. We made changes to the

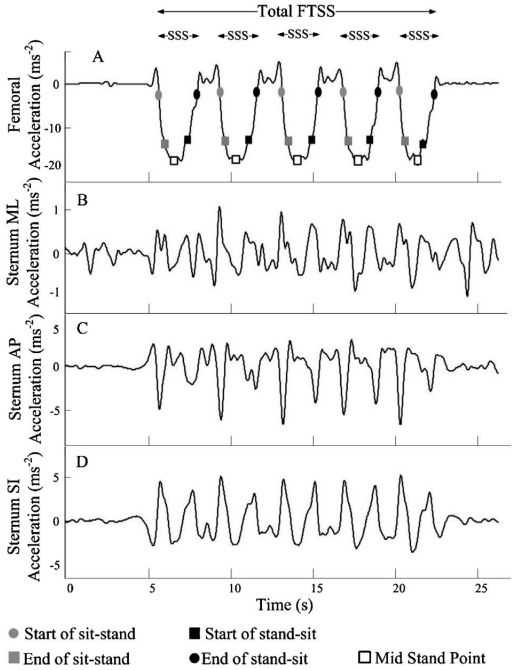

Figure 3.4: *Triaxial Accelerometers signals recorded during an FTSTS task. A) Vertical acceleration, accelerometer on right thigh. B) Mediolateral acceleration, accelerometer on the sternum. C) Anteroposterior acceleration, accelerometer on sternum D) Vertical acceleration, accelerometer on the sternum. The sit-stand-sit phased of the FTSTS were detected using the femoral acceleration. The Mid Stand Points were defined as the minimum acceleration during each phase. The mid standpoints with acceleration less than 0.8 of the minimum acceleration over all the performance were considered successful SSS attempts. The start and end of sit-stand and stand-sit were detected using thresholds empirically [35].*

algorithm accordingly to the sensors axis direction. Instead of the minimum acceleration, we individuated the Maximum Acceleration, A_{Max}. Since we recorded a single STS transition A_{ms} and A_{Max} coincided. The STS events were defined as follows:

- Start of Sit-Stand transition: the signal amplitude increased above 0.2 A_{ms}
- End of Sit-Stand transition: the signal amplitude increased above 0.8 A_{ms}
- Start of Stand-Sit transition:the signal amplitude fell below 0.8 A_{ms}
- End of Stand-Sit transition: the signal amplitude fell below $0.2A_{ms}$

We selected for our purposes only the *End of Sit-Stand* (used as end of the *Standing* phase and start of *Balance* phase) and *Start of Stand-Sit* used as end of the *Balance* phase and start of *Sitting* phase).

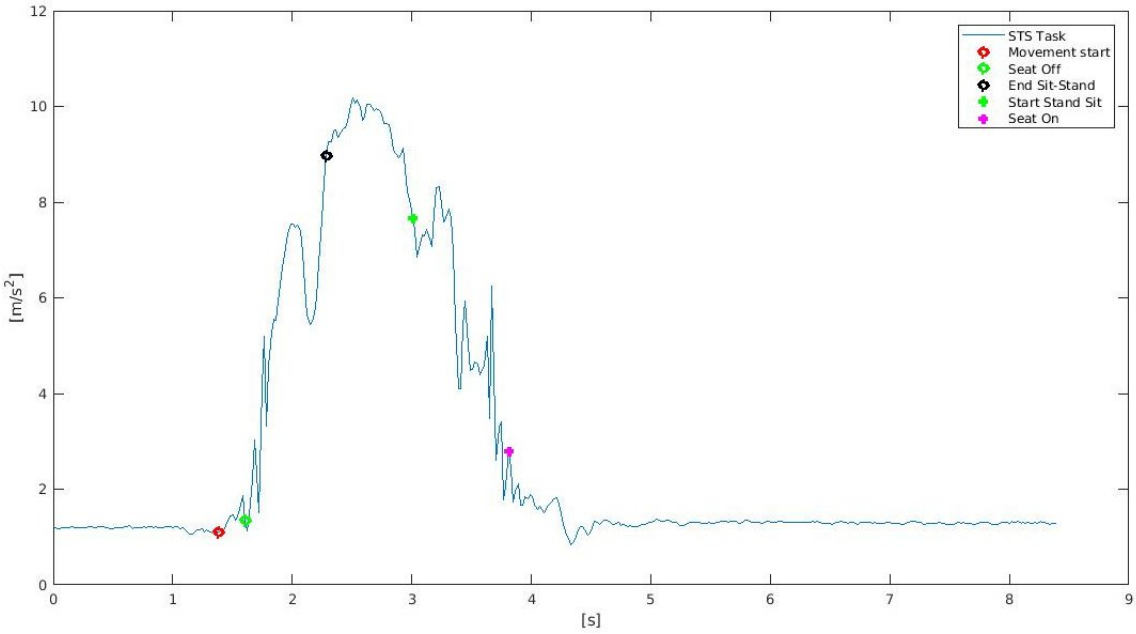

Figure 3.5: *Vertical acceleration recorded by the sensor placed on the left thigh. The X-Axis of the sensor is aligned to the femur axis and it has the same direction of the gravity. The key events reported in the picture. Red Circle: Start of the movement, green circle : Seat Off, black circle: End of Sit To Stand, green cross: Start of Stand Sit, magenta cross: Seat On.*

3.2.3 Classifier

Dataset

This report is an exploratory study aimed to build up a system able to detect the STS phases in real time. The fundamental issues related to the potential real-time Classifier were:

- the number of sample or time frame/epochs to compute the features;
- the number of inertial sensors;

To compare the classifier performances on epochs of different duration, we selected 0.1 s and 0.2 s as epoch duration. While to compare the classifier performances on a various number of inertial sensors, we used dataset including all sensors or some of them.
Hence, the datasets generated were four:

- $Dataset_1$: Epochs of 0.1 s, all inertial sensors included
- $Dataset_2$: Epochs of 0.2 s, inertial sensors on the chest, left and right thigh included
- $Dataset_3$: Epochs of 0.2 s, all inertial sensors included
- $Dataset_4$: Epochs of 0.1 s, inertial sensors on the chest, left and right thigh included

The wearability of the system could improve by reducing the number of sensors. As described in chapter 2, the sensor body placement could limit the quantity of the information. We selected sensors on the right and left thighs and chest as sensors subset. The clinical definition of the beginning of the STS coincides with the beginning of the trunk leaning. The sensor located on the chest measures the trunk acceleration and orienting allowing us to determine the beginning of the trunk

flexion (see 3.2.2), but it is unable to detect trunk movements with respect to the lower limbs, that could be components of the postural strategies [130].
Moreover, the starting and ending of the *Balance* phase have been detected by the thigh acceleration(see 3.2.2). To monitor potential limb impairment during the STS task, we included in the subset bot the sensors placed on the thigh. Elderly could suffer from Weight Bearing Asymmetry (WBA)[2] as a result of a stroke [139], arthroplasty [140] or muscle weakness. The WBA could contribute to falling during STS task [141, 142].
The datasets are matrices, in particular:

- each row corresponded to an epoch;
- each column corresponded to features;
- The last column contained the label for each epoch.

The table 3.2 is an example of how a dataset looks like.

	Features_1	Feature_2	Feature...	Features...	Labels
epoch_1					*C1*
epoch_2					*C1*
epoch_3					*TL*
epoch_4					...
epoch...					
epoch_m					*C1*

Table 3.2: *Example of a dataset template*

[2]Weight Bearing Asymmetry: It occurs when the body weight is not equally distributed between the legs. For example, as a result of a stroke or Total Knee Arthroplasty, patients load more the unaffected leg [138]

Model Evaluation

The Supervised Machine Learning aims to infer a function "f" able to make predictions based on input data. The system infers the function of learning from the data, i.e. the system learns general concepts from a specific example. The general concepts are used to make a prediction based on data unseen by the system. This process is called "Training." The goal of the Training is to find the best fit in order to maximize the predictions on the new data points [143]. If the system is too well trained, the noise will be memorized as data points by the system. This phenomenon is called *Overfitting* and it impacts negatively the performances of the model [143, 144]. The overfitting can be avoided by evaluating the performances of the model during the Training and adjusting the model parameters accordingly. The datasets were split into the Training set, from which the Validation set was extracted, and the Test Set in order to evaluate the model.
Beore to continue, we give some definitions:

- **Training Dataset**: The sample of data used to fit the model.
- **Validation Dataset**: The sample of data used to provide an unbiased evaluation of a model fit on the training dataset while tuning model hyperparameters. The evaluation becomes more biased as a skill on the validation dataset is incorporated into the model configuration. The validation set is used to evaluate a given model, but this is for frequent evaluation.
- **Test Dataset**: The sample of data used to provide an unbiased evaluation of a final model fit on the training dataset. The Test Set provides the gold standard used to evaluate the model. It is only used once a model is completely trained(using the train and validation sets). The test set is what is used to evaluate competing models. Usually, the validation set is used as the test set, but it is not good practice. The test set is generally well curated. It contains carefully sampled data that spans the various classes that the model would

face when used in the real world.

- **Hyperparameters**: parameters that have to be set/adjusted during the Training.

[144, 145]
The dataset was initially divided into the Training set and Test set. The Validation Set was extracted from the Training Set. As validation models, we compared K-Fold Cross-validation and Leaving-One-Subject-Out methods.

Validation model: K-Fold vs Leaving-One-Subject-Out

- **K-Fold Cross Validation** Cross-validation is a resampling procedure used to evaluate machine learning models on a limited data sample. The K-Fold Cross Validation consists of dividing the set of observation into k groups, or folds, of equal size. Iteratively, each fold is treated as a validation set. The Classifier is trained on the $k-1$ folds. The mean square error is computed on the hold-out observation. At the end of the iterations, the process resulted in k estimation of the mean square error. The validation set error rate is obtained by averaging the k mean square error [145]. The hyperparameters were automatically selected by the built-in functions of MatLab. The resulting dataset was split as follow:

  - Test set: For each subject, we selected the last sit to stand performed. These are excluded from the training set.
  - Training set: all the STS tests performed by subjects fewer ones included in the Test set.
  - Validation set: The validation set was extracted using the Classification Learner MatLab built-in functions. The hyperparameters tuning was completely automatic.

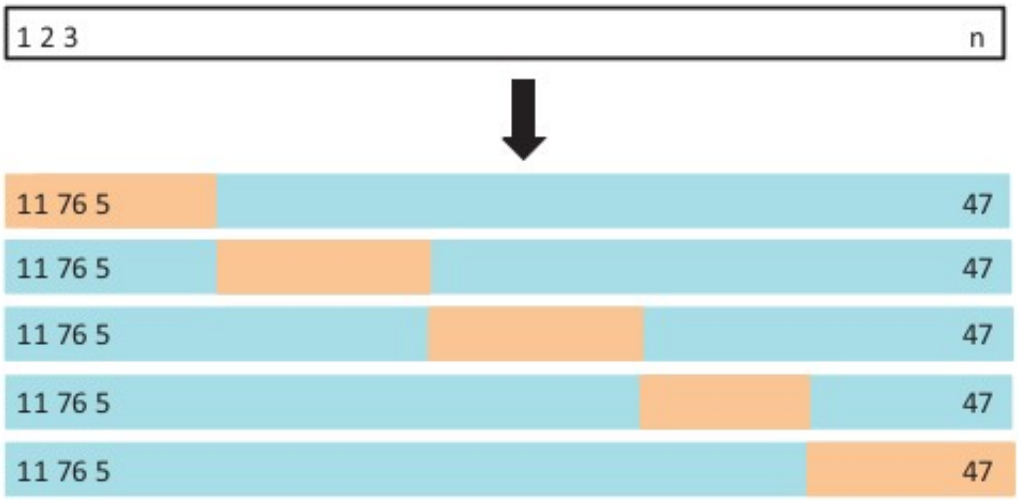

Figure 3.6: *A schematic display about 5-Cross Validation Model. The training set containing n observation is divided into k (five), not overlapping sets- folds- of equal size. The Classifier is trained k times, each time with a fold is used as a validation set and the remainder as the Training Set. The estimated error is the mean of the k mean square errors resulted at the end of the iterations [145].*

- **Leave One Subject out**(LOSO) This methodology consists of "*leaving out*" the data of one subject from the sample used for validation and training [146]. The dataset was split in the following way:

  – The Test set included all the STS recordings performed by one single subject.

  – The Training set included the remaining data, i.e. the exercises performed by all subjects less the subjects included in the Test set.

  – The Validation Set included all the STS tasks executed by one of the subjects included in the Training set.

  The splitting procedure was repeated n times: all the subjects were included in the Test set and Validation set.
  For each time, the mean error on the validation set was calculated. At the

end of all iterations, the loss curves were plotted. The hyperparameters corresponding to minimum errors were chosen. The chosen hyperparameters were used to train the best Classifier and for computing the accuracy of it on the Test Set. Accordingly to the classifier model, we manually tuned some hyperparameters.

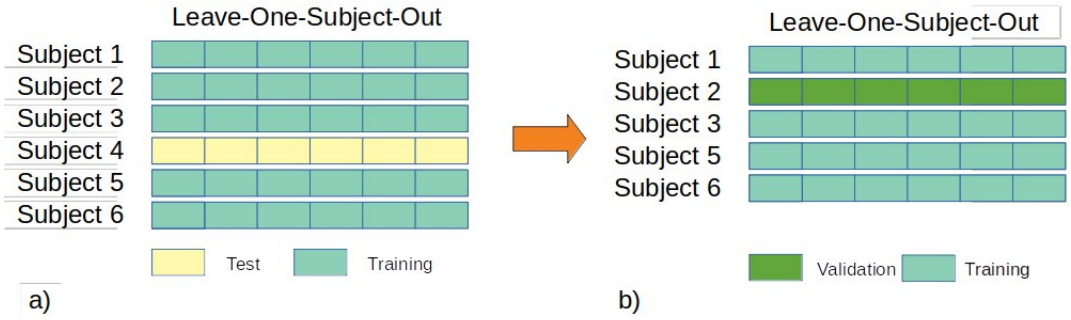

Figure 3.7: *a)Data is split into Training (blue), and Test (pink) sets to evaluate the performance of machine learning algorithms. The LOSO uses as Training set the data of one subject. b) The remaining data were split into Training (blue) and Validation (green). The data from one subject were added as the Validation Set. The procedure was repeated n times. Iteratively, one by one, all subjects were included in the Test Set and Validation Set.*

Metrics

The Classifier is evaluated by different performance metrics. We compared the classifiers performances using the confusion matrix and the F1 score.

– **Confusion matrix**: it is a table that summarizes information about actual values and predicted classification. The table 3.3 reports an example of a binary classification[3] matrix. The actual classifications are the rows, and the predicted ones are the columns [147].

[3]**Binary Classification:** the elements of a given dataset belong to only two classes.

Table 3.3: *Example of binary confusion matrix*

		Predicted		
		Positive	Negative	Total
Actual	Positive	TP	FN	$TP + FN$
	Negative	FP	TN	$FP + TN$
	Total	$TP + FP$	$FN + TP$	N

* **True Positive (TP)**: True positives were the cases when the actual class of the data point was 1 (True), and the predicted is also 1 (True) (The epochs have been correctly labelled as "x").
* **False Positive (FP)**: False positives were the cases when the actual class of the data point was 0 (False), and the predicted is 1 (True). False is because the model has mispredicted, and positive because the class predicted was a positive one (epochs have bee incorrectly labelled as "x" since they belong to the class "y").
* **False Negative (FN)**: False negatives were the cases when the actual class of the data point was 1 (True), and the predicted is 0 (False). False is because the model has mispredicted and negative because the class predicted was a negative one (epochs have been incorrectly labelled as "y," but they belong to class "x").
* **True Negative (TN)**: True negatives were the cases when the actual class of the data point was 0 (False), and the predicted is also 0 (False) (epochs have been correctly labelled as not belonging to the class "x").

Since there are more than two potential classes, this study addressed a multi-class classification task. Each sample is assigned to one and only one class. The confusion matrix results will be shown as in the table example 3.4.

The metrics for each class reported in the confusion matrix are :

* Accuracy: It measures how well the test predicts the true positive and

		Predicted					
		C1	C2	C3	C4	C5	
Actual	C1	AccC1	MisClass	MisClass	MisClass	MisClass	SensC1
	C2	MisClass	AccC2	MisClass	MisClass	MisClas	SensC2
	C3	MisClass	MisClass	AccC3	MisClass	MisClass	SensC3
	C4	MisClass	MisClass	MisClas	AccC4	MisClass	SensC4
	C5	MisClass	MisClass	MisClass	MisClass	AccC5	SensC5
		PrecC1	PrecC2	PrecC3	PrecC4	PrecC5	OverallAcc

Table 3.4: *Multi class confusion matrix template used in this study. The green cells contains the accuracy for each class (AccClass). The cyan cell the overall accuracy(OverallAcc). The last column contains the Sensitivity computed for each class(SensC), while last row contains the Precision computed for each class (PrecC). The cells MisClass are the fraction of the misclassified observation on the total of the observations.*

true negative observations.

$$Accuracy = \frac{TP + TN}{TP + TN + FP + FN} \tag{3.1}$$

* Precision: it's the fraction of the true positive observation over the retrieved observations.[4]. It measures how often the prediction is correct.

$$Precision = \frac{TP}{TP + FP} \tag{3.2}$$

* Sensitivity or Recall: it measures the proportion of the observation correctly classified over the total amount of relevant observations[5] .It measures how well the test predicts one category.

$$Sensitivity = \frac{TP}{TP + FN} \tag{3.3}$$

* Misclassified observation: the fraction of the misclassified observation(the number of observation in cells that not lie in matrix diagonal)on the total of the observations.

[4]**Retrieved Observations** The observation classified as positives -belongig to a specific class

[5]**Relevant Observations** all samples that should have been identified as positive

[148]

– F1 Score In statistical analysis, the F1 score (also F-score or F-measure) is a measure of a test's accuracy. It considers both the precision p and the recall r of the Test to compute the score: it is a comparison indicator between Precision and Recall. The F1 score is the harmonic average of the precision and recall, where an F1 score reaches its best value at 1 (perfect precision and recall) and worst at 0.

$$F1 = 2 * \frac{Precision * Recall}{Precision + Recall} \tag{3.4}$$

Classifier Models

Different classifiers perform differently, based on the application and datasets [136]. The study compared the performances of two different supervised classifiers models[6].

– K-nearest neighbour

– Support Vector Machine

All the above-cited classifiers are defined as non-parametric machine learning model: the model structure determined from the dataset. It means that there are not assumption about the form of the mapping function [144].

K-Nearest Neighbours

The K-Nearest Neighbours (KNN) algorithm is a non-parametric method used for classification and regression [7]. The principle behind the nearest neighbour

[6]In supervised learning, the class labels in the dataset are known

[7]The predictive models approximate a mapping function (f) from input variables (X) to an output variable (y).

classification consists in finding a predefined number, i.e. the k- of training samples closest in the distance to a new sample, which has to be classified [149]. These Neighbours will define the label of the new sample. The KNN classifiers assign the test sample(the observation to classify/label) to the majority class among the k nearest neighbours. The k neighbours can be fixed, or they have to be iteratively modified. The classifiers find the k nearest neighbours computing the distance between the test sample and the training set [150]. The distance can, in general, be any metric measure: standard Euclidean distance is the most common choice. Neighbours-based methods are known as non-generalizing machine learning methods since they "remember" all of its training data. Classification can be computed by a majority vote of the nearest Neighbours of the unknown sample.

Hyperparameters

- **Number of K neighbours**: the number varied between all numbers from 1 to 65.
- **Distance Weight**: the weight of the contribution of each of the k neighbours according to their distance to the query point. We compared:
  - "*Equal*": No weighting; the contribution of all Neighbours is the same.
  - "*Inverse*": Weight is 1/distance; the contribution of the most distant "neighbours" is lower than the nearest neighbours.

- **Distance Metrics** To classify an unknown instance represented by some feature vectors as a point in the feature space, the KNN Classifier calculates

---

– **Classification**: the output variable y is a discrete set of values (such as sunny, cloudy or rainy). The output variables are called labels or categories.

– **Regression**: the output variable y is a continuous variable, a number (such as tomorrow's temperature). The output variable is a conditional expectation of the real value of y.

[144]

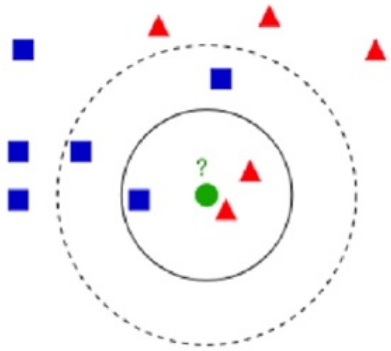

Figure 3.8: *An example of KNN classification. The solid line circle corresponds to the number of Neighbours K=3, while the dashed line circle to the number of neighbours=5. The training sample shown in this example contains only two classes: the blue square and the green triangle. The mission of the Classifier is to assign the green circle to one of those classes. The Classifier uses the distance function to find the K Neighbours to the sample. The test sample will be assigned to the class of the majority of the K-nearest Neighbours. So when K=3, the green circle is assigned to the red triangle class, while if K=5 it will be assigned to the blue square class[150].*

the distances between the point and points in the training data set. Then, it assigns the point to the class among its k nearest neighbours (where k is an integer)[151]. We compared two distance functions: Euclidean and Cosine. Given an mx n data matrix X, which is treated as mx (1-X-n) row vectors $x1, x2, ..., xm$, and an my X-n data matrix Y, which is treated as my (1-by-n) row vectors $y1, y2, ..., ym$, the various distances between the vector x_s and yt are defined as follows:

– Euclidean

$$d_{st}^2 = (x_s - y_t)(xs - t_t)' \tag{3.5}$$

– Cosine

$$d_{st} = 1 - \frac{(x_s y_t'}{\sqrt{(x_s x_s')(yty_t')}} \tag{3.6}$$

[152]

Support Vector Machine

The gaol of the support vector machine algorithm is to find a hyperplane [8] in an N-dimensional space that distinctly classifies the data point [153]. In two dimensional space, the hyperplane is a line dividing the plane into two parts were in each class lay on either side, see the figure 3.9.

Hyperparameters

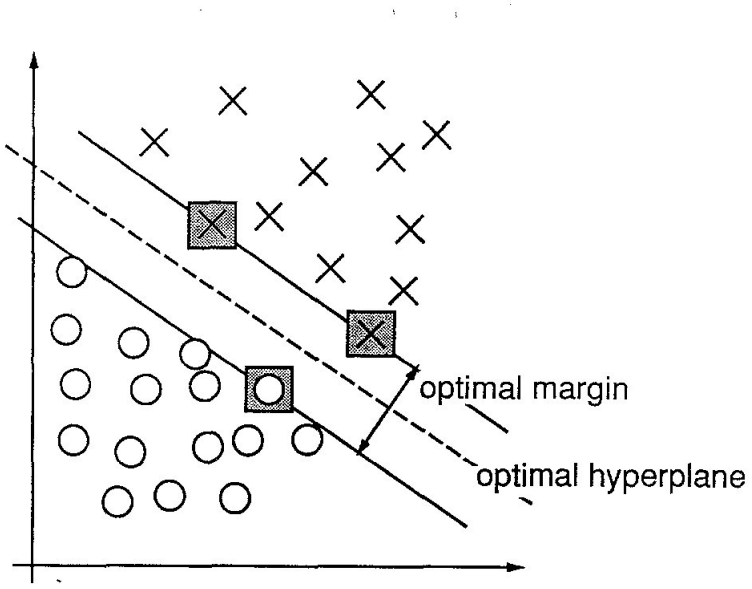

Figure 3.9: *An example of a separable problem in two dimensions. The heavy line is the maximum margin separator. The margin is the width of the area bounded by the dashed lines; it is large twice the distance from the separator to the nearest point. The support vectors, marked with gray, are the training data that determines the margin-they are the examples closest to the separator. The hyperplane is the function with the maximal margin between the vectors of two classes [144, 153].*

- **Box Constraints**: It is a parameter that controls the number of misclassified observations in the training set. It applies a cost to the misclassification.

[8] In n-dimensional space, a hyperplane is the $(n-1)$-dimensional solution set of one (homogeneous, non-trivial) linear equation: $a_1x_1 + a_2x_2 + ... + a_nx_n = 0$. An optimal hyperplane is defined as the linear decision function with the maximal margin between the vectors of the two classes [153]

The higher the box-constraint, the higher the cost of the misclassified points, leading to a more strict separation of the data [154].

3.3 Results and Discussion

The results found in this study are an exploratory step towards gaining knowledge about potential elements of a real-time phase detection system.
The main purpose of this study is to find an eligible system for real-time STS phases detection.
The STS movement has high variability both within and between subjects. It makes difficult finding and applying thresholds to detect STS phases [15]. Some solution to this problem included the use of adaptive thresholds [135] and the analysis of the slope variation of the trunk angle [134]. Both these methodologies cannot be applied in real-time, but off-line. Our methodology involves Machine Learning algorithms.

We used eight sensors to measure the movement. To increase the potential wearability of the system, we selected a subset of sensors and compared it against the complete set. We selected a subset the data from the sensors placed on the right and left thighs, and on the sternum
As shown in [22, 134, 135], one sensor placed on the back (L5) was enough to describe the trunk trajectory during the STS and to detect the STS movement phases. Due to the high lumbar spine mobility, the sensors placed on it could detect some postural strategies that elderly and neurodegenerative patients apply to prevent falls during rising from a chair [130]. Differently than [113], we did not assume that the STS movement is symmetrical. Indeed, Elderly could not equally distribute the loading between the lower limbs during the movement (Weight Bearing Asymmetry) increasing the falling risk[141, 142].

The 27 subjects performed 297 exercises. We discarded 16 exercises because:

- The exercises were performed wrongly (5) ;
- The data from the inertial sensors were missing (11);

The total dataset included 281 STS tasks. We did not apply any control autonomous quality control [155] for two main reasons:

- the complete dataset is limited to less than 300 tasks;
- use data more raw possible.

3.3.1 Phases duration

The table 3.5 reports the mean and standard deviation of the phases for all subjects. In general, accordingly to our results, the shortest phase is confirmed to be the *Trunk Leaning* phase, while the longest is the *Balance* phase. This finding differed from the results of [16], according to which the shortest phase is the *Momentum Transfer* phase, i.e. when the buttocks lifted from the seat. In our study the *Balance* phase included part of the extension phase, that Scheckman et al. [16] included in another phase. We guessed that this different phase definition could be main cause of disagreement between the studies.
While the results about the duration of the *Standing* and *Sitting* agreed with the results found by Doheny et al. [156].
The table 3.9 shows mean and standard deviation of phases duration for each subject.

Trunk Leaning [s]	Standing[s]	Balance[s]	Sitting [s]
0.486±0.317	0.574±0.237	1.166±0.662	0.865±0.352

Table 3.5: *Mean and standard deviation of phases duration*

3.3.2 DataSet and Features

This study aimed to compare datasets split in epochs of duration 0.1 s and 0.2 s and with different number of sensors. Four datasets were evaluated. The total number of features extracted is 336 for Dataset_1 and Dataset_4 (eight sensors, seven features and six signals), while the number of features for Dataset_2 and Dataset_3 is 126 (three sensors, seven features,six signals).
The table 3.6 summarizes the size of the datasets.

Dataset	N epochs (rows)	N Features (columns)
Dataset_1	32,001	336
Dataset_2	20,522	126
Dataset_3	32,001	126
Dataset_4	20,522	336

Table 3.6: *The table shows the size of the datasets evaluated in this study*

3.3.3 Model Validation

To avoid overfitting (i.e. the classifier fits too much with the data of the training set), the hyperparameters are tuned using the validation set as explained above. We compared the performances of datasets trained using the K-Fold and the LOSO validation.
The K-Fold Validation randomly splits the dataset into training set and test set. In a scenario where the aim is to generalize old and new subjects, the K-Fold validation could be misleading: both training set and test set included the observations from the same subject[157]. The LOSO technique have been introduced to reduce the bias due to the inclusion of the observation of a same subject both in training and data set [157, 158, 159].
We used the Classification Learner App of MatLab for training the classifiers using the K-Fold validation. The MatLab application automatically tuned the Hyperparameters.

We built custom scripts to train the classifier using the LOSO technique.
We coded two scripts: one for the KNN classifier, one for the SVM classifier.
The predictive inaccuracy of the models was obtained by Matlab built-in function "*loss*". The Loss function output could vary between 0 and 1. Lower loss output indicates better predictive model[160].

Leave-One-Subject-Out:KNN Classifiers The figures below display the loss curves of KNN Classifiers for each dataset varying the number of neighbours k, distance weight and metrics. The predictive inaccuracy of all models is less than 10%.
As shown by the table 3.7, the model EE is the more affected one by varying the number of the K neighbours (distance weight: Equal, distance metric: Euclidean). Indeed, the ratio between the minimum and the maximum points of the loss curve is around 80% for all datasets. However, considering the KNN classifier EE, the worst performance is obtained for the first dataset (all sensors, epochs of 0.1 s),the number of neighbours is 29 and the predictive inaccuracy is 8.1%. Still, less than 10%.

	CE[%]	CI[%]	EE [%]	EI[%]
Dataset_1	66	17	76	46
Dataset_2	76	50	83	24
Dataset_3	72	58	80	15
Dataset_4	74	7,3	81	12

Table 3.7: *Ratio between the minimum and maximum values of the Loss Curve for KNN classifiers: CE=Cosine, Equal; CI=Cosine, Inverse; EE=Euclidean, Equal; EI=Euclidean, Inverse*

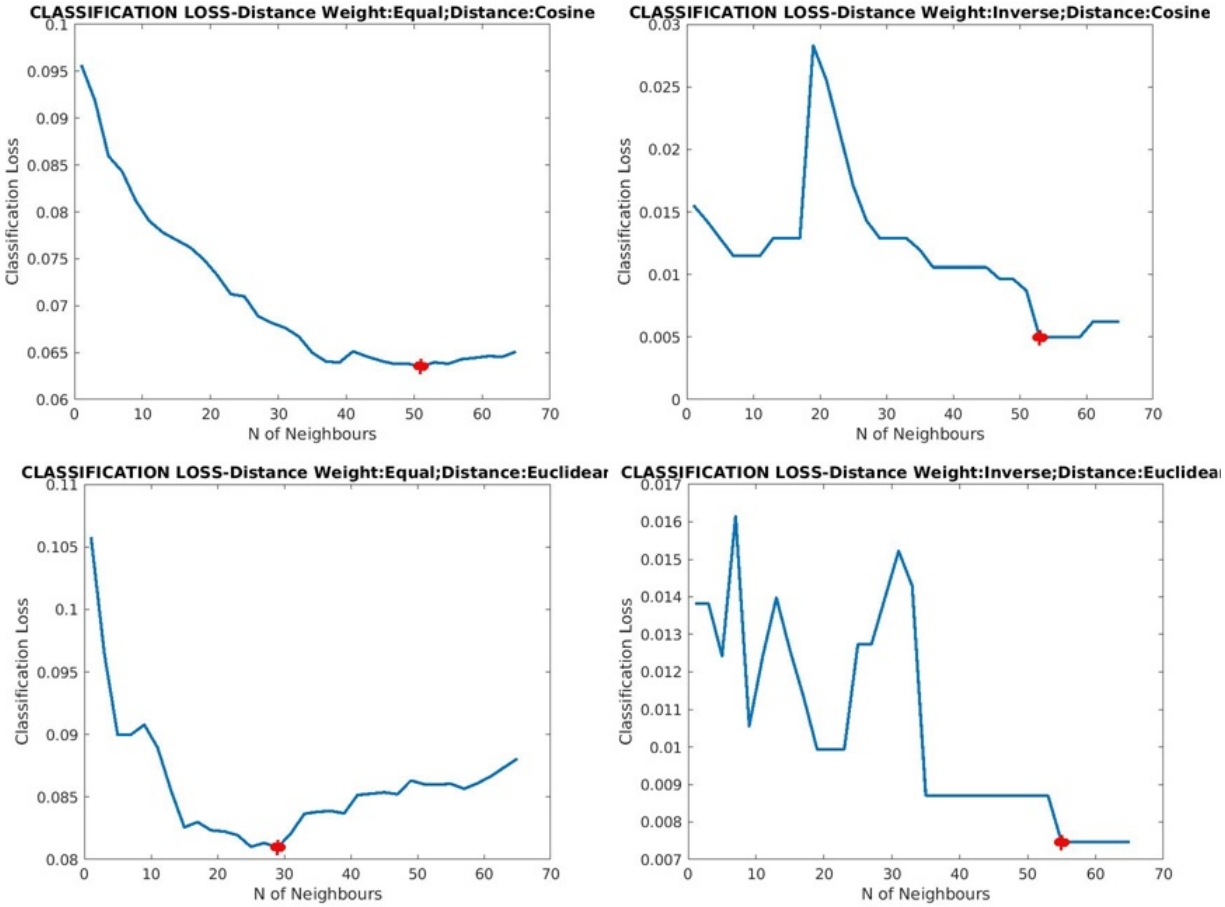

Figure 3.10: *The Loss curve is used for displaying the predictive inaccuracy of the model.Dataset_1 :a) k=51, L=0.0635.b)k=53, L=0.0050 c)k=29, L=0.0810 d)k=55, L=0.075*

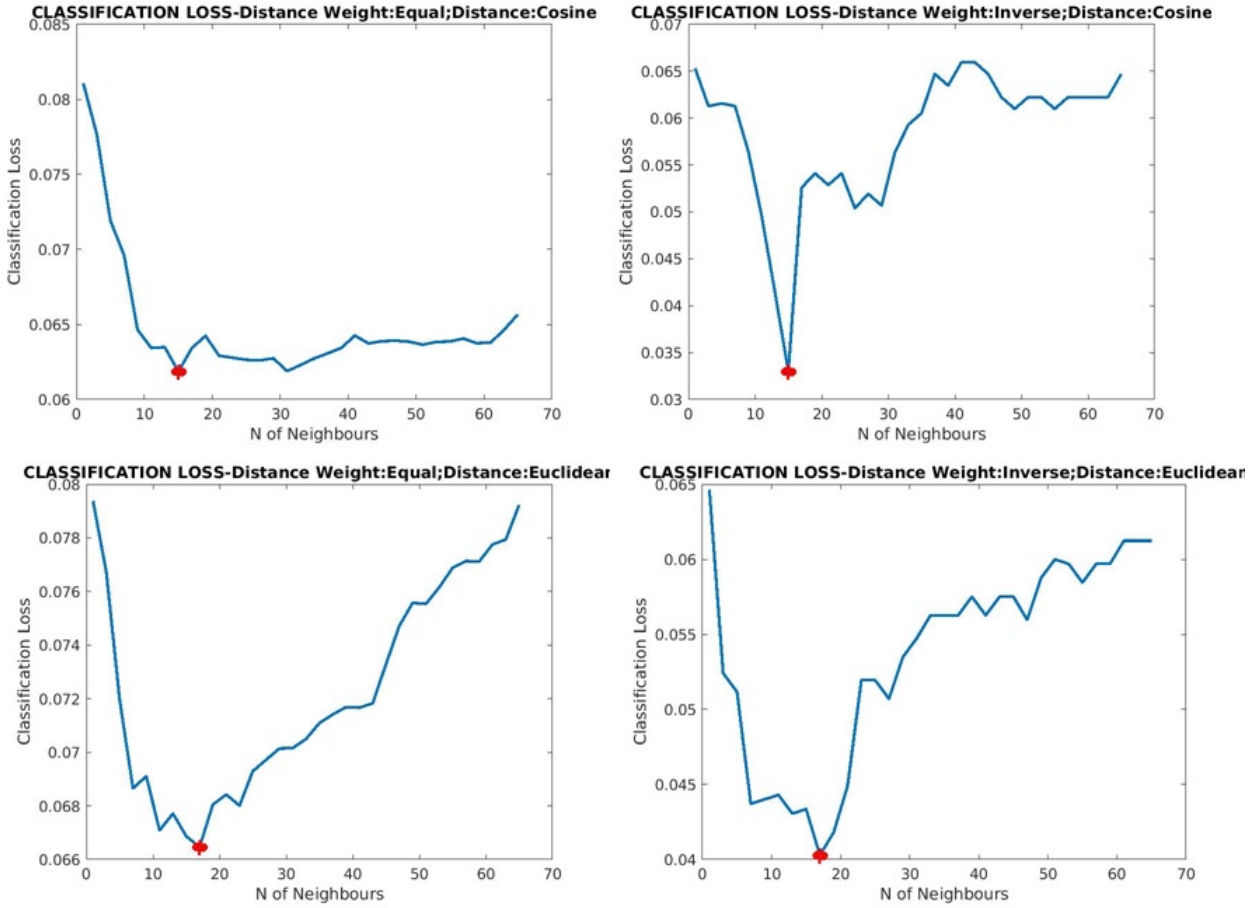

Figure 3.11: *The Loss curve is used for displaying the predictive inaccuracy of the model.Dataset_2 a) k=15, L=0.0619 b)k=15, L=0.0050 c)k=17, L=0.065 d)k=55, L=0.04*

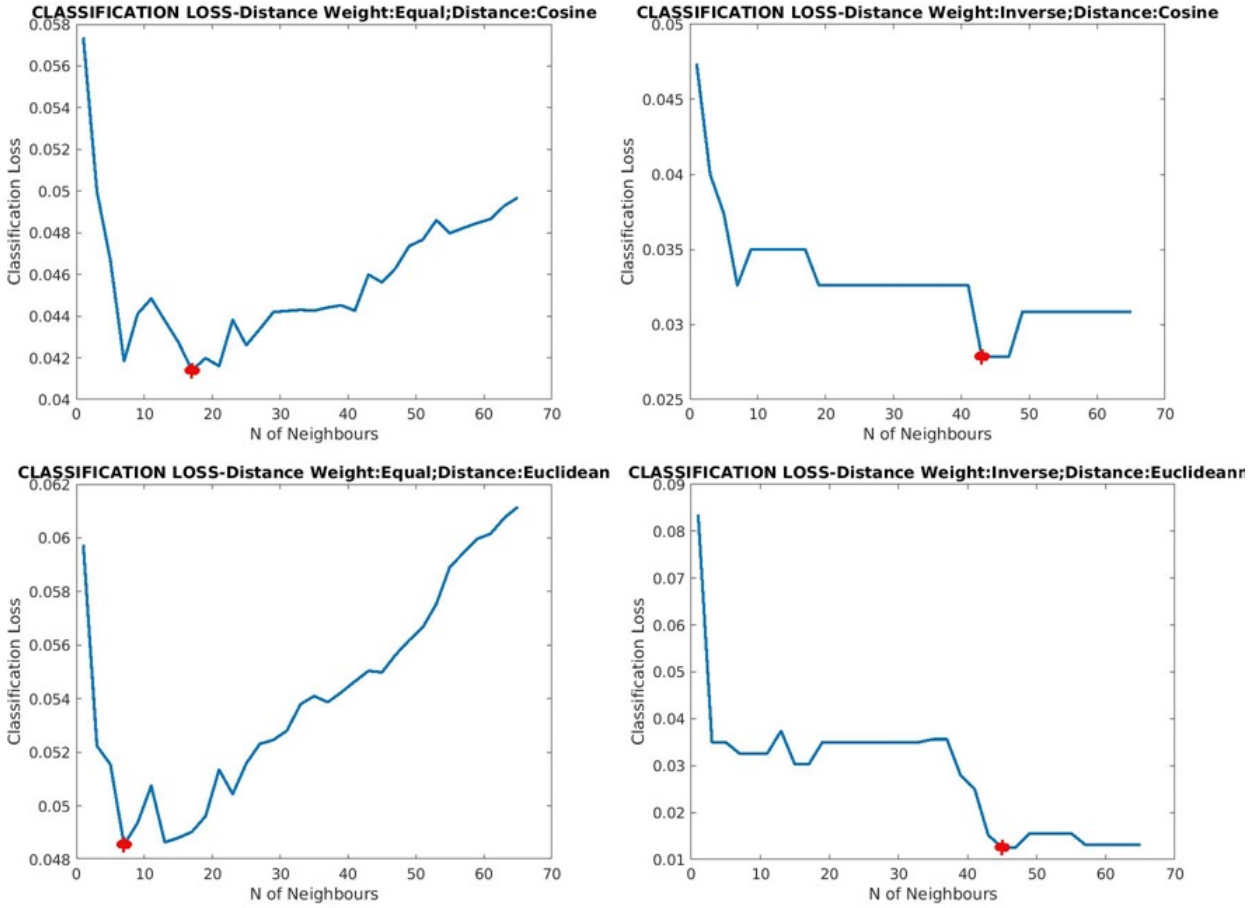

Figure 3.12: *The Loss curve is used for displaying the predictive inaccuracy of the model. Dataset_3 a)k=17, L=0.0414.b)k=43, L=0.0279 c)k=7, L=0.0665 d)k=45, L=0.0126*

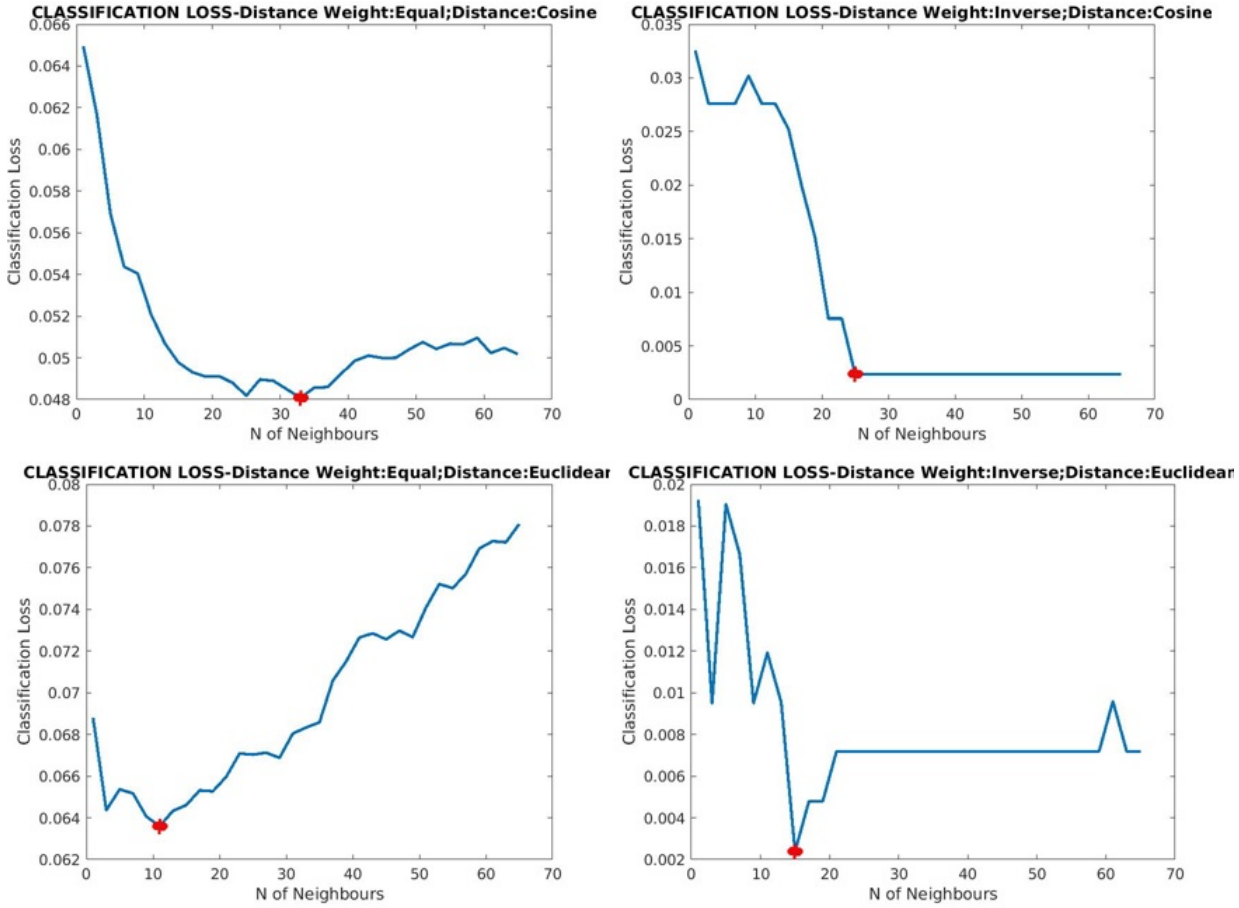

Figure 3.13: *The Loss curve is used for displaying the predictive inaccuracy of the model. Dataset_4: a)k=33, L=0.0481 b)k=25,L=0.024 c)k=11, L=0.0636 d)k=15 ,L=0.024*

Leave-One-Subject-Out:SVM Classifiers The figure 3.14 displays the loss curves of SVM Classifiers for each dataset varying the Box Constraints "C"(a parameter introduced that assigns penalty to the misclassification: as C increases as the strictness of the model increases). The predictive inaccuracy of all models is less than 5%: less than the KNN classifiers.

As shown by the table 3.8, the variation of the Box Constraint affected more the model trained on the Dataset_4. Indeed, the ratio between the minimum and the maximum points of the loss curve is around 82% .

The model trained on the Dataset_3 shows the lower Loss curve values: the maximum value is about 3.2%.

The Loss curves of SVM classifiers trained on Dataset_2, Dataset_3, Dataset_4 increased as the box constraint increased until to reach a plateau. The Loss curve of the SVM Classifier trained on Dataset_1 reached the highest point and after dropped until the plateau.

	[%]
Dataset_1	75
Dataset_2	78
Dataset_3	78
Dataset_4	82

Table 3.8: *Ratio between the minimum and maximum values of the Loss Curve for SVM classifiers*

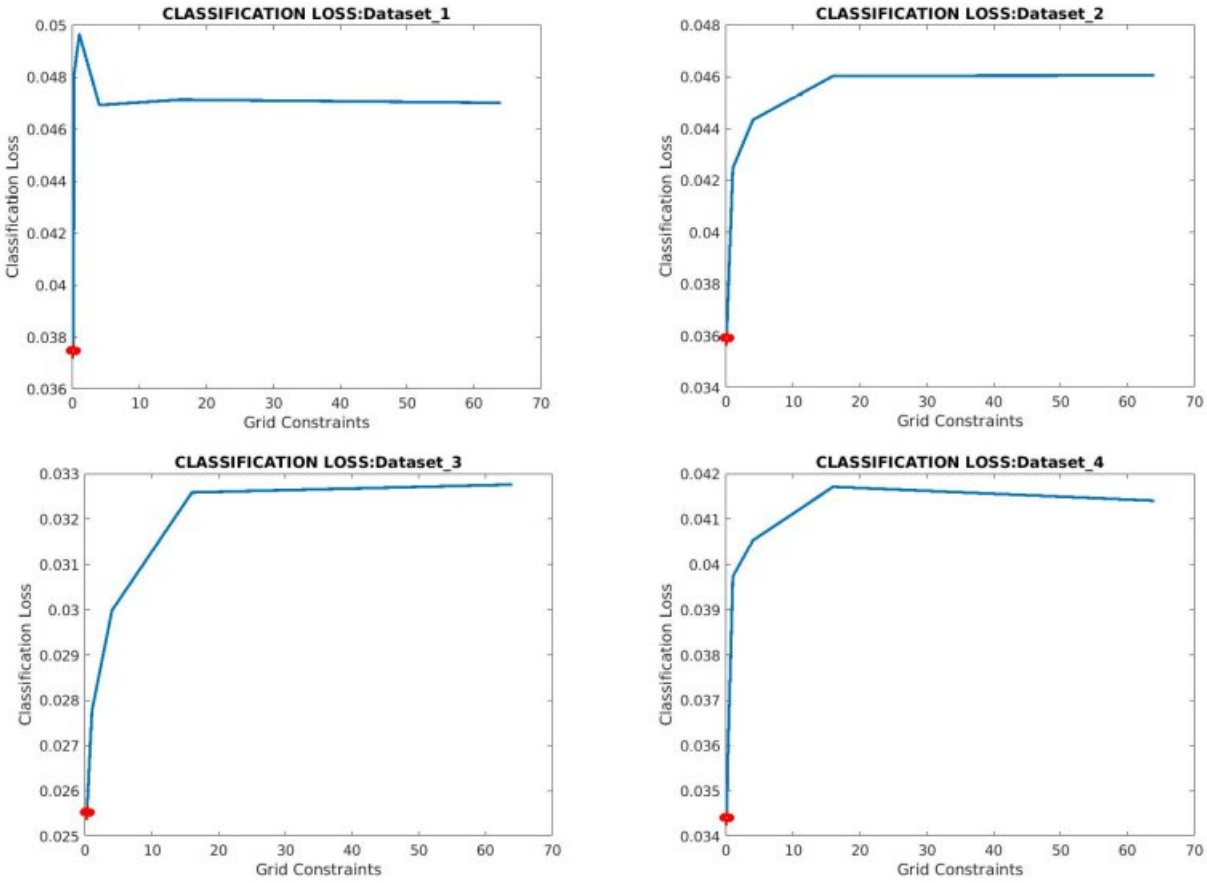

Figure 3.14: *The Loss curve is used for displaying the predictive inaccuracy of the model.a)Dataset_1,C=0.0625, L=0.0375; b)Dataset_2,C=0.0625, L=0.0359; c) Dataset_3 C=0.0625, L=0.0255; d)Dataset_4,C=0.0625, L=0.344*

3.3.4 Model Evaluation

We compared the performances of classifiers trained on the different datasets and with two validation model: KFold and LOSO. The performances have been evaluated using the confusion matrices(the tables from 3.10 to3.43) resulting from the test set evaluation.

The confusion matrices below (tables:3.10, 3.11,3.12, 3.13, 3.18, 3.17, 3.16, 3.15, 3.20, 3.21, 3.22, 3.23, 3.25, 3.26, 3.27, 3.28, 3.30, 3.31, 3.32, 3.33, 3.35, 3.36, 3.37, 3.38, 3.40, 3.41, 3.42, 3.43)display the classifiers accuracy at predicting each class

(the green cells along the diagonal cells); the last column represents the sensitivity of classifiers at predicting each class; the last row represents the precision of classifiers at predicting each class; the last value along the diagonal (the cyan cell) is the overall accuracy. The other cells of the matrices are the fraction of observations not correctly labelled over the total number of observations. Tables 3.14, 3.19, 3.24,3.29, 3.34, 3.39, 3.44 report the F1score values.

K-Fold vs. LOSO We would expect higher accuracy values for the classifiers using the K-Fold Validation. This technique randomly split the dataset into Training and Validation sets. So, the data of a certain subject were in both datasets. The prediction accuracy should improve, and hyperparameters tuning was biased by the presence of each subjects data in the validation set[157]. We evaluated the model on a test set including one STS exercise from each subject joined to the study.

In general, the predictive accuracy, precision, and sensitivity of the classifiers trained using the LOSO validation technique were higher than the metrics resulting from classifiers trained using the K-Fold validation model. The different size of Test Sets of the two validation models could cause a difference in the predictive accuracy. Also, we guessed that the low predictive accuracy of the K-Fold validation model could be affected by the high inter-subject variability. Indeed, the application tuned the hyperparameters taking into account phases from different subjects that could be misleading.

Another difference between the two validation models was the disagreement between the single-class and the overall accuracy in the K-Fold Validation model. Although the single-class predictive accuracy is high for each class, the overall accuracy is lower. The disagreement could be due to the predominance of some classes. We noticed that the Test Set included more instances of some classes. Also,

the number of True Positive observations of those classes was greater than the number of other classes True Positive observations. The True Positive observations of a certain class are included in the True Negative set of observations of another class. The numerator of the single-class accuracy formula increased resulting in higher accuracy output value. The accuracy is the proportion of correct classifications among all classifications. It is a very intuitive measure, but it could be misleading in case of imbalanced Class[9]. The Datasets used in this study were imbalanced because the duration of the phases displayed large inter-individual variability. So, it is likely having more observations of one class than others. Looking at the metrics values reported in the tables: 3.10, 3.11, 3.12, 3.13, 3.15, 3.16, 3.17, 3.18, among all classes the *REST* class is the one with lower accuracy, but with higher sensitivity and precision. The number of true positive observation of the *REST* class affected the accuracy evaluation of other classes. For this reason, the precision and sensitivity measures are more reliable to judge the quality of the classifier.
There is not disagreement between the predictive single-class accuracies and the overall accuracy. There is not the prevalence of the *REST* class respect to the others because of the smaller size of the Test Set. Aside from the better results, the LOSO technique is to prefer because we want to be able to build a model that generalize new subjects not included in the training or dataset. The LOSO validation model is the technique closest to how the system can be used.

KNN vs SVM LOSO[10] The performances of the two classifiers were quite similar and comparable.

[9]Imbalanced Class: The imbalanced class distribution has many more instances of some classes than others[161]

[10]Since, we tuned the hyperparameters in the LOSO validation model, we are going to comment only the results from LOSO

- **KNN**
  - The classifier trained using "Cosine" as distance metrics showed better performances than classifiers trained using Euclidean as distance metrics. The choice of the distance weight (Equal or inverse) did not influence the hyperparameters tuning.
  - The KNN showed better results using as dataset the Dataset_4.
- **SVM** We used the same Box Constraint for all four datasets. The only parameter that affected the classifier performance was the dataset choice. Dataset_3 showed the best performance. Nevertheless, we guessed that the best choice could be using a Dataset_2 because it included three sensors instead of ten(The wearability of the system improved) and the duration of the epoch are longer (to facilitate the data handling and processing for the system).

Both Classifiers performances could be affected by large unbalanced dataset (see the case of K-Fold, where the observations belonging to *REST* phase are higher than others)[161]. The KNN algorithm is an easier algorithm than the SVM, but the computational cost increases as increases the training size [162].

Subject	Trunk Leaning[s]	Sitting[s]	Balance[s]	Standing[s]
CNT_02	0.419± 0.192	0.56 ± 0.0709	1.06± 0.138	0.827±0.11
CNT_03	0.56±0.481	0.468 ± 0.125	0.484 ±0.143	0.566± 0.0566
CNT_04	0.391±0.197	0.7±0.0651	1.18±0.184	0.974±0.0951
CNT_05	0.348±0.245	0.689±0.272	1.01±0.325	0.6±0.322
CNT_06	0.469± 0.345	0.604±0.354	0.738±0.200	0.906±0.349
CNT_07	0.758±0.496	0.825±0.287	1.070±0.890	0.301±0.109
CNT_08	0.245±0.112	0.582±0.056	0.710±0.122	0.549±0.076
CNT_09	0.431±0.131	0.591±0.0968	0.504±0.167	0.533±0.069
CNT_10	0.226±0.139	0.699±0.0592	0.590±0.239	1.000±0.221
CNT_11	0.265± 0.100	0.698±0.086	0.979±0.113	0.855±0.144
CNT_13	0.441±0.154	0.493±0.125	1.100±0.0701	0.629±0.157
CNT_14	0.355±0.204	0.465±0.106	1.0±0.198	0.642±0.084
CNT_15	0.544±0.479	0.397±0.735	0.743±0.12	0.566±0.464
CNT_16	0.522±0.125	0.574±0.0415	0.918±0.105	0.622±0.0726
CNT_17	0.433±0.118	0.431±0.0385	0.376± 0.108	0.491±0.078
CNT_18	0.582±0.405	0.411±0.123	1.06±0.778	0.672±0.161
CNT_20	0.376±0.121	0.465±0.0412	1.160±0.138	0.892±0.104
CNT_21	0.622±0.437	0.392±0.515	0.977±0.278	0.735±0.492
CNT_22	0.684±0.377	0.481±0.0551	1.05±0.199	0.917±0.113
CNT_23	0.466±0.363	0.462±0.265	1.04±0.208	1.07±0.334
CNT_24	0.749±0.221	0.69±0.112	2.73±0.373	1.16±0.134
CNT_25	0.5±0.362	0.551±0.103	0.972±0.384	1.08±0.141
CNT_26	0.492±0.339	0.51±0.262	1.83±0.37	1.02±0.411
CNT_27	0.669±0.232	0.610±0.0774	2.300±0.256	1.210±0.243
CNT_28	0.496±0.433	0.558±0.062	0.993±0.291	1.2±0.207
CNT_29	0.459± 0.189	0.779±0.147	1.98±0.246	1.4±0.143
CNT_30	0.524±0.327	0.602±0.095	1.59±0.302	1.16±0.236

Table 3.9: *Mean and standard deviation of phases duration for each subject*

		Predicted					
		REST	TL	STANDING	BALANCE	SITTING	
Actual	REST	0.818	0.03	0.05	0.12	0.06	0.66
	TL	0.00	0.91	0.00	0.01	0.01	0.52
	STANDING	0.00	0.00	0.92	0.00	0.00	0.81
	BALANCE	0.00	0.00	0.00	0.85	0.00	0.94
	SITTING	0.00	0.00	0.00	0.00	0.90	0.91
		1.0	0.37	0.39	0.28	0.37	0.69

Table 3.10: *Classifier: KNN; Dataset_1; Validation Model: K-Fold. Hyperparameters automatically tuned by MatLab. The green cells along the matrix diagonal contains the classifier accuracy at predicting each class; the last column of the matrix reports the sensitivity of classifiers at predicting each class; the last row reports the precision of classifiers at predicting each class; the cyan cell is the overall accuracy. The other cells of the matrices are the fraction of misclassified observations over the total number of observations*

		Predicted					
		REST	TL	STANDING	BALANCE	SITTING	
Actual	REST	0.86	0.04	0.04	0.08	0.06	0.72
	TL	0.00	0.94	0.00	0.00	0.00	1.00
	STANDING	0.00	0.00	0.94	0.00	0.00	0.90
	BALANCE	0.00	0.00	0.00	0.91	0	0.95
	SITTING	0.00	0.00	0.00	0.00	0.92	0.84
		0.99	0.31	0.52	0.52	0.48	0.76

Table 3.11: *Classifier: KNN; Dataset_2; Validation Model: K-Fold. Hyperparameters automatically tuned by MatLab.The green cells along the matrix diagonal contains the classifier accuracy at predicting each class; the last column of the matrix reports the sensitivity of classifiers at predicting each class; the last row reports the precision of classifiers at predicting each class; the cyan cell is the overall accuracy. The other cells of the matrices are the fraction of misclassified observations over the total number of observations*

		Predicted					
		REST	TL	STANDING	BALANCE	SITTING	
Actual	REST	0.91	0.02	0.01	0.03	0.03	0.84
	TL	0.03	0.88	0.02	0.01	0.03	0.32
	STANDING	0.00	0.00	0.94	0.00	0.00	0.86
	BALANCE	0	0.00	0.00	0.95	0.00	0.98
	SITTING	0.00	0.00	0.00	0	0.92	0.95
		0.94	0.58	0.56	0.75	0.48	0.79

Table 3.12: *Classifier:KNN; Dataset_3; Validation Model: K-Fold. Hyperparameters automatically tuned by MatLab. The green cells along the matrix diagonal contained the classifier accuracy at predicting each class; the last column of the matrix reported the sensitivity of classifiers at predicting each class; the last row reported the precision of classifiers at predicting each class; the cyan cell is the overall accuracy.The other cells of the matrices are the fraction of misclassified observations over the total number of observations*

		Predicted					
		REST	TL	STANDING	BALANCE	SITTING	
Actual	REST	0.86	0.02	0.03	0.08	0.06	0.72
	TL	0.00	0.94	0.00	0.00	0.00	0.85
	STANDING	0.00	0.01	0.94	0.00	0.00	0.82
	BALANCE	0.00	0.00	0.00	0.89	0.00	0.95
	SITTING	0.00	0.00	0.00	0.00	0.92	0.96
		1.00	0.44	0.60	0.44	0.47	0.76

Table 3.13: *Classifier:KNN; Dataset_4; Validation Model: K-Fold. Hyperparameters automatically tuned by MatLab. The green cells along the matrix diagonal contains the classifier accuracy at predicting each class; the last column of the matrix reports the sensitivity of classifiers at predicting each class; the last row reports the precision of classifiers at predicting each class; the cyan cell is the overall accuracy. The other cells of the matrices are the fraction of misclassified observations over the total number of observations*

	REST	TL	STANDING	BALANCE	SITTING
Dataset_1	0.80	0.44	0 0.53	0.44	0.50
Dataset_2	0.83	0.47	0.65	0.67	0.61
Dataset_3	0.91	0.32	0.645	0.67	0.62
Dataset_4	0.97	0.23	0.73	0.62	0.59

Table 3.14: *KNN F1 score for the four datasets*

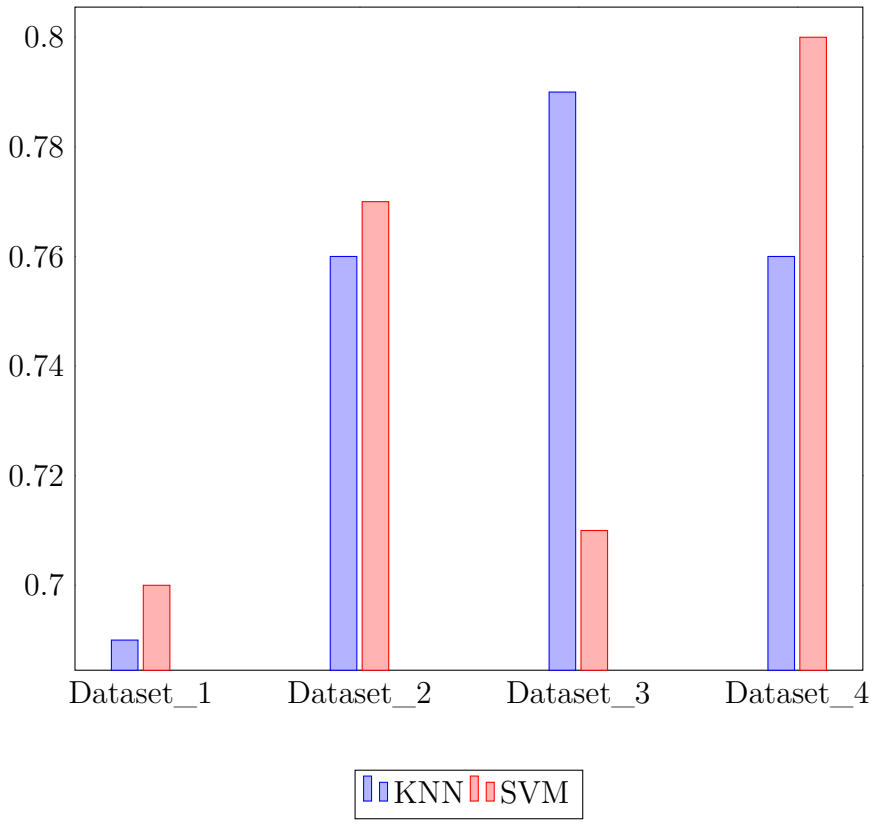

Figure 3.15: *The graph reports the overall accuracies of both KNN and SVM classifiers. The validation model is K-Fold.*

		Predicted					
		REST	TL	STANDING	BALANCE	SITTING	
Actual	REST	0.88	0.02	0.03	0.05	0.03	0.78
	TL	0.00	0.89	0.01	0.07	0.02	0.43
	STANDING	0.00	0.00	0.84	0.06	0.00	0.33
	BALANCE	0.00	0.00	0.00	0.85	0.00	0.98
	SITTING	0.00	0.00	0.00	0.00	0.91	0.88
		0.98	0.58	0.42	0.28	0.41	0.71

Table 3.15: *Classifier Algorithm: SVM,validation model:K-Fold, Dataset_1. Hyper-parameters automatically tuned by MatLab. The green cells along the matrix diagonal contains the classifier accuracy at predicting each class; the last column of the matrix reports the sensitivity of classifiers at predicting each class; the last row reports the precision of classifiers at predicting each class; the cyan cell is the overall accuracy. The other cells of the matrices are the fraction of misclassified observations over the total number of observations*

		Predicted					
		REST	TL	STANDING	BALANCE	SITTING	
Actual	REST	0.90	0.04	0.03	0.01	0.05	0.78
	TL	0.00	0.94	0.00	0.00	0.00	0.89
	STANDING	0.00	0.00	0.88	0.05	0.00	0.43
	BALANCE	0.00	0.00	0	0.91	0.00	0.97
	SITTING	0.00	0.00	0.00	0.00	0.92	0.89
		1.0	0.30	0.58	0.53	0.46	0.77

Table 3.16: *Classifier Algorithm: SVM,validation model:K-Fold,Dataset_2. Hyperparameters automatically tuned by MatLab. The green cells along the matrix diagonal contains the classifier accuracy at predicting each class; the last column of the matrix reports the sensitivity of classifiers at predicting each class; the last row reports the precision of classifiers at predicting each class; the cyan cell is the overall accuracy. The other cells of the matrices are the fraction of misclassified observations over the total number of observations*

		Predicted					
		REST	TL	STANDING	BALANCE	SITTING	
Actual	REST	0.93	0.00	0.00	0.00	0.00	0.98
	TL	0.08	0.80	0.03	0.00	0.05	0.24
	STANDING	0.00	0.01	0.84	0.09	0.00	0.35
	BALANCE	0.00	0.00	0.00	0.89	0.00	0.97
	SITTING	0.00	0.00	0.00	0.00	0.93	1.00
		0.84	0.75	0.60	0.47	0.52	0.71

Table 3.17: *Classifier Algorithm: SVM,validation model:K-Fold,Dataset_3.Hyperparamters automatically tuned by MatLab. The green cells along the matrix diagonal contains the classifier accuracy at predicting each class; the last column of the matrix reports the sensitivity of classifiers at predicting each class; the last row reports the precision of classifiers at predicting each class; the cyan cell is the overall accuracy. The other cells of the matrices are the fraction of misclassified observations over the total number of observations*

		Predicted					
		REST	TL	STANDING	BALANCE	SITTING	
Actual	REST	0.92	0.00	0.01	0.05	0.03	0.83
	TL	0.00	0.93	0.01	0.01	0.01	0.55
	STANDING	0.00	0.00	0.93	0.02	0.01	0.62
	BALANCE	0.00	0.00	0	0.90	0.00	0.98
	SITTING	0.00	0.00	0.00	0.00	0.92	0.88
		0.99	0.77	0.66	0.44	0.52	0.80

Table 3.18: *Classifier Algorithm: SVM,validation model:K-Fold, Dataset_4. Hyperparameters automatically tuned by MatLab. The green cells along the matrix diagonal contains the classifier accuracy at predicting each class; the last column of the matrix reports the sensitivity of classifiers at predicting each class; the last row reports the precision of classifiers at predicting each class; the cyan cell is the overall accuracy. The other cells of the matrices are the fraction of misclassified observations over the total number of observations*

	REST	TL	STANDING	BALANCE	SITTING
Dataset_1	0.87	0.49	0.37	0.43	0.56
Dataset_2	0.88	0.45	0.44	0.68	0.61
Dataset_3	0.91	0.36	0.44	0.64	0.68
Dataset_4	0.91	0.64	0.64	0.61	0.65

Table 3.19: *SVM F1 score for the four datasets*

		Predicted					
		REST	TL	STANDING	BALANCE	SITTING	
Actual	REST	0.97	0.00	0.00	0	0.00	0.97
	TL	0.00	0.97	0.00	0.00	0.00	0.93
	STANDING	0.00	0.00	0.98	0.00	0.00	0.91
	BALANCE	0.01	0.00	0.00	0.97	0.00	0.93
	SITTING	0.00	0.00	0.00	0.00	0.97	0.91
		0.96	0.74	0.87	0.97	0.89	0.93

Table 3.20: *Classifier Algorithm: KNN,validation model:LOSO,Dataset_1, distance weight: Equal, distance metrics: Cosine. The green cells along the matrix diagonal contains the classifier accuracy at predicting each class; the last column of the matrix reports the sensitivity of classifiers at predicting each class; the last row reports the precision of classifiers at predicting each class; the cyan cell is the overall accuracy. The other cells of the matrices are the fraction of misclassified observations over the total number of observations*

		Predicted					
		REST	TL	STANDING	BALANCE	SITTING	
Actual	REST	0.97	0.01	0.00	0.00	0.01	0.97
	TL	0.00	0.97	0.00	0.00	0.00	0.93
	STANDING	0.00	0.00	0.97	0.00	0.00	0.90
	BALANCE	0.00	0.00	0.00	0.97	0.00	0.93
	SITTING	0.00	0.00	0.00	0.00	0.97	0.90
		0.96	0.74	0.87	0.97	0.89	0.93

Table 3.21: *Classifier Algorithm: KNN,validation model:LOSO,Dataset_1, distance weight: Inverse, distance metrics: Cosine. The green cells along the matrix diagonal contains the classifier accuracy at predicting each class; the last column of the matrix reports the sensitivity of classifiers at predicting each class; the last row reports the precision of classifiers at predicting each class; the cyan cell is the overall accuracy. The other cells of the matrices are the fraction of misclassified observations over the total number of observations*

		Predicted					
		REST	TL	STANDING	BALANCE	SITTING	
Actual	REST	0.96	0.01	0.00	0.00	0.02	0.94
	TL	0.00	0.97	0.00	0.00	0.00	0.94
	STANDING	0.00	0.00	0.97	0.00	0.006	0.88
	BALANCE	0.00	0.00	0.00	0.97	0.00	0.93
	SITTING	0.00	0.00	0.00	0.00	0.96	0.87
		0.97	0.63	0.83	0.96	0.82	0.91

Table 3.22: *Classifier Algorithm: KNN,validation model:LOSO,Dataset_1, distance weight: Equal, distance metrics: Euclidean. The green cells along the matrix diagonal contains the classifier accuracy at predicting each class; the last column of the matrix reports the sensitivity of classifiers at predicting each class; the last row reports the precision of classifiers at predicting each class; the cyan cell is the overall accuracy. The other cells of the matrices are the fraction of misclassified observations over the total number of observations*

		Predicted					
		REST	TL	STANDING	BALANCE	SITTING	
Actual	REST	0.957	0.02	0.00	0.00	0.02	0.93
	TL	0.00	0.97	0.00	0.00	0.00	0.95
	STANDING	0.00	0.00	0.97	0.00	0.00	0.91
	BALANCE	0.01	0.00	0.00	0.97	0.00	0.93
	SITTING	0.00	0.00	0.00	0.00	0.96	0.88
		0.97	0.61	0.82	0.96	0.81	0.91

Table 3.23: *Classifier Algorithm: KNN,validation model:LOSO,Dataset_1, distance weight: Inverse, distance metrics: Euclidean. The green cells along the matrix diagonal contains the classifier accuracy at predicting each class; the last column of the matrix reports the sensitivity of classifiers at predicting each class; the last row reports the precision of classifiers at predicting each class; the cyan cell is the overall accuracy. The other cells of the matrices are the fraction of misclassified observations over the total number of observations*

Dataset_1	REST	TL	STANDING	BALANCE	SITTING
CE	0.96	0.81	0.87	0.93	0.89
CI	0.96	0.81	0.87	0.93	0.89
EE	0.95	0.72	0.83	0.93	0.84
EI	0.95	0.70	0.84	0.93	0.83

Table 3.24: *KNN-The table reports the F1score computed for the Dataset_1 varying the distance metrcs and weight. CE= distance weight equal, distance metric cosine; CI= distance weight inverse, distance metric cosine; EE= distance weight equal, distance metric euclidean; EE= distance weight inverse, distance metric euclidean*

		Predicted					
		REST	TL	STANDING	BALANCE	SITTING	
Actual	REST	0.97	0.01	0.00	0.00	0.00	0.96
	TL	0.00	0.97	0.00	0.00	0.00	0.88
	STANDING	0.00	0.00	0.98	0.00	0.00	0.91
	BALANCE	0.00	0.00	0.00	0.99	0.00	0.95
	SITTING	0.00	0.00	0.00	0.00	0.97	0.88
		0.98	0.73	0.87	0.99	0.87	0.94

Table 3.25: *Classifier Algorithm: KNN,Dataset_2, distance weight: Equal, distance metrics: Cosine. The green cells along the matrix diagonal contains the classifier accuracy at predicting each class; the last column of the matrix reports the sensitivity of classifiers at predicting each class; the last row reports the precision of classifiers at predicting each class; the cyan cell is the overall accuracy. The other cells of the matrices are the fraction of misclassified observations over the total number of observations.*

		Predicted					
		REST	TL	STANDING	BALANCE	SITTING	
Actual	REST	0.97	0.01	0.00	0.00	0.00	0.96
	TL	0.00	0.97	0.00	0	0.00	0.88
	STANDING	0.00	0.00	0.98	0.00	0.00	0.91
	BALANCE	0.00	0.00	0.00	0.99	0.00	0.95
	SITTING	0.00	0.00	0.00	0	0.97	0.88
		0.97	0.74	0.87	0.99	0.87	0.94

Table 3.26: *Classifier Algorithm: KNN,Dataset_2, distance weight: Inverse, distance metrics: Cosine. The green cells along the matrix diagonal contains the classifier accuracy at predicting each class; the last column of the matrix reports the sensitivity of classifiers at predicting each class; the last row reports the precision of classifiers at predicting each class; the cyan cell is the overall accuracy. The other cells of the matrices are the fraction of misclassified observations over the total number of observations.*

		Predicted					
		REST	TL	STANDING	BALANCE	SITTING	
Actual	REST	0.97	0.02	0.00	0	0.01	0.94
	TL	0.00	0.97	0.00	0.00	0.00	0.93
	STANDING	0	0.00	0.98	0.00	0.00	0.93
	BALANCE	0	0	0.00	0.99	0.00	0.96
	SITTING	0.00	0.00	0.01	0	0.97	0.87
		0.98	0.64	0.85	0.98	0.87	0.93

Table 3.27: *Classifier Algorithm: KNN,Dataset_2, distance weight: Equal, distance metrics: Euclidean. The green cells along the matrix diagonal contains the classifier accuracy at predicting each class; the last column of the matrix reports the sensitivity of classifiers at predicting each class; the last row reports the precision of classifiers at predicting each class; the cyan cell is the overall accuracy. The other cells of the matrices are the fraction of misclassified observations over the total number of observations.*

		Predicted					
		REST	TL	STANDING	BALANCE	SITTING	
Actual	REST	0.97	0.02	0.00	0.00	0.01	0.94
	TL	0.00	0.97	0.00	0.00	0.00	0.93
	STANDING	0.00	0.00	0.98	0.00	0.00	0.93
	BALANCE	0.00	0.00	0.00	0.99	0.00	0.96
	SITTING	0.00	0.00	0.00	0	0.97	0.87
		0.98	0.64	0.85	0.98	0.87	0.93

Table 3.28: *Classifier Algorithm: KNN,Dataset_2, distance weight: Inverse, distance metrics: Euclidean. The green cells along the matrix diagonal contains the classifier accuracy at predicting each class; the last column of the matrix reports the sensitivity of classifiers at predicting each class; the last row reports the precision of classifiers at predicting each class; the cyan cell is the overall accuracy. The other cells of the matrices are the fraction of misclassified observations over the total number of observations.*

Dataset_2	REST	TL	STANDING	BALANCE	SITTING
CE	0.96	0.80	0.87	0.94	0.89
CI	0.96	0.81	0.87	0.94	0.89
EE	0.95	0.72	0.83	0.93	0.84
EI	0.95	0.70	0.84	0.93	0.83

Table 3.29: *KNN-The table reports the F1score computed for the Dataset_2 varying the distance metrcs and weight. CE= distance weight equal, distance metric cosine; CI= distance weight inverse, distance metric cosine; EE= distance weight equal, distance metric euclidean; EE= distance weight inverse, distance metric euclidean*

		Predicted					
		REST	TL	STANDING	BALANCE	SITTING	
Actual	REST	0.98	0.00	0.00	0.00	0.01	0.97
	TL	0.00	0.98	0.00	0.00	0.00	0.91
	STANDING	0.00	0.00	0.99	0.00	0.00	0.95
	BALANCE	0.00	0.00	0.00	0.99	0.00	0.96
	SITTING	0.00	0.00	0.00	0	0.98	0.93
		0.98	0.81	0.92	0.99	0.91	0.96

Table 3.30: *Classifier Algorithm: KNN,validation model:LOSO,Dataset_3, distance weight: Equal, distance metrics: Cosine. The green cells along the matrix diagonal contains the classifier accuracy at predicting each class; the last column of the matrix reports the sensitivity of classifiers at predicting each class; the last row reports the precision of classifiers at predicting each class; the cyan cell is the overall accuracy. The other cells of the matrices are the fraction of misclassified observations over the total number of observations.*

		Predicted					
		REST	TL	STANDING	BALANCE	SITTING	
Actual	REST	0.98	0.01	0.00	0.00	0.01	0.96
	TL	0.00	0.98	0.00	0.00	0.00	0.91
	STANDING	0.00	0.00	0.98	0.00	0.00	0.95
	BALANCE	0.00	0.00	0.00	0.99	0.00	0.95
	SITTING	0.00	0.00	0.00	0.00	0.98	0.93
		0.99	0.80	0.91	0.99	0.90	0.95

Table 3.31: *Classifier Algorithm: KNN,validation model:LOSO,Dataset_3, distance weight: Inverse, distance metrics: Cosine. The green cells along the matrix diagonal contains the classifier accuracy at predicting each class; the last column of the matrix reports the sensitivity of classifiers at predicting each class; the last row reports the precision of classifiers at predicting each class; the cyan cell is the overall accuracy. The other cells of the matrices are the fraction of misclassified observations over the total number of observations.*

		Predicted					
		REST	TL	STANDING	BALANCE	SITTING	
Actual	REST	0.98	0.01	0.00	0.00	0.01	0.96
	TL	0.00	0.98	0.00	0.00	0.00	0.93
	STANDING	0.00	0.00	0.98	0.00	0.00	0.95
	BALANCE	0.00	0.00	0.00	0.99	0.00	0.97
	SITTING	0.00	0.00	0.00	0.00	0.97	0.90
		0.98	0.76	0.89	0.99	0.91	0.95

Table 3.32: *Classifier Algorithm: KNN,validation model:LOSO,Dataset_3, distance weight: Equal, distance metrics: Euclidean. The green cells along the matrix diagonal contains the classifier accuracy at predicting each class; the last column of the matrix reports the sensitivity of classifiers at predicting each class; the last row reports the precision of classifiers at predicting each class; the cyan cell is the overall accuracy. The other cells of the matrices are the fraction of misclassified observations over the total number of observations.*

		Predicted					
		REST	TL	STANDING	BALANCE	SITTING	
Actual	REST	0.97	0.02	0.00	0.00	0.01	0.94
	TL	0.00	0.97	0.00	0.00	0.00	0.93
	STANDING	0.00	0.00	0.98	0.00	0.00	0.96
	BALANCE	0.00	0.00	0.00	0.99	0.00	0.97
	SITTING	0.00	0.00	0.00	0.00	0.97	0.93
		0.99	0.70	0.88	0.99	0.88	0.94

Table 3.33: *Classifier Algorithm: KNN,validation model:LOSO,Dataset_3, distance weight: Inverse, distance metrics: Euclidean. The green cells along the matrix diagonal contains the classifier accuracy at predicting each class; the last column of the matrix reports the sensitivity of classifiers at predicting each class; the last row reports the precision of classifiers at predicting each class; the cyan cell is the overall accuracy. The other cells of the matrices are the fraction of misclassified observations over the total number of observations.*

Dataset_3	REST	TL	STANDING	BALANCE	SITTING
CE	0.98	0.85	0.93	0.98	0.91
CI	0.98	0.84	0.93	0.97	0.90
EE	0.97	0.81	0.91	0.98	0.90
EI	0.96	0.75	0.91	0.98	0.89

Table 3.34: *KNN-The table reports the F1score computed for the Dataset_3 varying the distance metrcs and weight. CE= distance weight equal, distance metric cosine; CI= distance weight inverse, distance metric cosine; EE= distance weight equal, distance metric euclidean; EE= distance weight inverse, distance metric euclidean*

		Predicted					
		REST	TL	STANDING	BALANCE	SITTING	
Actual	REST	0.98	0.00	0.00	0.00	0.00	0.98
	TL	0.00	0.98	0.00	0.00	0.00	0.95
	STANDING	0.00	0.00	0.98	0.00	0.00	0.934
	BALANCE	0.01	0.00	0.00	0.97	0.00	0.94
	SITTING	0.00	0.00	0.00	0	0.98	0.94
		0.97	0.84	0.91	0.98	0.92	0.95 0.958

Table 3.35: *Classifier Algorithm: KNN,validation model:LOSO,Dataset_4, distance weight: Equal, distance metrics: Cosine. The green cells along the matrix diagonal contains the classifier accuracy at predicting each class; the last column of the matrix reports the sensitivity of classifiers at predicting each class; the last row reports the precision of classifiers at predicting each class; the cyan cell is the overall accuracy. The other cells of the matrices are the fraction of misclassified observations over the total number of observations.*

		Predicted					
		REST	TL	STANDING	BALANCE	SITTING	
Actual	REST	0.97	0.00	0.00	0.00	0.00	0.98
	TL	0.00	0.98	0.00	0.00	0.00	0.95
	STANDING	0.00	0.00	0.98	0.00	0.00	0.93
	BALANCE	0.01	0.00	0.00	0.97	0.00	0.94
	SITTING	0.00	0.00	0.00	0.00	0.98	0.94
		0.97	0.84	0.91	0.98	0.92	0.95

Table 3.36: *Classifier Algorithm: KNN,validation model:LOSO,Dataset_4, distance weight: Inverse, distance metrics: Cosine. The green cells along the matrix diagonal contains the classifier accuracy at predicting each class; the last column of the matrix reports the sensitivity of classifiers at predicting each class; the last row reports the precision of classifiers at predicting each class; the cyan cell is the overall accuracy. The other cells of the matrices are the fraction of misclassified observations over the total number of observations.*

		Predicted					
		REST	TL	STANDING	BALANCE	SITTING	
Actual	REST	0.97	0.01	0.00	0	0.01	0.95
	TL	0	0.98	0.00	0.00	0.00	0.97
	STANDING	0.00	0.00	0.97	0.00	0.00	0.92
	BALANCE	0.01	0.00	0.00	0.98	0.00	0.94
	SITTING	0.00	0.00	0.00	0.00	0.97	0.90
		0.97	0.75	0.87	0.96	0.88	0.93

Table 3.37: *Classifier Algorithm: KNN,validation model:LOSO,Dataset_4, distance weight: Equal, distance metrics: Euclidean. The green cells along the matrix diagonal contains the classifier accuracy at predicting each class; the last column of the matrix reports the sensitivity of classifiers at predicting each class; the last row reports the precision of classifiers at predicting each class; the cyan cell is the overall accuracy. The other cells of the matrices are the fraction of misclassified observations over the total number of observations.*

		Predicted					
		REST	TL	STANDING	BALANCE	SITTING	
Actual	REST	0.97	0.01	0.00	0.00	0.01	0.95
	TL	0.00	0.98	0.00	0.00	0.00	0.97
	STANDING	0.00	0.00	0.97	0.00	0.00	0.92
	BALANCE	0.00	0.00		0.000.98	0.00	0.94
	SITTING	0.00	0.00	0.00	0.00	0.97	0.90
		0.97	0.74	0.87	0.96	0.88	0.93

Table 3.38: *Classifier Algorithm: KNN,validation model:LOSO,Dataset_4, distance weight: Inverse, distance metrics: Euclidean. The green cells along the matrix diagonal contains the classifier accuracy at predicting each class; the last column of the matrix reports the sensitivity of classifiers at predicting each class; the last row reports the precision of classifiers at predicting each class; the cyan cell is the overall accuracy. The other cells of the matrices are the fraction of misclassified observations over the total number of observations.*

Dataset_4	REST	TL	STANDING	BALANCE	SITTING
CE	0.98	0.85	0.93	0.98	0.91
CI 2	0.98	0.84	0.93	0.97	0.90
EE	0.97	0.81	0.91	0.98	0.90
EI	0.96	0.75	0.91	0.98	0.89

Table 3.39: *KNN,model Validation LOSO -The table reports the F1score computed for the Dataset_4 varying the distance metrcs and weight. CE= distance weight equal, distance metric cosine; CI= distance weight inverse, distance metric cosine; EE= distance weight equal, distance metric euclidean; EE= distance weight inverse, distance metric euclidean.*

		Predicted					
		REST	TL	STANDING	BALANCE	SITTING	
Actual	REST	0.98	0.00	0.00	0.00	0.00	0.98
	TL	0.00	0.97	0.00	0.00	0.00	0.89
	STANDING	0.00	0.00	0.98	0.00	0.00	0.91
	BALANCE	0.00	0.00	0.00	0.99	0.00	0.99
	SITTING	0.00	0.00	0.00	0.00	0.97	0.91
		0.98	0.81	0.90	0.98	0.93	0.95

Table 3.40: *Classifier Algorithm: SVM, validation model: LOSO, Dataset_1, C=0.0625. The green cells along the matrix diagonal contains the classifier accuracy at predicting each class; the last column of the matrix reports the sensitivity of classifiers at predicting each class; the last row reports the precision of classifiers at predicting each class; the cyan cell is the overall accuracy. The other cells of the matrices are the fraction of misclassified observations over the total number of observations.*

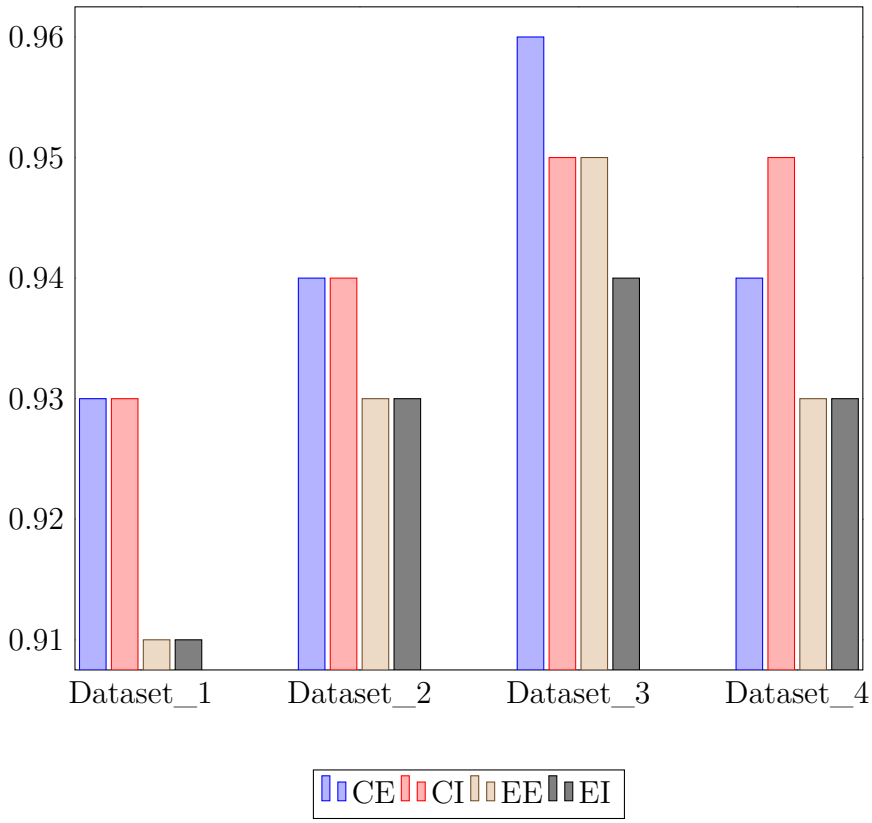

Figure 3.16: *Classifier: KNN, Validation Model: LOSO. The graph shows how the overall accuracy of the four datasets changed accordingly to the hyperparameters choice.*

		Predicted					
		REST	TL	STANDING	BALANCE	SITTING	
Actual	REST	0.98	0.00	0.00	0.00	0.00	0.98
	TL	0.00	0.97	0.00	0.00	0.00	0.87
	STANDING	0.00	0.00	0.98	0.00	0.00	0.95
	BALANCE	0.00	0.00	0.00	0.99	0.00	0.99
	SITTING	0.00	0.00	0.00	0.00	0.98	0.92
		0.98	0.84	0.88	0.99	0.95	0.96

Table 3.41: *Classifier Algorithm: SVM,validation model: LOSO, Dataset_2, C=0.0625. The green cells along the matrix diagonal contains the classifier accuracy at predicting each class; the last column of the matrix reports the sensitivity of classifiers at predicting each class; the last row reports the precision of classifiers at predicting each class; the cyan cell is the overall accuracy. The other cells of the matrices are the fraction of misclassified observations over the total number of observations.*

		Predicted					
		REST	TL	STANDING	BALANCE	SITTING	
Actual	REST	0.99	0.00	0.00	0.00	0.00	0.99
	TL	0.00	0.98	0.00	0	0.00	0.90
	STANDING	0.00	0.00	0.98	0.00	0.00	0.96
	BALANCE	0.00	0.00	0.00	0.99	0	0.99
	SITTING	0.00	0.00	0.00	0.00	0.99	0.95
		0.99	0.91	0.92	0.99	0.97	0.97

Table 3.42: *Classifier Algorithm: SVM, validation model: LOSO, Dataset_3, C=0.0625. The green cells along the matrix diagonal contains the classifier accuracy at predicting each class; the last column of the matrix reports the sensitivity of classifiers at predicting each class; the last row reports the precision of classifiers at predicting each class; the cyan cell is the overall accuracy. The other cells of the matrices are the fraction of misclassified observations over the total number of observations.*

		Predicted					
		REST	TL	STANDING	BALANCE	SITTING	
Actual	REST	0.98	0.00	0.00	0.00	0.00	0.99
	TL	0.00	0.98	0.00	0.00	0.00	0.93
	STANDING	0.00	0.00	0.98	0.00	0.00	0.94
	BALANCE	0.00	0.00	0.00	0.99	0.00	0.96
	SITTING	0.00	0.00	0.00	0.00	0.98	0.90
		0.98	0.87	0.92	0.99	0.96	0.96

Table 3.43: *Classifier Algorithm: SVM, validation model: LOSO, Dataset_4, C=0.0625. The green cells along the matrix diagonal contains the classifier accuracy at predicting each class; the last column of the matrix reports the sensitivity of classifiers at predicting each class; the last row reports the precision of classifiers at predicting each class; the cyan cell is the overall accuracy. The other cells of the matrices are the fraction of misclassified observations over the total number of observations.*

	REST	TL	STANDING	BALANCE	SITTING
Dataset_1	0.98	0.83	0.9	0.99	0.90
Dataset_2	0.98	0.84	0.90	0.99	0.93
Dataset_3	0.99	0.892	0.927	0.994	0.96
Dataset_4	0.98	0.89	0.93	0.97	0.92

Table 3.44: *SVM, model Validation LOSO-the table reports the F1score for the four datasets*

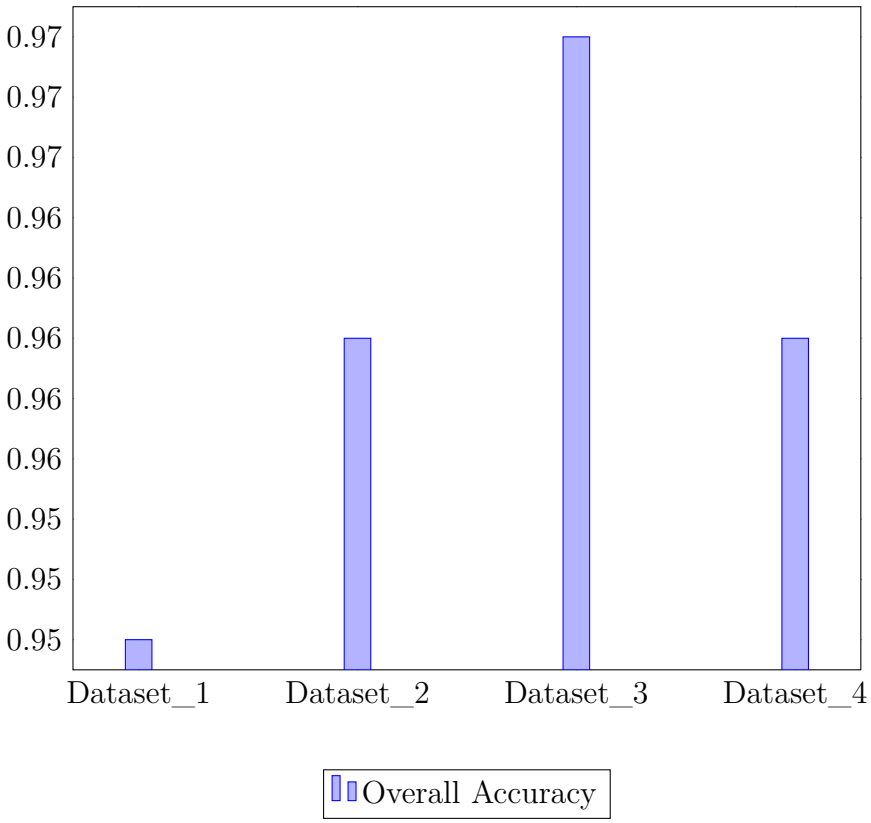

Figure 3.17: *Classifier: SVM, Validation Model: LOSO. The graph shows the overall accuracy across of the four datasets.*

Conclusion

The purpose of this preliminary study is to characterize the dynamic events occurring as rising from a chair. The study of the distinct events-or phases- of the STS movement would result in a most effective description about:

- the contribution of each single body element involved in the movement;
- the kinematic and kinetic variables during the movement and their changes related to specific diseases;
- the pain point that could cause the failure of the movement.

The STS exercises have been recorded by the inertial sensors. In contrast with devices as force platforms or optoelectronics cameras, the inertial sensors are small, wearable and not expensive. They could be used outside the laboratory environment.
Because of the high inter and intra-variability of the STS movement, the STS detection using thresholds related to kinematic and kinetic data could be inaccurate. We tried to solve the problem using Machine Learning.
The machine learning aims to generalize model from experience, i.e. from the real data. In particular, in this study, we trained two classifier models: KNN and SVM. We compared two classifier algorithms performances varying the duration of the epoch, the number of sensors, and the validation model used to train the classifier. The classifier performances were evaluated by confusion matrices and the F1 scores.

We compared the K-Fold and Leave One Subject Out validation models. The K-Fold validation model randomly extracts observations to use as the validation set. The LOSO validation model use as validation model data from one subject. The classifier is validated by data that classifier does not know. The results of our study suggested that the predictive accuracy, precision, and recall of classifier trained were higher using the LOSO. This is because the size of test set was smaller than the size of K-Fold validation set resulting in a less unbalanced dataset. Furthermore, the LOSO validation technique was closer to how the system will be used. Indeed, the system should be able to generalize new subjects.

The hyperparameters varied in the KNN model were the distance metrics(the function that calculates the distance between the query point and the neighbours) and distance weight(the weight of the contribution of each of the k neighbours according to their distance to the query point). The classifier performances was more affected by The distance metrics than the the distance weight

The SVM classifiers performed better with lower box constraints(penalties assigned to the misclassification). More than box constraints the SVM classifiers were affected by the dataset choice.

In the case of LOSO, the KNN and SVM classifier model showed high-performance metrics and were quite similar, but KNN performed better (0.3% better than SVM). Both Classifiers performances could be affected by a large unbalanced dataset. The KNN algorithm is an easier algorithm than the SVM, but, generally, the computational cost increases as increase the training size.

The SVM Classifier trained on Dataset_3 (three sensors-sternum, right and left thigh-0.1 epoch duration) showed the best results. Although this study presents high accuracy values, several issues that still need to be addressed before such techniques could be used in a more applied setting.

Next Steps

- We discarded the task performed wrongly and missing data recordings. We assumed that all the picked measurements were good, so we did not apply any quality control algorithm to discard potential bad "*sequences*." To estimate how the reliability and accuracy of the sensors' measurement could influence the classifier performances it could be useful to apply a quality control algorithm. In the case, it is necessary to estimate the time to evaluate the quality of the sequence.

- Use the classifier in real time;

- This study included a small data sample (27 healthy subjects and 281 STS exercises). It would be interesting to increase the data sample and investigating if and how will change the predictive accuracy;

- To estimate the potential variation of the overall predictive accuracy and single phases accuracy, it would b useful including healthy elderly subjects and elderly with history fall.

- It would be interesting evaluating the ability of the classifier to recognize the STS phases when the task is performed wrongly.

- The clinical relevance of this system could be enhanced by combining it with classical clinical tools as falls and functional questionnaires. The questionnaires could be useful in identifying functional status. The sensor-based measures will be correlated with the outcomes of the clinical tools adding a diagnostic significance to the measures.

Appendix: Publications and Research Activities

PUBLICATIONS AND PROCEEDINGS

- Marco Testa, Anna Di Marco, Raffaele Pertusio, Peter Van Roy, Erik Cattrysse, Silvestro Roatta, A validation study of a new instrument for low cost bite force measurement, Journal of Electromyography and Kinesiology, Volume 30, October 2016,Pages 243-248, ISSN 1050-6411, http://dx.doi.org/10.1016/j.jelekin.2016.08.00

- A. Di Marco, M. Testa (2017,October), Real time detection of sit-to-stand phases: An early study, presented at Italian Society of Clinical Movement Analysis Congress in Turin, Italy

RESEARCH ACTIVITIES

Movement to sound, from sound to movement: Progettazione e validazione di un Sistema di feedback uditivo applicato al Sit To Stand(STS)
The main aim of this study is the development of an auditory feedback to facilitate the re-learning of Sit-To-Stand (STS) movement, using inertial sensors (IS).

IS detect the movement of the limbs involved in the STS movement and, by the elaboration of the data collected, should permit the individuation of a movement pattern associable to STS. The pattern will be the basis for the development of an auditory-musical feedback system. The quality of the sound generated by the system will be related to the adherence of the actual sit to stand to the ideal pattern of execution, indicating precision and quality of the performance of the subject. The data processing involves temporal features extraction (mean, standard deviation,RMS, maximum and minimum) and machine learning application, that should allow the identification of a pattern relative to STS.

Visual feedback system for the biting and pinching force control The objective evaluation of pinching or biting accuracy can be of support to monitor the progress of neuromuscular pathologies and it gives a reference point for creating personalized rehabilitation therapies. During my first year of PhD studies, I have been working to refine an already existent visual feedback software prototype for the evaluation of the biting and pinching force control. In particular, the graphic interface of the software and the acquisition from the force sensors have been optimized. Moreover, the system has been set for being used coupled with surface emg.

Study of prevalence and mechanical pathogenetic factors of neck pain in the Judoka Among the most common martial arts, judo is the one that has the highest number of reported injuries to the head and neck.The aim of this study was to quantitatively analyze, using inertial sensors applied on the Judoka's body, forces really acting on the athlete's neck during the repeated execution of imbalance techniques. Obtained data will be compared with pathogenic mechanisms already extensively studied including, in particular, those of whiplash, to assess any similarities and develop, therefore, more effective strategies for the prevention of neck pain in Judo.Two inertial sensors (MTw, wireless motion Tracker, Xsens Technologies

B.V.,Enschede, Netherlands)have been used, one placed on the middle of forehead and the other placed on the upper part of the sternum. The preliminary analysis of the collected data seems to confirm that in Judo, the stresses acting on the neck while performing unbalancing techniques are comparable to those recorded in whiplash 67 and, however, characterized by a propagation speed, from the trunk to the head, lower than that of the activation of the muscular response. Faced with a similar antero-posterior acceleration of the head, it was not recorded a vertical acceleration of the head, a mechanism that, in the light of current knowledge on whiplash, seems to be the one the more harmful and primarily responsible for the disorders associated with whiplash.

Inter-muscular adaptations in presence of Trigger Point Musculoskeletal pain of myofascial origin is one of the major causes of increased national health services' costs because of the elevated request of diagnostic imaging and treatments together with the impact on economic costs due to productivity loss. The most accredited cause of myofascial pain is the trigger point(TrP). The present project aim at investigating the relationship between the presence of myofascial trigger point and muscles' recruitment analyzed by means of muscle synergies during a reaching Surface EMG signals were recorded with OT Bioelettronica EMG-USB system. The surface EMG acquisition was conducted simultaneously with the motor performance recordings In order to qualify and quantify the deviation from the desired trajectory, the subjects was equipped with inertial sensors (MTw, wireless motion Tracker, Xsens Technologies B.V.,Enschede, Netherlands to register the motion of the arm in terms of articular angles in a three-dimensional space, velocity and acceleration. The inertial sensors were positioned on the forearm, the arm, on top of the acromion and on the Lewis's sternal angle. The results of this preliminary experiment have shown that muscles with TrP contribute less to the relative activation of synergies containing them in the movement space of reference

Journal of Electromyography and Kinesiology 30 (2016) 243–248

Contents lists available at ScienceDirect

Journal of Electromyography and Kinesiology

journal homepage: www.elsevier.com/locate/jelekin

A validation study of a new instrument for low cost bite force measurement

Marco Testa [a,*], Anna Di Marco [a], Raffaele Pertusio [b], Peter Van Roy [c], Erik Cattrysse [c], Silvestro Roatta [b]

[a] Department of Neuroscience, Rehabilitation, Ophthalmology, Genetics, Maternal and Child Health, University of Genova, Campus of Savona, Italy
[b] Department of Neuroscience, University of Torino, Italy
[c] Department of Experimental Anatomy, Vrije Universiteit Brussel, Belgium

ARTICLE INFO

Article history:
Received 2 July 2016
Received in revised form 1 August 2016
Accepted 8 August 2016

Keywords:
Motor control
Bite Force
Mandible
Masseter muscle
Force transducer

ABSTRACT

Quantitative assessment of force in masticatory muscles is not a routine clinical test, probably due to the lack of an "easy-to-use" device. Aim of this study is (1) to present a low cost bite force instrument located in a custom-made housing, designed to guarantee a comfortable and effective bite action, (2) to evaluate its mechanical characteristics, in order to implement it in clinical settings and in experimental setups.

Linearity, repeatability and adaptation over time were assessed on a set of four different sensors in bare and housed condition. Application of the housing to the transducer may appreciably alter the transducer's response. Calibration of the housed transducer is thus necessary in order to correctly record real bite force. This solution may represent a low cost and reliable option for biting force measurement and objective assessment of individual force control in the scientific and clinical setting.

1. Introduction

Bite force is a biological variable that has been frequently used to assess the function of the masticatory system. Variations of maximum voluntary bite force and precision seem related to different conditions as acutely provoked pain (Wang et al., 2010), chronic orofacial pain (Pereira et al., 2009) and temporomandibular disorders (Bakke and Hansdottir, 2008; Kogawa et al., 2006), occlusal factors (Koc et al., 2011; Trawitzki et al., 2011), wearing dentures (Caloss et al., 2011) or prosthetic implants (Rismanchian et al., 2009) and can be considered as useful indicator in diagnosing the functional status of the masticatory system and monitoring the effectiveness of a therapy.

The first experimental attempt to measure bite force was conducted by Giovanni Alfonso Borrelli and described in his book De Motu Animalium in 1680 (Ortug, 2002). Since then, depending on the available technologies, bite force was measured in different ways. As examples, Castroflorio et al. (2008) used intraoral load cells embedded in customized acrylic splint, Hoyuela et al. (2015) measured jaw elevator muscles force in rheumatoid arthritis women by a bite fork mounted with strain gauge and complex extra oral devices were used to assess bite force and oral reflexes (Turker et al., 2004). The bite force in clinical setting is not yet used as routine outcome measure, while it is extensively measured in research by study-customized devices. Indeed, only few commercial devices for measuring bite force are available and were tested for their reliability. Tscan III (Tekscan Inc, South Boston, USA), a widely used system for assessing forces on dental surfaces, did not show an adequate level of validity in measuring the absolute bite force value, due to individual response behaviour of the pressure sensors utilized by the system (Cerna et al., 2015).

GM10 occlusal force-meter (Nagano Keiki Japan) is a portable bite force gauge that demonstrated a good accuracy and reliability in clinical setting but was found to be uncomfortable due to excessive hardness of the bite (Serra and Manns, 2013). Major practical and technical problems related to measuring the force of bite are:

(1) thickness of the intraoral sensor: excessive interocclusal distance alters the physiological posture of the mandible and affects the developed force. On the other hand miniature load cells are delicate, expensive and not adequate for routine clinical use;
(2) positioning of the sensor: when a single force transducer is placed between the incisors it requires a protrusion of the mandible, which affects the biting force, while placement of the sensor in the premolar or molar region makes the precise repositioning of the sensors more difficult, thus affecting repeatability;

* Corresponding author.
E-mail address: marco.testa@unige.it (M. Testa).

http://dx.doi.org/10.1016/j.jelekin.2016.08.005
1050-6411/

(3) costs: extra oral apparatuses have been developed, connected with servo controlled motors, adequate to investigate motor function and reflexes (Turker et al., 2004; van der Bilt et al., 2006) however, due to their cost and complexity, these systems are more suited for research purposes than for routine clinical examination. Some authors have used load cells mounted on a customized dental (Castroflorio et al., 2008) device to evaluate bite force, but also this approach results in a complex and costly technical procedure.

Aim of this study is to present a much simpler and practical solution, based on a low cost and versatile piezo-resistive force sensor, adequate to measure bite force in a clinical setting. A thin commercial transducer is accommodated within a protective rubberized housing and characterized from the electro-mechanical point of view.

2. Material and methods

2.1. Sensor housing description

Force measurement was based on the piezoresistive force transducer Flexiforce A201 (Tekscan, Boston, MA, USA), featuring a load range of 100 lb, equivalent to 440 N, and a sensitivity of 0.01 V/N. The *FlexiForce* force sensor is a flexible printed circuit with at one end an active sensing area made of pressure-sensitive ink of 1 cm of diameter. The circuit is embedded within two polyester film layers with a final thickness of 0.2 mm (Fig. 1A).

Forces exerted on the active sensing area cause a roughly proportional change of the sensor's conductance. A special housing was developed in order to protect the sensor from mechanical damage and to reduce discomfort for the subject during clenching. The force transducer was inserted in a home made "sandwich structure" composed of different plastic foils and a steel disc, stuck together by bi-adhesive film. The multi-layer "L" shaped housing was developed as shown in Fig. 1B and C. The external layer is made of a silicone rubber material, commonly used in preparing dental orthotics (Bioplast – Scheudental - Germany). This layer provides the possibility of small yielding of the surface under the teeth, thereby generating a wider contact surface, thus lowering local pressure. It also provides improved comfort during clenching, as compared to a hard surface. An internal thinner layer is made of two hard plastic foils, which provide a flexible support as well as a graduated handle for the housed sensor. The force transducer is inserted in-between the two plastic foils, coupled with a metal disc (diameter = 10 mm, thickness 0.8 mm) located exactly below the sensory area of the transducer and fixed by bi-adhesive film to the plastic foil and the transducer. The steel disc ensures that virtually all the force lines between upper and lower teeth are conveyed through that area, according to recommendation given by the manufacturer in the flexiforce user manual (https://www.tekscan.com/support/faqs/flexiforce-user-manual). The lateral, short arm of the "L" structure can be shortened by simply cutting the excess with scissors in order to adapt to the latero-lateral dimension of the subject's mouth.

Since the sensor does not tolerate heat or immersion sterilization, it should be inserted into a disposable latex or nitrile glove in order to prevent contact with saliva and thus exclude the need for sterilization. Final thickness of the housed sensor is about 7 mm and decreases to (5–6) mm after some pressure is exerted by the teeth, slightly accommodating in the superficial layer. This allows jaw-elevator muscles fibers to work at optimal length, therefore permitting an adequate expression of force (Fernandes et al., 2003; Manns et al., 1979).

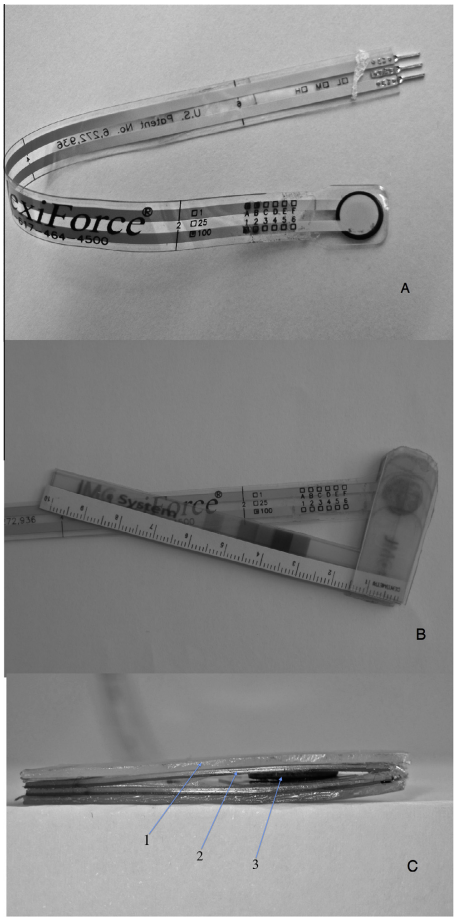

Fig. 1. (A) – The piezoresistive film sensor. (B) – Housed transducer, top view. (C) – Housed transducer, lateral view: (1) external silicone layer, (2) internal hard plastic layer, (3) metal disc.

A graduated handle allows for accurate repositioning along the antero-posterior direction, in different experimental sessions. Moreover, the "L" shape of the housing allows both the sensor and the graduated handle to exit the mouth through the interincisal opening, thus preventing damage by canine teeth.

2.2. Device characterization

Force-output measurements of bare and housed transducer have been performed on a set of four A 201 Flexiforce devices. The sensor under test was first preconditioned according to the manufacturer recommendations (https://www.tekscan.com/support/faqs/flexiforce-user-manual). The preconditioning consisted of loading the sensor up to 490 N for 30 s for three times. This treatment was actually repeated few more times to improve

stability of the transducer. A lever system and a set of weights was used to apply controlled loads in the range 0–314 N.

The lever system was progressively loaded and unloaded in eight steps of 39 N. (0-39-78-118-157-196-235-274-314-314-274 -235-196-157-118-78-39-0). The whole procedure lasted about 5 min. The load was exerted perpendicularly to the sensor surface through a conic head of 10 mm in diameter, corresponding to the active area of the flexiforce transducer and was measured by a load cell. In order to assess relative and absolute reliability of the measurement in both conditions, this procedure was performed on the bare and on the housed sensor and repeated after 24 h.

In addition, in order to test the dependence of the sensor response on the contact surface, four transducer were loaded (300 N) against a smooth or rough Plexiglas surface.

Finally, the application of a constant load of 390 N for 4 min was performed to investigate the output drift over time.

Electric signals generated by the cell and by the Flexiforce transducer were amplified, sampled at 15 Hz and digitally-converted (16 bit) by a dedicated hardware (Cal4met, OT Bioelettronica, Torino, Italy) and transmitted to a personal computer (via USB). Numerical data were acquired and stored by a custom-made software written in Matlab (Mathworks, Natick, Massachusetts, USA). Measures from the load cell are expressed in Newton (N), while readings from the sensors are in Volt (V). Linear fitting of sensor load/unload-response curve provided a measure of the sensor sensitivity (slope) and of linearity (R^2) in both the bare and housed condition. Hysteresis has been defined as difference between the areas under the loading and unloading curves, divided to the area under the loading curve, and the relative means were calculated on absolute values. Relative reliability was assessed by Intraclass Correlation Coefficient (ICC) and absolute reliability by Standard Error of Measurement (SEM) and by Bland and Altman's 95% Limits of Agreement (LOA). Calculations were conducted using "R" software (R Core Team, 2013).

3. Results

3.1. Sensor characterization

The characteristic load-response curves of four different sensors in bare and housed conditions have been measured in two consecutive days. Their qualitative behaviour is given in Fig. 2.

Table 1
Values of intercept (in V) and slope (in V/N) of each sensors in bare and housed conditions and in two days.

	Condition	Day	Intercept (V)	Slope (V/N)	R^2	p
SENSOR 1	Bare	*First*	0.23	0.0039	0.97	<0.001
		Second	0.24	0.0039	0.96	<0.001
	Housed	*First*	0.30	0.0054	0.97	<0.001
		Second	0.29	0.0052	0.96	<0.001
SENSOR 2	Bare	*First*	0.34	0.0051	0.95	<0.001
		Second	0.34	0.0055	0.95	<0.001
	Housed	*First*	0.27	0.0063	0.98	<0.001
		Second	0.31	0.0058	0.96	<0.001
SENSOR 3	Bare	*First*	0.22	0.0038	0.97	<0.001
		Second	0.23	0.0032	0.96	<0.001
	Housed	*First*	0.23	0.0056	0.99	<0.001
		Second	0.25	0.0059	0.98	<0.001
SENSOR 4	Bare	*First*	0.21	0.0042	0.98	<0.001
		Second	0.21	0.0039	0.98	<0.001
	Housed	*First*	0.24	0.0060	0.98	<0.001
		Second	0.26	0.0061	0.98	<0.001

The different sensors showed a similar load-response curve, slightly decreasing the slope at increasing load.

Regression analysis of the curve for each sensor in bare and housed condition and in the two days was performed (Table 1). It can be observed that the slope of the regression line, i.e. the sensor sensitivity, may appreciably change in the different sensors (e.g.: 0.004–0.005 V/N, bare sensors, day 1). Moreover, it was systematically higher in the housed than in the bare condition. As for the intercept, ranging between 0.15 and 0.34 V, it is to be attributed to a specific feature of the hardware, which introduces a positive offset in order to avoid negative output at 0 load. Linearity of the curves was in all cases very high (R^2 > 0.94) and little affected by the housing.

Mean absolute values of hysteresis, calculated over all sensors and both days was about 0.9% either in bare (range: 0.002–2.177%) and in housed condition (range: 0.065-4.707%).

Between days relative reliability was very high: ICC1: 0.99; CI: 0.98–0.99 (bare sensors) and ICC1: 0.98; CI: 0.97–0.99 (housed sensors) as such as absolute reliability described by SEM (0.04 V

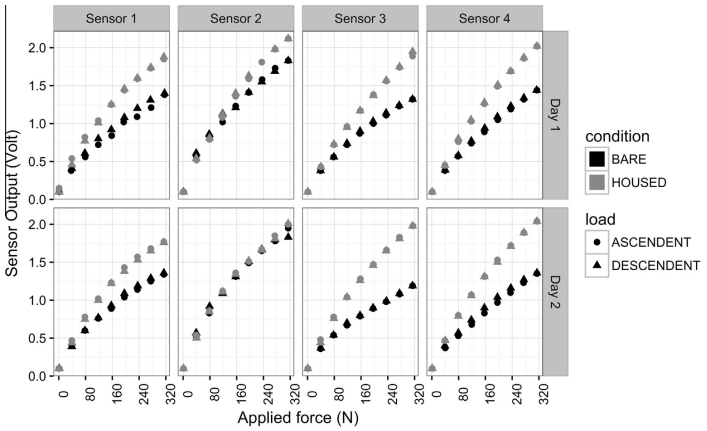

Fig. 2. Individual load-response curve of the four sensors in bare and housed conditions. Ascending (circle) and descending (triangle) for the bare (black) and housed sensor (grey).

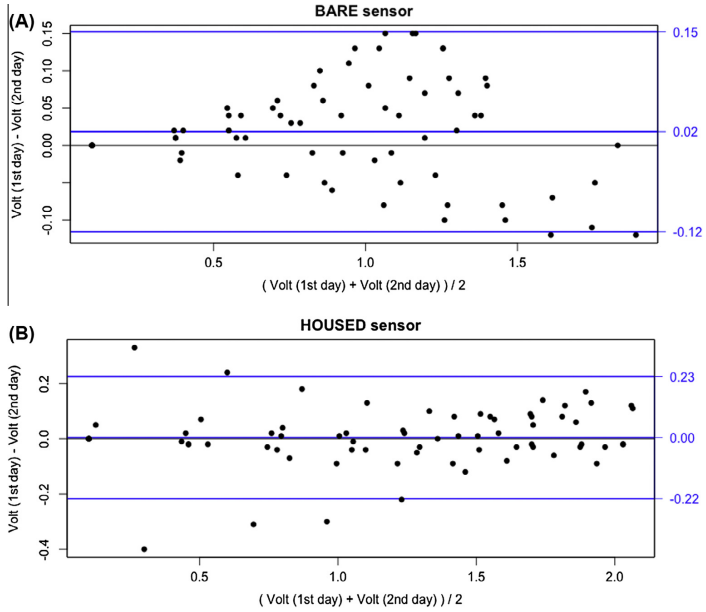

Fig. 3. Limit of Agreement of the four sensors: (A) in bare condition; (B) in housed condition.

for the bare and 0.06 V for the housed) and by Bland & Altman plots (Fig. 3A and B).

When the sensors were loaded with a constant force of 300 N against a smooth Plexiglas surface the average output was 1.015 ± 0.126 V and consistently decreased to 0.645 ± 0.104 V when loaded against a rough surface, individual decrease ranging from 33 to 40% in the different sensors.

The response to a sustained load of 390 N for 4 min conducted on bare sensors produced a small drift in the output of 0.7 ± 0.6% at 1 min, stabilizing at 1 ± 0.5% at 4 min.

4. Discussion

The low-cost system for the measurement of biting force here described provides a satisfactory performance in terms of linearity, reliability and response to constant load.

The load-response curves in bare and housed condition showed that sensitivity (1) is highly variable between different sensors. (2) slightly decreases at increasing load due to non-perfect linearity; (3) is substantially increased by application of the housing (by 35%, on average).

It was surprising to see the sensitivity of the sensor increased after application of the housing.

In fact, a decrease of sensitivity was expected instead of an increase, considering that in the housed sensor part of the load could be transmitted through the housing rather than through the piezoresistive area of the sensor. To prevent this risk and to make experimental measurements less dependent on the shape of the contact surface of the teeth, increased separation between upper and lower surfaces of the housing, was pursued by the insertion of the metal disks (Fig. 1). The increased sensitivity introduced by the housing must then be attributed to the different nature (hardness, roughness. . .) of the surfaces taking direct contact with the sensor. In fact, when the same load was tested against a rough rather then a smooth plexiglas surface the force reading was shown to decrease by as much as 40%.

The observed non linearity is very small ($R^2 > 0.94$) and is most likely to be attributed to the signal conditioning, based on a non inverting amplifier and also implementing low-pass filtering and electrical isolation. This non-linearity and the individual variability of the sensitivity may potentially result in a systematic error. However this error may be easily prevented by implementing a multi-point sensor calibration, in the specific load range of the measurement. In this way reliable recording of absolute force values can be achieved. Due to the large dependence of the sensor response on the contact surfaces, it is advisable to apply the housing prior to calibration.

As already mentioned in the results, a little offset (sensor output at 0 load) is introduced by the housing. This offset needs to be accounted for by the calibration procedure and removed, in order to prevent large errors at low load conditions.

Although we did not assess the effect of temperature change on the sensor output, the variation reported by the manufacturer in the user manual of the flexiforce sensor (https://www.tekscan.com/support/faqs/flexiforce-user-manual) is about 0.36%/°C. If we account for 15–17 degrees of temperature difference between the sensor when tested at the bench and when located in the mouth, this variation would be in the order of 5–6%. However, a similar variation is expected to occur in all subjects thus producing negligible changes in the comparisons between subjects or between sides of the same subject.

Sensors operating in the mouth are also potentially exposed to high humidity, whose effect has not been tested in the present

study, however exposure to saliva and humidity may be prevented by shielding the sensor with a latex or nitrile finger glove.

Plastic and rubber shielding of the sensor was proven to improve comfort and stability of the force signal (Fernandes et al., 2003; Waltimo and Kononen, 1993). The present results indicate that, although increasing the sensitivity of the sensor, as discussed above, the housing does not affect its linearity. The nominal working range of the sensor (440 N) is adequate for use with adult subjects. In case a wider or smaller range of registration is needed, it could be scaled up or down by adjusting the sensor's dynamic range by tweaking its external drive circuit. The values of interday relative and absolute reliability obtained by testing the sensors in bare and housed condition were quite high. Bland and Altman plots revealed a slightly better performance of the sensors in housed condition. The present device has already been employed in two preclinical studies. In a sample of seventeen volunteers the control of unilateral bite force was assessed during a reach and hold task (Testa et al., 2011) This trial demonstrated a good reliability of the measurements (ICC ranged between 74% and 88%). In a subsequent study, the device was employed to assess bilateral control of bite force, two sensors being placed between left and right molars during an isometric task requiring independent adjustment of force on the two sides. Also in this case, the reliability was quite good (ICC of different force indices ranging from 0.66 to 0.78) (Testa et al., 2015b).

Recently, the system for bite force recording was used, coupled with surface electromyography, in a group of patients affected by chronic neck pain to assess the modification of masticatory muscles recruitment during bite force reach and hold tasks (Testa et al., 2015a).

In each of the above described trials the housed sensors were well tolerated, thanks to the limited thickness (5–6) mm and the rubber surface. When inserting a device of such thickness between the first or second molar, the mouth opens by no >2–3 mm of inter-incisal distance. It means that the condyles stay almost centred in the fossa temporalis, the position corresponding to most of the common jaw activities (Osborn, 1989). The inter-incisal space allows the passage of the graduated handle (long arm of the "L" shaped sensor), proving useful for accurate device repositioning. Film-based force sensors provide a potentially interesting means to measure biting force, given their very low thickness and low cost, however only few applications have been presented in the dentistry field up to now (Baba et al., 2003; Fernandes et al., 2003; Maki et al., 2001; Miura et al., 2001; Rottner and Richter, 2004; Takeuchi et al., 2001). The reason of this scarce utilization could be that these sensors are still considered less precise and accurate than load cells, even if in one study the film sensors compared with a conventional bite force transducer demonstrated a better performance (Fernandes et al., 2003). The system proposed by Fernandes et al. (2003) adopted a steel disc presenting a small bulge in the centre, aimed to exert pressure on the transducer. In case of repetitive measurements, this solution, could damage the sensor and reduce its life. The presented customized housing provided with a flat steel disc permits to re-use several times the film sensors (up to 6–8 times in our experience), significantly reducing the costs of each exam.

A system called T-SCAN and its upgrade (*T-SCAN II and III*) had a good success and diffusion in clinical practice among dentists. (***Tekscan, Inc.*** *307 West First Street. South Boston, MA. 02127-1309, USA*) This system uses a film sensor to record the distribution of occlusal forces which is graphically described over the occlusal surface by a qualitative colorimetric representation of dental contact-intensity. The information given by the system can support clinical decision in prosthetic dentistry, but has limited value in giving information about the neuromuscular control of the bite force.

In other studies film sensors were embedded in splints for long duration recordings (Baba et al., 2003; Takeuchi et al., 2001). Recently Castroflorio et al. (2008) proposed a system of bite force registration that is based on customized upper and lower dental appliances. These systems must be customized for each subject with significant extra costs. In addition, the complexity of the procedure limits its application within dentistry departments. The piezo-resistive force transducer used in the present study has comparable shape and dimensions to the one used by Fernandes et al. (2003) and shows similar characteristics in terms of measurement errors, making this sensor a potentially useful tool for routine clinical examinations, provided sensor calibration in its working condition is carefully accomplished.

5. Conclusions

A simple instrument to measure bite force, based on a commercially available sensor inserted in a protective housing and connected to a simple hardware has been developed. The limited thickness of the developed sensor, the easy repositioning of the device in the mouth and its low cost overcome the most common problems encountered in bite force measuring. Indeed, the housing of the sensor can be assembled by hand and the signal conditioning can be obtained by adopting the hardware recommended by the manufacturer or another equivalent solution like the one we have used in the present work.

The characterization tests showed that the presence of the housing layers does not worsen, but on the contrary enhance the sensitivity of the sensor. Accurate preconditioning and subsequent calibration of the housed sensor in its working conditions, by acquisition of the I/O response curve over the load range of interest, is recommended in order to account for the many limitation including non linearity, individual variability of the sensitivity and dependence of the output response on the nature of the contact surfaces.

The proposed transducer may be a handy solution to assess the bite force in the clinical setting and a valid support for standardization of EMG studies on jaw-closing muscles.

Conflict of interest

The authors declare that there is no conflict of interests regarding the publication of this paper.

Acknowledgements

The authors thank Tommaso Geri for his valuable support to the statistical analysis of the data.

References

Baba, K., Clark, G.T., Watanabe, T., Ohyama, T., 2003. Bruxism force detection by a piezoelectric film-based recording device in sleeping humans. J. Orofacial Pain. 17, 58–64.
Bakke, M., Hansdottir, R., 2008. Mandibular function in patients with temporomandibular joint pain: a 3-year follow-up. Oral Surg. Oral Med. Oral Pathol. Oral Radiol. Endod. 106, 227–234.
Caloss, R., Al-Arab, M., Finn, R.A., Throckmorton, G.S., 2011. The effect of denture stability on bite force and muscular effort. J. Oral Rehabil. 38, 434–439.
Castroflorio, T., Bracco, P., Farina, D., 2008. Surface electromyography in the assessment of jaw elevator muscles. J. Oral Rehabil. 35, 638–645.
Cerna, M., Ferreira, R., Zaror, C., Navarro, P., Sandoval, P., 2015. Validity and reliability of the T-Scan((R)) III for measuring force under laboratory conditions. J. Oral Rehabil. 42, 544–551.
Fernandes, C.P., Glantz, P.O., Svensson, S.A., Bergmark, A., 2003. A novel sensor for bite force determinations. Dent. Mater. 19, 118–126.
Hoyuela, C.P., Furtado, R.N., Chiari, A., Natour, J., 2015. Oro-facial evaluation of women with rheumatoid arthritis. J. Oral Rehabil. 42, 370–377.
Koc, D., Dogan, A., Bek, B., 2011. Effect of gender, facial dimensions, body mass index and type of functional occlusion on bite force. J. Appl. Oral Sci. 19, 274–279.
Kogawa, E.M., Calderon, P.S., Lauris, J.R., Araujo, C.R., Conti, P.C., 2006. Evaluation of maximal bite force in temporomandibular disorders patients. J. Oral Rehabil. 33, 559–565.

Maki, K., Nishioka, T., Morimoto, A., Naito, M., Kimura, M., 2001. A study on the measurement of occlusal force and masticatory efficiency in school age Japanese children. Int. J. Pediatr. Dent. 11, 281–285.
Manns, A., Miralles, R., Palazzi, C., 1979. EMG, bite force, and elongation of the masseter muscle under isometric voluntary contractions and variations of vertical dimension. J. Prosthet. Dent. 42, 674–682.
Miura, H., Watanabe, S., Isogai, E., Miura, K., 2001. Comparison of maximum bite force and dentate status between healthy and frail elderly persons. J. Oral Rehabil. 28, 592–595.
Ortug, G., 2002. A new device for measuring mastication force (Gnathodynamometer). Ann Anat. 184, 393–396.
Osborn, J.W., 1989. The temporomandibular ligament and the articular eminence as constraints during jaw opening. J. Oral Rehabil. 16, 323–333.
Pereira, L.J., Steenks, M.H., de Wijer, A., Speksnijder, C.M., van der Bilt, A., 2009. Masticatory function in subacute TMD patients before and after treatment. J. Oral Rehabil. 36, 391–402.
R Core Team, 2013. R: A Language and Environment for Statistical Computing. R Foundation for Statistical Computing, Vienna, Austria.
Rismanchian, M., Bajoghli, F., Mostajeran, Z., Fazel, A., Eshkevari, P., 2009. Effect of implants on maximum bite force in edentulous patients. J. Oral Implantol. 35, 196–200.
Rottner, K., Richter, E.J., 2004. Effect of occlusal morphology on the accuracy of bite force measurements using thin film transducers. Int. J. Prosthodontics. 17, 518–523.
Serra, C.M., Manns, A.E., 2013. Bite force measurements with hard and soft bite surfaces. J. Oral Rehabil. 40, 563–568.
Takeuchi, H., Ikeda, T., Clark, G.T., 2001. A piezoelectric film-based intrasplint detection method for bruxism. J. Prosthet. Dent. 86, 195–202.
Testa, M., Geri, T., Gizzi, L., Petzke, F., Falla, D., 2015a. Alterations in masticatory muscle activation in people with persistent neck pain despite the absence of orofacial pain or temporomandibular disorders. J. Oral Facial Pain Headache 29, 340–348.
Testa, M., Geri, T., Signori, A., Roatta, S., 2015b. Visual feedback of bilateral bite force to assess motor control of the mandible in isometric condition. Mot. Control 19, 312–324.
Testa, M., Rolando, M., Roatta, S., 2011. Control of jaw-clenching forces in dentate subjects. J. Orofacial Pain. 25, 250–260.
Trawitzki, L.V., Silva, J.B., Regalo, S.C., Mello-Filho, F.V., 2011. Effect of class II and class III dentofacial deformities under orthodontic treatment on maximal isometric bite force. Arch. Oral Biol. 56, 972–976.
Turker, K.S., Brinkworth, R.S., Abolfathi, P., Linke, I.R., Nazeran, H., 2004. A device for investigating neuromuscular control in the human masticatory system. J. Neurosci. Methods 136, 141–149.
van der Bilt, A., Engelen, L., Pereira, L.J., van der Glas, H.W., Abbink, J.H., 2006. Oral physiology and mastication. Physiol. Behav. 89, 22–27.
Waltimo, A., Kononen, M., 1993. A novel bite force recorder and maximal isometric bite force values for healthy young adults. Scand. J. Dent. Res. 101, 171–175.
Wang, M.Q., He, J.J., Zhang, J.H., Wang, K., Svensson, P., Widmalm, S.E., 2010. SEMG activity of jaw-closing muscles during biting with different unilateral occlusal supports. J. Oral Rehabil. 37, 719–725.

Marco Testa was born in Alassio on May 16 1962. Graduated in Physical Education in 1985 and in Physiotherapy in 1988. He works as assistant professor at the Department of Neuroscience, Rehabilitation, Ophthalmology, Genetic, Maternal and Child Health of the University of Genova – Campus of Savona. He is president of the Master in Rehabilitation of Musculoskeletal Disorders (www.masteromt.unige.it). He teaches Manual Therapy in the School of Physiotherapy and Physical Medicine and Rehabilitation at the Medical Specialty of Rheumatology of the University of Genova.

Anna Di Marco was born in Gaeta (Italy) in 1987. She graduated in Biomedical Engineering from Politecnico di Torino in 2013 with a master thesis on the development of an high magnetic field compatible optical encoder conducted at Imperial College of London in UK. From April 2014 to September 2014 she has worked at LiSIN in Torino. Since October 2014 she is a PhD fellow in Neuroscience at University of Genova. From February 2015 to April 2015 She has conducted a research project focus on correlation between Neck Pain and Jaw Muscle force at the Department of Neurorehabilitation Engineering in Gottingen in Germany. Her research interest mainly focus on biomedical signal processing for EMG investigation and movement analysis. Actually she is working on analysis of Sit to stand.

Raffaele Pertusio (PhD) is a biomedical engineer, working as technician at the Department of Neuroscience of the University of Torino, Italy. After graduation from the Polytechnic of Turin in 1999, he started working at the Mechanical Department and currently collaborates with the Integrative Physiology Group.

Peter Van Roy (PhD, PT) is professor emeritus of anatomy and applied biomechanics at the Departments of Experimental Anatomy and Manual Therapy of the Vrije Universiteit Brussel (VUB), Brussels, Belgium (1989–2012). In the first part of his career, he worked as physiotherapist, and as lecturer in schools of physiotherapy in Brussels (BE), Utrecht (NL) and Landquart (CH). He has been director of schools of physiotherapy in Belgium and Switzerland. In 1989, he received the Sport Science Award of the I.O.C.-President for the paper "Three-Dimensional Kinematic Study of the Screw-Home Movement of the Knee Joint Using Magnetic Resonance Imaging". Subsequently, he developed an academic career at the VUB with the following topics of research: anatomical variants of the musculoskeletal system, 3D joint kinematics, and correlative anatomy with medical imaging. This resulted in numerous publications in national and international scientific journals, congress proceedings and books. He has been vice-dean (2004–2008) and dean (2008–2012) of the faculty of Physical Education and Physiotherapy of the VUB. At present, he is president of the Federal Council for Physiotherapy in Belgium.

Erik Cattrysse has a PhD in Rehabilitation Sciences and Physiotherapy and a master of Science in Manual Therapy. He is assistant Professor and head of the Experimental Anatomy research department. His main field of interest concerns the study of anatomy and its variations and kinematics of the cervical spine in-vitro and in-vivo.

Silvestro Roatta received his degree in Electrical Engineering from Politecnico di Torino (1993) and his Ph.D in Physiology from the University of Torino (1997). Currently, he is Associate Professor of Physiology and head of the Integrative Physiology Lab, at the Dept of Neuroscience, University of Torino. His research interests include stress and sympathetic modulation of muscle and motor function, motor control of the mandible in health and disease and the control blood flow in skeletal muscle. He teaches Human Physiology at the School of Dentistry, and at the School of Biomedical Engineering and is director of the Master in Echography for Nurses and Obstetricians (MEPIO) He published over 40 articles on peer-reviewed journals.

Bibliography

[1] S. Bajelan and M. R. Azghani. Musculoskeletal analysis of sit-to-stand maneuver in order to compare the various standing up strategies. In *2011 18th Iranian Conference of Biomedical Engineering (ICBME)*, pages 215–220, Dec 2011. doi: 10.1109/ICBME.2011.6168559.

[2] S.S. Coghlin and B.J. McFadyen. Transfer strategies used to rise from a chair in normal and low back pain subjects. *Clinical Biomechanics*, 9(2):85 – 92, 1994. ISSN 0268-0033. doi: https://doi.org/10.1016/0268-0033(94)90029-9. URL http://www.sciencedirect.com/science/article/pii/0268003394900299.

[3] Amy Gross McMillan and John P Scholz. Early development of coordination for the sit-to-stand task. *Human Movement Science*, 19(1):21 – 57, 2000. ISSN 0167-9457. doi: https://doi.org/10.1016/S0167-9457(00)00007-5. URL http://www.sciencedirect.com/science/article/pii/S0167945700000075.

[4] Kaiyu Tong and Malcolm H Granat. A practical gait analysis system using gyroscopes. *Medical Engineering & Physics*, 21(2):87 – 94, 1999. ISSN 1350-4533. doi: https://doi.org/10.1016/S1350-4533(99)00030-2. URL http://www.sciencedirect.com/science/article/pii/S1350453399000302.

[5] Jennifer Howcroft, Jonathan Kofman, and Edward D. Lemaire. Review of fall risk assessment in geriatric populations using inertial sensors. *Journal*

of NeuroEngineering and Rehabilitation, 10(1):91, Aug 2013. ISSN 1743-0003. doi: 10.1186/1743-0003-10-91. URL https://doi.org/10.1186/1743-0003-10-91.

[6] Mohammad Ashfak Habib, Mas S. Mohktar, Shahrul Bahyah Kamaruzzaman, Kheng Seang Lim, Tan Maw Pin, and Fatimah Ibrahim. Smartphone-based solutions for fall detection and prevention: Challenges and open issues. *Sensors*, 14(4):7181–7208, 2014. ISSN 1424-8220. doi: 10.3390/s140407181. URL http://www.mdpi.com/1424-8220/14/4/7181.

[7] Diane Podsiadlo and Sandra Richardson. The timed "up & go": A test of basic functional mobility for frail elderly persons. *Journal of the American Geriatrics Society*, 39(2):142–148, 1991. doi: 10.1111/j.1532-5415.1991.tb01616.x. URL https://onlinelibrary.wiley.com/doi/abs/10.1111/j.1532-5415.1991.tb01616.x.

[8] Pao-Tsai Cheng, Mei-Yun Liaw, May-Kuen Wong, Fuk-Tan Tang, Ming-Yih Lee, and Pay-Shin Lin. The sit-to-stand movement in stroke patients and its correlation with falling. *Archives of Physical Medicine and Rehabilitation*, 79(9):1043 – 1046, 1998. ISSN 0003-9993. doi: https://doi.org/10.1016/S0003-9993(98)90168-X. URL http://www.sciencedirect.com/science/article/pii/S000399939890168X.

[9] Yuan-Yang Cheng, Shun-Hwa Wei, Po-Yin Chen, Mei-Wun Tsai, I.-Chung Cheng, Ding-Hao Liu, and Chung-Lan Kao. Can sit-to-stand lower limb muscle power predict fall status? *Gait & Posture*, 40(3):403 – 407, 2014. ISSN 0966-6362. doi: https://doi.org/10.1016/j.gaitpost.2014.05.064. URL http://www.sciencedirect.com/science/article/pii/S0966636214005967.

[10] Susan L Whitney, Diane M Wrisley, Gregory F Marchetti, Michael A Gee, Mark S Redfern, and Joseph M Furman. Clinical measurement of sit-to-stand

performance in people with balance disorders: Validity of data for the five-times-sit-to-stand test. *Physical Therapy*, 85(10):1034–1045, 2005. doi: 10.1093/ptj/85.10.1034. URL http://dx.doi.org/10.1093/ptj/85.10.1034.

[11] Richard W. Bohannon. Sit-to-stand test for measuring performance of lower extremity muscles. *Perceptual and Motor Skills*, 80(1):163–166, 1995. doi: 10.2466/pms.1995.80.1.163. URL https://doi.org/10.2466/pms.1995.80.1.163. PMID: 7624188.

[12] Jack M. Guralnik Eleanor M. Simonsick Luigi Ferrucci Robert J. Glynn Lisa F. Berkman Dan G. Blazer Paul A. Scherr Robert B. Wallace. A short physical performance battery assessing lower extremity function: Association with self-reported disability and prediction of mortality and nursing home admission. *Journal of Gerontology*, 49:M85–M94, March 1994. doi: https://doi.org/10.1093/geronj/49.2.M85.

[13] Erick K. McCarthy, Michael A. Horvat, Philip A. Holtsberg, and Joseph M. Wisenbaker. Repeated chair stands as a measure of lower limb strength in sexagenarian women. *The Journals of Gerontology: Series A*, 59(11):1207–1212, 2004. doi: 10.1093/gerona/59.11.1207. URL http://dx.doi.org/10.1093/gerona/59.11.1207.

[14] J. Ghika, A. W. Wiegner, J. J. Fang, L. Davies, R. R. Young, and J. H. Growdon. Portable system for quantifying motor abnormalities in parkinson's disease. *IEEE Transactions on Biomedical Engineering*, 40(3):276–283, March 1993. ISSN 0018-9294. doi: 10.1109/10.216411.

[15] Bruce Etnyre and David Q Thomas. Event standardization of sit-to-stand movements. *Physical Therapy*, 87(12):1651–1666, 2007. doi: 10.2522/ptj.20060378. URL http://dx.doi.org/10.2522/ptj.20060378.

[16] Margaret Schenkman, Richard A Berger, Patrick Riley, Robert W Mann, and

W Andrew Hodge. Whole-body movements during rising to standing from sitting. *Physical therapy*, 70:638–48; discussion 648, 11 1990. doi: 10.1093/ptj/70.10.638.

[17] Eline van der Kruk and Marco M. Reijne. Accuracy of human motion capture systems for sport applications; state-of-the-art review. *European Journal of Sport Science*, 18(6):806–819, 2018. doi: 10.1080/17461391.2018.1463397. URL https://doi.org/10.1080/17461391.2018.1463397. PMID: 29741985.

[18] Jennifer Howcroft, Jonathan Kofman, and Edward D. Lemaire. Review of fall risk assessment in geriatric populations using inertial sensors. *Journal of NeuroEngineering and Rehabilitation*, 10(1):91, Aug 2013. ISSN 1743-0003. doi: 10.1186/1743-0003-10-91. URL https://doi.org/10.1186/1743-0003-10-91.

[19] CJ Thompson and MG Bemben. Reliability and comparability of the accelerometer as a measure of muscular power. *Medicine and science in sports and exercise*, 31(6):897—902, June 1999. ISSN 0195-9131. doi: 10.1097/00005768-199906000-00020. URL https://doi.org/10.1097/00005768-199906000-00020.

[20] Milica D. Djurić-Jovičić, Nenad S. Jovičić, and Dejan B. Popović. Kinematics of gait: New method for angle estimation based on accelerometers. *Sensors*, 11(11):10571–10585, 2011. ISSN 1424-8220. doi: 10.3390/s111110571. URL http://www.mdpi.com/1424-8220/11/11/10571.

[21] A. Godfrey, A.K. Bourke, G.M. Ólaighin, P. van de Ven, and J. Nelson. Activity classification using a single chest mounted tri-axial accelerometer. *Medical Engineering & Physics*, 33(9):1127 – 1135, 2011. ISSN 1350-4533.

doi: https://doi.org/10.1016/j.medengphy.2011.05.002. URL http://www.sciencedirect.com/science/article/pii/S1350453311001111.

[22] B. Najafi, K. Aminian, F. Loew, Y. Blanc, and P. A. Robert. Measurement of stand-sit and sit-stand transitions using a miniature gyroscope and its application in fall risk evaluation in the elderly. *IEEE Transactions on Biomedical Engineering*, 49(8):843–851, Aug 2002. ISSN 0018-9294. doi: 10.1109/TBME.2002.800763.

[23] Y. Higashi, K. Yamakoshi, T. Fujimoto, M. Sekine, and T. Tamura. Quantitative evaluation of movement using the timed up-and-go test. *IEEE Engineering in Medicine and Biology Magazine*, 27(4):38–46, July 2008. ISSN 0739-5175. doi: 10.1109/MEMB.2008.919494.

[24] Alejandro Galán-Mercant and Antonio I. Cuesta-Vargas. Differences in trunk accelerometry between frail and non-frail elderly persons in functional tasks. *BMC Research Notes*, 7(1):100, Feb 2014. ISSN 1756-0500. doi: 10.1186/1756-0500-7-100. URL https://doi.org/10.1186/1756-0500-7-100.

[25] Alejandro Galán-Mercant and Antonio I Cuesta-Vargas. Differences in trunk accelerometry between frail and nonfrail elderly persons in sit-to-stand and stand-to-sit transitions based on a mobile inertial sensor. *JMIR Mhealth Uhealth*, 1(2):e21, Aug 2013. ISSN 2291-5222. doi: 10.2196/mhealth.2710. URL http://mhealth.jmir.org/2013/2/e21/.

[26] B. Aguiar, T. Rocha, J. Silva, and I. Sousa. Accelerometer-based fall detection for smartphones. In *2014 IEEE International Symposium on Medical Measurements and Applications (MeMeA)*, pages 1–6, June 2014. doi: 10.1109/MeMeA.2014.6860110.

[27] C. Tacconi, S. Mellone, and L. Chiari. Smartphone-based applications for

investigating falls and mobility. In *2011 5th International Conference on Pervasive Computing Technologies for Healthcare (PervasiveHealth) and Workshops*, pages 258–261, May 2011. doi: 10.4108/icst.pervasivehealth.2011.246060.

[28] Shu Nishiguchi, Minoru Yamada, Koutatsu Nagai, Shuhei Mori, Yuu Kajiwara, Takuya Sonoda, Kazuya Yoshimura, Hiroyuki Yoshitomi, Hiromu Ito, Kazuya Okamoto, Tatsuaki Ito, Shinyo Muto, Tatsuya Ishihara, and Tomoki Aoyama. Reliability and validity of gait analysis by android-based smartphone. *Telemedicine and e-Health*, 18(4):292–296, 2012. doi: 10.1089/tmj.2011.0132. URL https://doi.org/10.1089/tmj.2011.0132. PMID: 22400972.

[29] Farzin Dadashi, Benoit Mariani, Stephane Rochat, Christophe J. Büla, Brigitte Santos-Eggimann, and Kamiar Aminian. Gait and foot clearance parameters obtained using shoe-worn inertial sensors in a large-population sample of older adults. *Sensors*, 14(1):443–457, 2014. ISSN 1424-8220. doi: 10.3390/s140100443. URL http://www.mdpi.com/1424-8220/14/1/443.

[30] A. M. Sabatini, C. Martelloni, S. Scapellato, and F. Cavallo. Assessment of walking features from foot inertial sensing. *IEEE Transactions on Biomedical Engineering*, 52(3):486–494, March 2005. ISSN 0018-9294. doi: 10.1109/TBME.2004.840727.

[31] Barry R. Greene, Denise McGrath, Ross O'Neill, Karol J. O'Donovan, Adrian Burns, and Brian Caulfield. An adaptive gyroscope-based algorithm for temporal gait analysis. *Medical & Biological Engineering & Computing*, 48(12):1251–1260, Dec 2010. ISSN 1741-0444. doi: 10.1007/s11517-010-0692-0. URL https://doi.org/10.1007/s11517-010-0692-0.

[32] Carolin Jakob, Patrick Kugler, Felix Hebenstreit, Samuel Reinfelder, Ulf

Jensen, Dominik Schuldhaus, Matthias Lochmann, and Bjoern M. Eskofier. Estimation of the knee flexion-extension angle during dynamic sport motions using body-worn inertial sensors. In *Proceedings of the 8th International Conference on Body Area Networks*, BodyNets '13, pages 289–295, ICST, Brussels, Belgium, Belgium, 2013. ICST (Institute for Computer Sciences, Social-Informatics and Telecommunications Engineering). ISBN 978-1-936968-89-3. doi: 10.4108/icst.bodynets.2013.253613. URL http://dx.doi.org/10.4108/icst.bodynets.2013.253613.

[33] A. J. Wixted, D. C. Billing, and D. A. James. Validation of trunk mounted inertial sensors for analysing running biomechanics under field conditions, using synchronously collected foot contact data. *Sports Engineering*, 12(4): 207–212, Aug 2010. ISSN 1460-2687. doi: 10.1007/s12283-010-0043-2. URL https://doi.org/10.1007/s12283-010-0043-2.

[34] Miranda C. Boonstra, Rienk M.A. van der Slikke, Noël L.W. Keijsers, Rob C. van Lummel, Maarten C. de Waal Malefijt, and Nico Verdonschot. The accuracy of measuring the kinematics of rising from a chair with accelerometers and gyroscopes. *Journal of Biomechanics*, 39(2):354 – 358, 2006. ISSN 0021-9290. doi: https://doi.org/10.1016/j.jbiomech.2004.11.021. URL http://www.sciencedirect.com/science/article/pii/S0021929004005871.

[35] Emer P. Doheny, Cathal Walsh, Timothy Foran, Barry R. Greene, Chie Wei Fan, Clodagh Cunningham, and Rose Anne Kenny. Falls classification using tri-axial accelerometers during the five-times-sit-to-stand test. *Gait & Posture*, 38(4):1021 – 1025, 2013. ISSN 0966-6362. doi: https://doi.org/10.1016/j.gaitpost.2013.05.013. URL http://www.sciencedirect.com/science/article/pii/S0966636213002439.

[36] R. Ganea, A. Paraschiv-Ionescu, C. Büla, S. Rochat, and K. Aminian. Multiparametric evaluation of sit-to-stand and stand-to-sit transitions in elderly

people. *Medical Engineering & Physics*, 33(9):1086 – 1093, 2011. ISSN 1350-4533. doi: https://doi.org/10.1016/j.medengphy.2011.04.015. URL http://www.sciencedirect.com/science/article/pii/S1350453311000968.

[37] Nora Millor, Pablo Lecumberri, Marisol Gómez, Alicia Martínez-Ramírez, and Mikel Izquierdo. An evaluation of the 30-s chair stand test in older adults: frailty detection based on kinematic parameters from a single inertial unit. *Journal of NeuroEngineering and Rehabilitation*, 10(1):86, Aug 2013. ISSN 1743-0003. doi: 10.1186/1743-0003-10-86. URL https://doi.org/10.1186/1743-0003-10-86.

[38] A Weiss, T Herman, M Plotnik, M Brozgol, N Giladi, and J M Hausdorff. An instrumented timed up and go: the added value of an accelerometer for identifying fall risk in idiopathic fallers. *Physiological Measurement*, 32(12): 2003, 2011. URL http://stacks.iop.org/0967-3334/32/i=12/a=009.

[39] S. B. Kotsiantis. Supervised machine learning: A review of classification techniques. In *Proceedings of the 2007 Conference on Emerging Artificial Intelligence Applications in Computer Engineering: Real Word AI Systems with Applications in eHealth, HCI, Information Retrieval and Pervasive Technologies*, pages 3–24, Amsterdam, The Netherlands, The Netherlands, 2007. IOS Press. ISBN 978-1-58603-780-2. URL http://dl.acm.org/citation.cfm?id=1566770.1566773.

[40] G.Sophia Reena (HOD of BCA Department) Asha Rajkumar M.phil (Computer Science). Diagonsis of heaer disease using datamining algorithm. *Global Journal of Computer Science and Technology*, 2010. ISSN 0975-4172. URL https://computerresearch.org/index.php/computer/article/view/1028.

[41] Kemal Polat and Salih Güneş. An expert system approach based on principal

component analysis and adaptive neuro-fuzzy inference system to diagnosis of diabetes disease. *Digital Signal Processing*, 17(4):702 – 710, 2007. ISSN 1051-2004. doi: https://doi.org/10.1016/j.dsp.2006.09.005. URL http://www.sciencedirect.com/science/article/pii/S1051200406001370.

[42] Resul Das, Ibrahim Turkoglu, and Abdulkadir Sengur. Effective diagnosis of heart disease through neural networks ensembles. *Expert Systems with Applications*, 36(4):7675 – 7680, 2009. ISSN 0957-4174. doi: https://doi.org/10.1016/j.eswa.2008.09.013. URL http://www.sciencedirect.com/science/article/pii/S095741740800657X.

[43] Y. Xing, J. Wang, Z. Zhao, and a. Gao. Combination data mining methods with new medical data to predicting outcome of coronary heart disease. In *2007 International Conference on Convergence Information Technology (ICCIT 2007)*, pages 868–872, Nov 2007. doi: 10.1109/ICCIT.2007.204.

[44] S. Palaniappan and R. Awang. Intelligent heart disease prediction system using data mining techniques. In *2008 IEEE/ACS International Conference on Computer Systems and Applications*, pages 108–115, March 2008. doi: 10.1109/AICCSA.2008.4493524.

[45] G. Yadav, Y. Kumar, and G. Sahoo. Predication of parkinson's disease using data mining methods: A comparative analysis of tree, statistical and support vector machine classifiers. In *2012 NATIONAL CONFERENCE ON COMPUTING AND COMMUNICATION SYSTEMS*, pages 1–8, Nov 2012. doi: 10.1109/NCCCS.2012.6413034.

[46] Charissa Ann Ronao and Sung-Bae Cho. Human activity recognition with smartphone sensors using deep learning neural networks. *Expert Systems with Applications*, 59:235 – 244, 2016. ISSN 0957-4174. doi: https://doi.org/10.

1016/j.eswa.2016.04.032. URL http://www.sciencedirect.com/science/article/pii/S0957417416302056.

[47] R. K. Begg, M. Palaniswami, and B. Owen. Support vector machines for automated gait classification. *IEEE Transactions on Biomedical Engineering*, 52(5):828–838, May 2005. ISSN 0018-9294. doi: 10.1109/TBME.2005.845241.

[48] R. Williamson and B. J. Andrews. Gait event detection for fes using accelerometers and supervised machine learning. *IEEE Transactions on Rehabilitation Engineering*, 8(3):312–319, Sep. 2000. ISSN 1063-6528. doi: 10.1109/86.867873.

[49] Megan Herrmann Arun Jayaraman Mark V. Albert, Konrad Kording. Fall classification by machine learning using mobile phones. *PLoS ONE*, 7(5), 2012. doi: https://doi.org/10.1371/journal.pone.0036556.

[50] Erick K. McCarthy, Michael A. Horvat, Philip A. Holtsberg, and Joseph M. Wisenbaker. Repeated chair stands as a measure of lower limb strength in sexagenarian women. *The Journals of Gerontology: Series A*, 59(11):1207–1212, 2004. doi: 10.1093/gerona/59.11.1207. URL http://dx.doi.org/10.1093/gerona/59.11.1207.

[51] Shinsuke Yoshioka, Akinori Nagano, Dean C. Hay, and Senshi Fukashiro. The minimum required muscle force for a sit-to-stand task. *Journal of Biomechanics*, 45(4):699 – 705, 2012. ISSN 0021-9290. doi: https://doi.org/10.1016/j.jbiomech.2011.11.054. URL http://www.sciencedirect.com/science/article/pii/S0021929011007482.

[52] P.J. Cordo, V.S. Gurfinkel, T.C. Smith, P.W. Hodges, S.M.P. Verschueren, and S. Brumagne. The sit-up: complex kinematics and muscle activity in voluntary axial movement. *Journal of Electromyography and Kinesiology*, 13(3):239 – 252, 2003. ISSN 1050-6411. doi: https://doi.org/10.1016/

S1050-6411(03)00023-3. URL http://www.sciencedirect.com/science/article/pii/S1050641103000233.

[53] Shinsuke Yoshioka, Akinori Nagano, Dean C. Hay, and Senshi Fukashiro. Biomechanical analysis of the relation between movement time and joint moment development during a sit-to-stand task. *BioMedical Engineering OnLine*, 8(1):27, Oct 2009. ISSN 1475-925X. doi: 10.1186/1475-925X-8-27. URL https://doi.org/10.1186/1475-925X-8-27.

[54] Mary Klein, Mukul Talaty, Alberto Esquenazi, John Whyte, and Mary Keenan. Analysis of the effect of lower limb weakness on performance of a sit-stand task. In *6th Annual International Conference on Industrial Engineering*, November 18-20 2001.

[55] Albert B. Schultz, Neil B. Alexander, and James A. Ashton-Miller. Biomechanical analyses of rising from a chair. *Journal of Biomechanics*, 25(12):1383 – 1391, 1992. ISSN 0021-9290. doi: https://doi.org/10.1016/0021-9290(92)90052-3. URL http://www.sciencedirect.com/science/article/pii/0021929092900523.

[56] Claudia Mazzà, Francesco Benvenuti, Carlo Bimbi, and Steven J. Stanhope. Association between subject functional status, seat height, and movement strategy in sit-to-stand performance. *Journal of the American Geriatrics Society*, 52(10):1750–1754, 2004. doi: 10.1111/j.1532-5415.2004.52472.x. URL https://onlinelibrary.wiley.com/doi/abs/10.1111/j.1532-5415.2004.52472.x.

[57] Susan L Whitney, Diane M Wrisley, Gregory F Marchetti, Michael A Gee, Mark S Redfern, and Joseph M Furman. Clinical measurement of sit-to-stand

performance in people with balance disorders: Validity of data for the five-times-sit-to-stand test. *Physical Therapy*, 85(10):1034–1045, 2005. doi: 10.1093/ptj/85.10.1034. URL http://dx.doi.org/10.1093/ptj/85.10.1034.

[58] C Weng, N Wang, and L Liu. The five times sit to stand test: a useful assessment tool for predicting falls in elderly. *Chinese Journal of Rehabilitation Medicine*, 27:908–912, 10 2012. doi: 10.3969/j.issn.1001-1242.2012.10.004.

[59] Severine Buatois, Christine Perret-Guillaume, Rene Gueguen, Patrick Miget, Guy Vançon, Philippe Perrin, and Athanase Benetos. A Simple Clinical Scale to Stratify Risk of Recurrent Falls in Community-Dwelling Adults Aged 65 Years and Older. *Physical Therapy*, 90(4):550–560, 04 2010. ISSN 0031-9023. doi: 10.2522/ptj.20090158. URL https://dx.doi.org/10.2522/ptj.20090158.

[60] Severine Buatois, Darko Miljkovic, Patrick Manckoundia, Rene Gueguen, Patrick Miget, Guy Vançon, Philippe Perrin, and Athanase Benetos. Five times sit to stand test is a predictor of recurrent falls in healthy community-living subjects aged 65 and older. *Journal of the American Geriatrics Society*, 56(8):1575–1577, 2008. doi: 10.1111/j.1532-5415.2008.01777.x. URL https://onlinelibrary.wiley.com/doi/abs/10.1111/j.1532-5415.2008.01777.x.

[61] Ryan P. Duncan, Abigail L. Leddy, and Gammon M. Earhart. Five times sit-to-stand test performance in parkinson's disease. *Archives of Physical Medicine and Rehabilitation*, 92(9):1431 – 1436, 2011. ISSN 0003-9993. doi: https://doi.org/10.1016/j.apmr.2011.04.008. URL http://www.sciencedirect.com/science/article/pii/S000399931100253X.

[62] C. Jessie Jones, Roberta E. Rikli, and William C. Beam. A 30-s chair-stand test as a measure of lower body strength in community-residing older adults.

Research Quarterly for Exercise and Sport, 70(2):113–119, 1999. doi: 10.1080/02701367.1999.10608028. URL https://doi.org/10.1080/02701367.1999.10608028. PMID: 10380242.

[63] Natalie A. de Morton, Megan Davidson, and Jennifer L. Keating. The de morton mobility index (demmi): An essential health index for an ageing world. *Health and Quality of Life Outcomes*, 6(1):63, Aug 2008. ISSN 1477-7525. doi: 10.1186/1477-7525-6-63. URL https://doi.org/10.1186/1477-7525-6-63.

[64] Inge Bruun, Birgitte Nørgaard, Berit Schiøttz-Christensen, Christian Mogensen, and Thomas Maribo. The 30-second chair stand test and habitual mobility predict reduced physical ability after acute admission. *Physiotherapy*, 102, 11 2016. doi: 10.1016/j.physio.2016.10.277.

[65] Małgorzata Wilk Anna Różańska-Kirschke, Piotr Kocur. The fullerton fitness test as an index of fitness in the elderly. *Medical Rehabilitation*, 10(2):15–19, 2006.

[66] Joan McMeeken, Barry Stillman, Ian Story, Peter Kent, and Jenni Smith. The effects of knee extensor and flexor muscle training on the timed-up-and-go test in individuals with rheumatoid arthritis. *Physiotherapy Research International*, 4(1):55–67, 1999. doi: 10.1002/pri.1999.4.1.55. URL https://onlinelibrary.wiley.com/doi/abs/10.1002/pri.1999.4.1.55.

[67] Anne Marie Norén, Ulrika Bogren, Jenny Bolin, and Christina Stenström. Balance assessment in patients with peripheral arthritis: applicability and reliability of some clinical assessments. *Physiotherapy Research International*, 6(4):193–204, 2001. doi: 10.1002/pri.228. URL https://onlinelibrary.wiley.com/doi/abs/10.1002/pri.228.

[68] Catherine M. Arnold and Robert A. Faulkner. The history of falls and

the association of the timed up and go test to falls and near-falls in older adults with hip osteoarthritis. *BMC Geriatrics*, 7(1):17, Jul 2007. ISSN 1471-2318. doi: 10.1186/1471-2318-7-17. URL https://doi.org/10.1186/1471-2318-7-17.

[69] Shamay S. Ng and Christina W. Hui-Chan. The timed up & go test: Its reliability and association with lower-limb impairments and locomotor capacities in people with chronic stroke. *Archives of Physical Medicine and Rehabilitation*, 86(8):1641 – 1647, 2005. ISSN 0003-9993. doi: https://doi.org/10.1016/j.apmr.2005.01.011. URL http://www.sciencedirect.com/science/article/pii/S0003999305002194.

[70] Thóra B. Hafsteinsdóttir, Marijke Rensink, and Marieke Schuurmans. Clinimetric properties of the timed up and go test for patients with stroke: A systematic review. *Topics in Stroke Rehabilitation*, 21(3):197–210, 2014. doi: 10.1310/tsr2103-197. URL https://doi.org/10.1310/tsr2103-197. PMID: 24985387.

[71] Susan Morris, Meg E Morris, and Robert Iansek. Reliability of Measurements Obtained With the Timed "Up & Go" Test in People With Parkinson Disease. *Physical Therapy*, 81(2):810–818, 02 2001. ISSN 0031-9023. doi: 10.1093/ptj/81.2.810. URL https://dx.doi.org/10.1093/ptj/81.2.810.

[72] Joe R. Nocera, Elizabeth L. Stegemöller, Irene A. Malaty, Michael S. Okun, Michael Marsiske, and Chris J. Hass. Using the timed up & go test in a clinical setting to predict falling in parkinson's disease. *Archives of Physical Medicine and Rehabilitation*, 94(7):1300 – 1305, 2013. ISSN 0003-9993. doi: https://doi.org/10.1016/j.apmr.2013.02.020. URL http://www.sciencedirect.com/science/article/pii/S0003999313001998.

[73] David A. Winter. *A.B.C. (anatomy, Biomechanics and Control) of Balance During Standing and Walking*. Waterloo Biomechanics, 1995.

[74] Martin Hora, Vladimır Sládek, Libor Soumar, Stráníková Kateřina, and Tomáš Michálek. Influence of body mass and lower limb length on knee flexion angle during walking in humans. *Folia Zoologica -Praha-*, 61:330–339, 11 2012. doi: 10.25225/fozo.v61.i3.a15.2012.

[75] MA Dettmann, M T Linder, and S B Sepic. Relationships among walking performance, postural stability, and functional assessments of the hemiplegic patient. *American journal of physical medicine & Rehabilitation*, 66:77–90, 05 1987.

[76] Mary E. Tinetti, Mark Speechley, and Sandra F. Ginter. Risk factors for falls among elderly persons living in the community. *New England Journal of Medicine*, 319(26):1701–1707, 1988. doi: 10.1056/NEJM198812293192604. URL https://doi.org/10.1056/NEJM198812293192604. PMID: 3205267.

[77] M.E. Roebroeck, C.A.M. Doorenbosch, J. Harlaar, R. Jacobs, and G.J. Lankhorst. Biomechanics and muscular activity during sit-to-stand transfer. *Clinical Biomechanics*, 9(4):235 – 244, 1994. ISSN 0268-0033. doi: https://doi.org/10.1016/0268-0033(94)90004-3. URL http://www.sciencedirect.com/science/article/pii/0268003394900043.

[78] Pao-Tsai Cheng, Mei-Yun Liaw, May-Kuen Wong, Fuk-Tan Tang, Ming-Yih Lee, and Pay-Shin Lin. The sit-to-stand movement in stroke patients and its correlation with falling. *Archives of Physical Medicine and Rehabilitation*, 79(9):1043 – 1046, 1998. ISSN 0003-9993. doi: https://doi.org/10.1016/S0003-9993(98)90168-X. URL http://www.sciencedirect.com/science/article/pii/S000399939890168X.

[79] Roberto Merletti and Philip Parker. *Electromyography: Physiology, Engineering and Noninvasive Applications*. John Wiley & Sons,Ltd, 2004.

[80] Laura Guidetti, Gianfranco Rivellini, and Francesco Figura. Emg patterns during running: Intra- and inter-individual variability. *Journal of Electromyography and Kinesiology*, 6(1):37 – 48, 1996. ISSN 1050-6411. doi: https://doi.org/10.1016/1050-6411(95)00015-1. URL http://www.sciencedirect.com/science/article/pii/1050641195000151.

[81] J.H. Sanchez, M. Solomonow, R.V. Baratta, and R. D'Ambrosia. Control strategies of the elbow antagonist muscle pair during two types of increasing isometric contractions. *Journal of Electromyography and Kinesiology*, 3(1):33 – 40, 1993. ISSN 1050-6411. doi: https://doi.org/10.1016/1050-6411(93)90021-N. URL http://www.sciencedirect.com/science/article/pii/105064119390021N.

[82] M. Cesarelli, P. Bifulco, and M. Bracale. Study of the control strategy of the quadriceps muscles in anterior knee pain. *IEEE Transactions on Rehabilitation Engineering*, 8(3):330–341, Sep. 2000. ISSN 1063-6528. doi: 10.1109/86.867875.

[83] R. H. T. Edwards. *Human Muscle Function and Fatigue*, chapter 1, pages 1–18. John Wiley & Sons, Ltd, 2008. ISBN 9780470715420. doi: 10.1002/9780470715420.ch1. URL https://onlinelibrary.wiley.com/doi/abs/10.1002/9780470715420.ch1.

[84] Carlo J. De Luca. The use of surface electromyography in biomechanics. *Journal of Applied Biomechanics*, 13:135–163, 05 1997. doi: 10.1123/jab.13.2.135.

[85] Mario Cifrek, Vladimir Medved, Stanko Tonković, and Saša Ostojić. Surface

emg based muscle fatigue evaluation in biomechanics. *Clinical Biomechanics*, 24(4):327 – 340, 2009. ISSN 0268-0033. doi: https://doi.org/10.1016/j.clinbiomech.2009.01.010. URL http://www.sciencedirect.com/science/article/pii/S0268003309000254.

[86] Fátima Rodrigues de Paula Goulart and Josep Valls-Solé. Patterned electromyographic activity in the sit-to-stand movement. *Clinical Neurophysiology*, 110(9):1634 – 1640, 1999. ISSN 1388-2457. doi: https://doi.org/10.1016/S1388-2457(99)00109-1. URL http://www.sciencedirect.com/science/article/pii/S1388245799001091.

[87] P T Cheng, Chia-Ling Chen, Chin-Man Wang, and Wei-Hsien Hong. Leg muscle activation patterns of sit-to-stand movement in stroke patients. *American journal of physical medicine & rehabilitation*, 83 1:10–6, 2004.

[88] David T. Felson. Osteoarthritis of the knee. *New England Journal of Medicine*, 354(8):841–848, 2006. doi: 10.1056/NEJMcp051726. URL https://doi.org/10.1056/NEJMcp051726. PMID: 16495396.

[89] Sheila C O'Reilly, Adrian Jones, Ken R Muir, and Michael Doherty. Quadriceps weakness in knee osteoarthritis: the effect on pain and disability. *Annals of the Rheumatic Diseases*, 57(10):588–594, 1998. ISSN 0003-4967. doi: 10.1136/ard.57.10.588. URL https://ard.bmj.com/content/57/10/588.

[90] Leena MD Sharma. Local factors in osteoarthritis. *Current Opinion in Rheumatology*, 13(5):441–446, September 2001.

[91] Yi–Chung Pai, Huan J. Chang, Rowland W. Chang, James M. Sinacore, and Jack L. Lewis. alteration in multijoint dynamics in patients with bilateral knee osteoarthritis. *Arthritis & Rheumatism*, 37(9):1297–1304, 1994. doi: 10.1002/art.1780370905. URL https://onlinelibrary.wiley.com/doi/abs/10.1002/art.1780370905.

[92] Glykeria Patsika, Eleftherios Kellis, and Ioannis G. Amiridis. Neuromuscular efficiency during sit to stand movement in women with knee osteoarthritis. *Journal of Electromyography and Kinesiology*, 21(5):689 – 694, 2011. ISSN 1050-6411. doi: https://doi.org/10.1016/j.jelekin.2011.05.006. URL http://www.sciencedirect.com/science/article/pii/S1050641111000800.

[93] Sara J Farquhar, Darcy S Reisman, and Lynn Snyder-Mackler. Persistence of altered movement patterns during a sit-to-stand task 1 year following unilateral total knee arthroplasty. *Physical Therapy*, 88(5):567–579, 2008. doi: 10.2522/ptj.20070045. URL http://dx.doi.org/10.2522/ptj.20070045.

[94] CENTER OF MASS LAB. http://oregonstate.edu/instruct/exss323/CM_Lab/Center%20of%20Mass.htm. Accessed: 2018-10-25.

[95] Joseph Hamill, K.M. Knutzen, and Timothy Derrick. *Biomechanical basis of human movement*. 01 2014. ISBN 978-1451177305.

[96] Manuela Galli, Marcello Crivellini, F Sibella, Angelo Montesano, P Bertocco, and C Parisio. Sit-to-stand movement analysis in obese subjects. *International journal of obesity and related metabolic disorders : journal of the International Association for the Study of Obesity*, 24:1488–92, 12 2000. doi: 10.1038/sj.ijo.0801409.

[97] F Sibella, Manuela Galli, Marianna Romei, Angelo Montesano, and Marcello Crivellini. Biomechanical analysis of sit-to-stand movement in normal and obese subjects. *Clinical biomechanics (Bristol, Avon)*, 18:745–50, 11 2003. doi: 10.1016/S0268-0033(03)00144-X.

[98] A. Kerr, V.P. Pomeroy, P.J. Rowe, P. Dall, and D. Rafferty. Measuring movement fluency during the sit-to-walk task. *Gait & Posture*, 37 (4):598 – 602, 2013. ISSN 0966-6362. doi: https://doi.org/10.1016/

j.gaitpost.2012.09.026. URL http://www.sciencedirect.com/science/article/pii/S0966636212003724.

[99] Kazusuke Maenaka. Mems inertial sensors and their applications. In *2008 5th International Conference on Networked Sensing Systems*, pages 71–73, June 2008. doi: 10.1109/INSS.2008.4610859.

[100] Matthew Shaw, Clayton J. Adam, Maree T. Izatt, Paul Licina, and Geoffrey N. Askin. Use of the iphone for cobb angle measurement in scoliosis. *European Spine Journal*, 21(6):1062–1068, Jun 2012. ISSN 1432-0932. doi: 10.1007/s00586-011-2059-0. URL https://doi.org/10.1007/s00586-011-2059-0.

[101] Antonio I Cuesta-Vargas, Alejandro Galán-Mercant, and Jonathan M Williams. The use of inertial sensors system for human motion analysis. *Physical Therapy Reviews*, 15(6):462–473, 2010. doi: 10.1179/1743288X11Y.0000000006. URL https://doi.org/10.1179/1743288X11Y.0000000006. PMID: 23565045.

[102] N. Yazdi, F. Ayazi, and K. Najafi. Micromachined inertial sensors. *Proceedings of the IEEE*, 86(8):1640–1659, Aug 1998. ISSN 0018-9219. doi: 10.1109/5.704269.

[103] Anthony J. Wheeler andAhmad R. Ganji. *Introduction to Engineering Experiments*. Pearson Education, London, UK, 2010.

[104] A. Beliveau, G. T. Spencer, K. A. Thomas, and S. L. Roberson. Evaluation of mems capacitive accelerometers. *IEEE Design Test of Computers*, 16(4):48–56, Oct 1999. ISSN 0740-7475. doi: 10.1109/54.808209.

[105] Glen Cooper, Ian Sheret, Louise McMillian, Konstantinos Siliverdis, Ning Sha, Diana Hodgins, Laurence Kenney, and David Howard. Inertial sensor-based knee flexion/extension angle estimation. *Journal of Biomechanics*,

42(16):2678 – 2685, 2009. ISSN 0021-9290. doi: https://doi.org/10.1016/j.jbiomech.2009.08.004. URL http://www.sciencedirect.com/science/article/pii/S002192900900459X.

[106] Manon Kok, Jeroen D. Hol, and Thomas B. Schön. Using inertial sensors for position and orientation estimation. *CoRR*, abs/1704.06053, 2017. URL http://arxiv.org/abs/1704.06053.

[107] F. Gulmammadov. Analysis, modeling and compensation of bias drift in mems inertial sensors. In *2009 4th International Conference on Recent Advances in Space Technologies*, pages 591–596, June 2009. doi: 10.1109/RAST.2009.5158260.

[108] A. Grossmann and J. Morlet. Decomposition of hardy functions into square integrable wavelets of constant shape. *SIAM Journal on Mathematical Analysis*, 15(4):723–736, 1984. doi: 10.1137/0515056. URL https://doi.org/10.1137/0515056.

[109] Stephen J Preece, John Y Goulermas, Laurence P J Kenney, Dave Howard, Kenneth Meijer, and Robin Crompton. Activity identification using body-mounted sensors—a review of classification techniques. *Physiological Measurement*, 30(4):R1, 2009. URL http://stacks.iop.org/0967-3334/30/i=4/a=R01.

[110] X. Yun and E. R. Bachmann. Design, implementation, and experimental results of a quaternion-based kalman filter for human body motion tracking. *IEEE Transactions on Robotics*, 22(6):1216–1227, Dec 2006. ISSN 1552-3098. doi: 10.1109/TRO.2006.886270.

[111] H. J. Luinge and P. H. Veltink. Measuring orientation of human body segments using miniature gyroscopes and accelerometers. *Medical and Biological*

Engineering and Computing, 43(2):273–282, Apr 2005. ISSN 1741-0444. doi: 10.1007/BF02345966. URL https://doi.org/10.1007/BF02345966.

[112] E. R. Bachmann, , and C. W. Peterson. An investigation of the effects of magnetic variations on inertial/magnetic orientation sensors. In *IEEE International Conference on Robotics and Automation, 2004. Proceedings. ICRA '04. 2004*, volume 2, pages 1115–1122 Vol.2, April 2004. doi: 10.1109/ROBOT.2004.1307974.

[113] Josip Music, Roman Kamnik, and Marko Munih. Model based inertial sensing of human body motion kinematics in sit-to-stand movement. *Simulation Modelling Practice and Theory*, 16(8):933 – 944, 2008. ISSN 1569-190X. doi: https://doi.org/10.1016/j.simpat.2008.05.005. URL http://www.sciencedirect.com/science/article/pii/S1569190X08001019. EUROSIM 2007.

[114] R. A. da Paixão, P. F. F. Rosa, and J. M. M. Neto. An attitude heading and reference system: Basic concepts and prototype. In *2011 IEEE International Symposium on Industrial Electronics*, pages 2225–2230, June 2011. doi: 10.1109/ISIE.2011.5984507.

[115] Karina Lebel, Patrick Boissy, Hung Nguyen, and Christian Duval. Inertial measurement systems for segments and joints kinematics assessment: towards an understanding of the variations in sensors accuracy. *BioMedical Engineering OnLine*, 16(1):56, May 2017. doi: 10.1186/s12938-017-0347-6. URL https://doi.org/10.1186/s12938-017-0347-6.

[116] R. M. Guimaraes and Bernard Isaacs. Characteristics of the gait in old people who fall. *International Rehabilitation Medicine*, 2(4):177–180, 1980. doi: 10.3109/09638288009163984. URL https://doi.org/10.3109/09638288009163984. PMID: 7239777.

[117] Chiung-Yu Cho and Gary Kamen. Detecting balance deficits in frequent fallers using clinical and quantitative evaluation tools. *Journal of the American Geriatrics Society*, 46(4):426–430, 1998. doi: 10.1111/j.1532-5415.1998.tb02461.x. URL https://onlinelibrary.wiley.com/doi/abs/10.1111/j.1532-5415.1998.tb02461.x.

[118] Sebastijan Sprager and Matjaz B. Juric. Inertial sensor-based gait recognition: A review. *Sensors*, 15(9):22089–22127, 2015. ISSN 1424-8220. doi: 10.3390/s150922089. URL http://www.mdpi.com/1424-8220/15/9/22089.

[119] Merryn J Mathie, Adelle C F Coster, Nigel H Lovell, and Branko G Celler. Accelerometry: providing an integrated, practical method for long-term, ambulatory monitoring of human movement. *Physiological Measurement*, 25(2): R1, 2004. URL http://stacks.iop.org/0967-3334/25/i=2/a=R01.

[120] Jan Rueterbories, Erika G. Spaich, Birgit Larsen, and Ole K. Andersen. Methods for gait event detection and analysis in ambulatory systems. *Medical Engineering & Physics*, 32(6):545 – 552, 2010. ISSN 1350-4533. doi: https://doi.org/10.1016/j.medengphy.2010.03.007. URL http://www.sciencedirect.com/science/article/pii/S1350453310000718.

[121] R. Williamson and B. J. Andrews. Gait event detection for fes using accelerometers and supervised machine learning. *IEEE Transactions on Rehabilitation Engineering*, 8(3):312–319, Sept 2000. ISSN 1063-6528. doi: 10.1109/86.867873.

[122] K. Aminian, B. Najafi, C. Büla, P.-F. Leyvraz, and Ph. Robert. Spatio-temporal parameters of gait measured by an ambulatory system using miniature gyroscopes. *Journal of Biomechanics*, 35(5):689 – 699, 2002. ISSN 0021-9290. doi: https://doi.org/10.1016/S0021-9290(02)00008-8. URL http://www.sciencedirect.com/science/article/pii/S0021929002000088.

[123] Kaiyu Tong and Malcolm H Granat. A practical gait analysis system using gyroscopes. *Medical Engineering & Physics*, 21(2):87 – 94, 1999. ISSN 1350-4533. doi: https://doi.org/10.1016/S1350-4533(99)00030-2. URL http://www.sciencedirect.com/science/article/pii/S1350453399000302.

[124] Thomas Seel, Jörg Raisch, and Thomas Schauer. Imu-based joint angle measurement for gait analysis. *Sensors*, 14(4):6891–6909, 2014. ISSN 1424-8220. doi: 10.3390/s140406891. URL http://www.mdpi.com/1424-8220/14/4/6891.

[125] Tinetti ME and Kumar C. The patient who falls: "it's always a trade-off". *JAMA*, 303(3):258–266, 2010. doi: 10.1001/jama.2009.2024. URL +http://dx.doi.org/10.1001/jama.2009.2024.

[126] Stephen R. Lord, Susan M. Murray, Kirsten Chapman, Bridget Munro, and Anne Tiedemann. Sit-to-stand performance depends on sensation, speed, balance, and psychological status in addition to strength in older people. *The Journals of Gerontology: Series A*, 57(8):M539–M543, 2002. doi: 10.1093/gerona/57.8.M539. URL http://dx.doi.org/10.1093/gerona/57.8.M539.

[127] Linda P. Fried, Catherine M. Tangen, Jeremy Walston, Anne B. Newman, Calvin Hirsch, John Gottdiener, Teresa Seeman, Russell Tracy, and Willem J. Kop. Frailty in older adults: evidence for a phenotype. *Journal of Gerontology, Biological Sciences and Medical Sciences*, pages 146–156, 2001.

[128] Brandon Rohrer, Susan Fasoli, Hermano Igo Krebs, Richard Hughes, Bruce Volpe, Walter R. Frontera, Joel Stein, and Neville Hogan. Movement smoothness changes during stroke recovery. *Journal of Neuroscience*, 22(18):8297–8304, 2002. ISSN 0270-6474. doi: 10.1523/JNEUROSCI.22-18-08297.2002. URL http://www.jneurosci.org/content/22/18/8297.

[129] Neville Hogan and Dagmar Sternad. Sensitivity of smoothness measures to

movement duration, amplitude, and arrests. *Journal of Motor Behavior*, 41 (6):529–534, 2009. doi: 10.3200/35-09-004-RC. URL https://doi.org/10.3200/35-09-004-RC. PMID: 19892658.

[130] José Ailton Oliveira Carneiro, Taiza Elaine Grespan Santos-Pontelli, José Fernando Colafêmina, Antonio Adilton Oliveira Carneiro, and Eduardo Ferriolli. A pilot study on the evaluation of postural strategies in young and elderly subjects using a tridimensional electromagnetic system. *Brazilian Journal of Otorhinolaryngology*, 79(2):219 – 225, 2013. ISSN 1808-8694. doi: https://doi.org/10.5935/1808-8694.20130038. URL http://www.sciencedirect.com/science/article/pii/S1808869415302986.

[131] N.B. Alexander, A.T. Galecki, L.V. Nyquist, M.R. Hofmeyer, J.C. Grunawalt, M.L. Grenier, and J.L. Medell. Chair and bed rise performance in adl-impaired congregate housing residents. *Journal of the American Geriatrics Society*, 48(5):526–533, 2000. doi: 10.1111/j.1532-5415.2000.tb04999.x. URL https://onlinelibrary.wiley.com/doi/abs/10.1111/j.1532-5415.2000.tb04999.x.

[132] Mei-Yun Liaw May-Kuen Wong Fuk-Tan Tang Ming-Yih Lee Pay-Shin Lin Pao-Tsai Cheng, Pao-Tsai Cheng. The sit-to-stand movement in stroke patients and its correlation with falling. *Archives of Physical Medicine and Rehabilitation*, 79(9):1043–1046, 2000. doi: 10.1111/j.1532-5415.2000.tb04999.x. URL https://onlinelibrary.wiley.com/doi/abs/10.1111/j.1532-5415.2000.tb04999.x.

[133] Y. Hsu, S. Yang, H. Chang, and H. Lai. Human daily and sport activity recognition using a wearable inertial sensor network. *IEEE Access*, 6:31715–31728, 2018. ISSN 2169-3536. doi: 10.1109/ACCESS.2018.2839766.

[134] R.C. Van Lummel, E. Ainsworth, U. Lindemann, W. Zijlstra, L. Chiari,

P. Van Campen, and J.M. Hausdorff. Automated approach for quantifying the repeated sit-to-stand using one body fixed sensor in young and older adults. *Gait & Posture*, 38(1):153 – 156, 2013. ISSN 0966-6362. doi: https://doi.org/10.1016/j.gaitpost.2012.10.008. URL http://www.sciencedirect.com/science/article/pii/S0966636212003815.

[135] Daniele Giansanti, Giovanni Maccioni, Francesco Benvenuti, and Velio Macellari. Inertial measurement units furnish accurate trunk trajectory reconstruction of the sit-to-stand manoeuvre in healthy subjects", journal="medical & biological engineering & computing. 45(10):969–976, Oct 2007. ISSN 1741-0444. doi: 10.1007/s11517-007-0224-8. URL https://doi.org/10.1007/s11517-007-0224-8.

[136] Abul Doulah, Xiangrong Shen, and Edward Sazonov. Early detection of the initiation of sit-to-stand posture transitions using orthosis-mounted sensors. *Sensors*, 17:2712, 11 2017. doi: 10.3390/s17122712.

[137] James Diebel. Representing attitude: Euler angles, unit quaternions, and rotation vectors. *Matrix*, 58(15-16):1–35, 2006.

[138] Panagiotis Tsaklis PhD, Wilhelmus Grooten, and Erika Franzén. Effects of weight-shift training on balance control and weight distribution in chronic stroke: A pilot study. *Topics in stroke rehabilitation*, 19:23–31, 01 2012. doi: 10.1310/tsr1901-23.

[139] Catherine M. Sackley. The relationships between weight-bearing asymmetry after stroke, motor function and activities of daily living. *Physiotherapy Theory and Practice*, 6(4):179–185, 1990. doi: 10.3109/09593989009048293.

[140] Ryan L. Mizner and Lynn Snyder-Mackler. Altered loading during walking and sit-to-stand is affected by quadriceps weakness after total knee

arthroplasty. *Journal of Orthopaedic Research*, 23(5):1083–1090, 2005. doi: 10.1016/j.orthres.2005.01.021.

[141] Ali H. Alnahdi, Joseph A. Zeni, and Lynn Snyder-Mackler. Quadriceps strength asymmetry predicts loading asymmetry during sit-to-stand task in patients with unilateral total knee arthroplasty. *Knee Surgery, Sports Traumatology, Arthroscopy*, 24(8):2587–2594, Aug 2016. doi: 10.1007/s00167-015-3827-x.

[142] P T Cheng, Mei-Yun Liaw, M K Wong, Feng Tang, Ming-Yih Lee, and Pay-Shin Lin. The sit-to-stand movement in stroke patients and its correlation with falling. *Archives of physical medicine and rehabilitation*, 79:1043–6, 10 1998. doi: 10.1016/S0003-9993(98)90168-X.

[143] Tom Dietterich. Overfitting and undercomputing in machine learning. *ACM Comput. Surv.*, 27(3):326–327, September 1995. ISSN 0360-0300. doi: 10.1145/212094.212114. URL http://doi.acm.org/10.1145/212094.212114.

[144] Stuart Russell and Peter Norvig. *Artificial Intelligence: A Modern Approach*. Prentice Hall Press, Upper Saddle River, NJ, USA, 3rd edition, 2009. ISBN 0136042597, 9780136042594.

[145] Gareth James, Daniela Witten, Trevor Hastie, and Robert Tibshirani. *An Introduction to Statistical Learning: With Applications in R*. Springer Publishing Company, Incorporated, 2014. ISBN 1461471370, 9781461471370.

[146] Sylvain Arlot, Alain Celisse, et al. A survey of cross-validation procedures for model selection. *Statistics surveys*, pages 40–79, 2010.

[147] Ron Kohavi and Foster Provost. Glossary of terms. *Machine Learning*, 30(2):271–274, Feb 1998. ISSN 1573-0565. doi: 10.1023/A:1017181826899. URL https://doi.org/10.1023/A:1017181826899.

[148] Nataraj CC Haj Mohamad TT, Samadani MM. Rolling element bearing diagnostics using extended phase space topology. *Journal of Vibration and Acoustics*, 140(6):061009–061009–9, 2018. doi: 10.1115/1.4040041.

[149] N. S. Altman. An introduction to kernel and nearest-neighbor nonparametric regression. *The American Statistician*, 46(3):175–185, 1992. ISSN 00031305. URL http://www.jstor.org/stable/2685209.

[150] V. B. Surya Prasath, Haneen Arafat Abu Alfeilat, Omar Lasassmeh, and Ahmad B. A. Hassanat. Distance and similarity measures effect on the performance of k-nearest neighbor classifier - A review. *CoRR*, abs/1708.04321, 2017. URL http://arxiv.org/abs/1708.04321.

[151] Li-Yu Hu, Min-Wei Huang, Shih-Wen Ke, and Chih-Fong Tsai. The distance function effect on k-nearest neighbor classification for medical datasets. *SpringerPlus*, 5, 12 2016. doi: 10.1186/s40064-016-2941-7.

[152] Classification Using Nearest Neighbors pairwise distance metrics. https://it.mathworks.com/help/stats/classification-using-nearest-neighbors.html#bsfjytu-1, . Accessed: 2019-01-15.

[153] Corinna Cortes and Vladimir Vapnik. Support-vector networks. *Machine Learning*, 20(3):273–297, Sep 1995. ISSN 1573-0565. doi: 10.1007/BF00994018. URL https://doi.org/10.1007/BF00994018.

[154] fitcsvm box constraints. https://it.mathworks.com/help/stats/fitcsvm.html#bt8v_z4-1, . Accessed: 2019-01-15.

[155] Karina Lebel, Patrick Boissy, Hung Nguyen, and Christian Duval. Autonomous quality control of joint orientation measured with inertial sensors. *Sensors*, 16(7), 2016. ISSN 1424-8220. doi: 10.3390/s16071037. URL http://www.mdpi.com/1424-8220/16/7/1037.

[156] E. P. Doheny, C. W. Fan, T. Foran, B. R. Greene, C. Cunningham, and R. A. Kenny. An instrumented sit-to-stand test used to examine differences between older fallers and non-fallers. In *2011 Annual International Conference of the IEEE Engineering in Medicine and Biology Society*, pages 3063–3066, Aug 2011. doi: 10.1109/IEMBS.2011.6090837.

[157] Sohrab Saeb, Luca Lonini, Arun Jayaraman, David C. Mohr, and Konrad P. Kording. The need to approximate the use-case in clinical machine learning. *GigaScience*, 6(5):gix019, 2017. doi: 10.1093/gigascience/gix019. URL http://dx.doi.org/10.1093/gigascience/gix019.

[158] Michael Esterman, Benjamin J. Tamber-Rosenau, Yu-Chin Chiu, and Steven Yantis. Avoiding non-independence in fmri data analysis: Leave one subject out. *NeuroImage*, 50(2):572 – 576, 2010. ISSN 1053-8119. doi: https://doi.org/10.1016/j.neuroimage.2009.10.092. URL http://www.sciencedirect.com/science/article/pii/S1053811909013184.

[159] K. V. R. Ravi and R. Palaniappan. Leave-one-out authentication of persons using 40 hz eeg oscillations. In *EUROCON 2005 - The International Conference on "Computer as a Tool"*, volume 2, pages 1386–1389, Nov 2005. doi: 10.1109/EURCON.2005.1630219.

[160] loss classification loss. https://it.mathworks.com/help/stats/classificationkernel.loss.html?s_tid=srchtitle#mw_757aea83-5228-4963-9933-9e0a83f7bcd4l, . Accessed: 2019-01-14.

[161] YANMIN SUN, ANDREW K. C. WONG, and MOHAMED S. KAMEL. Classification of imbalanced data: A review. *International Journal of Pattern Recognition and Artificial Intelligence*, 23(04):687–719, 2009. doi: 10.1142/S0218001409007326.

[162] Maleq Khan, Qin Ding, and William Perrizo. K-nearest neighbor classification

on spatial data streams using p-trees. 12 2001. doi: 10.1007/3-540-47887-6_51.